Oxford Brookes University

Faculty of Health and Life Sciences

Beyond membrane curvature; Clade 6 reticulons and their role within the plant endoplasmic reticulum

---

A thesis submitted for the award of;

Doctor of Philosophy (PhD)

Author:

Stefan Wojcik

Supervisors:

Dr Verena Kriechbaumer

Dr Patrick Moreau

December 2021

PhD programme funded by the Nigel Groome Studentship

Abstract

The endoplasmic reticulum (ER) is a dynamic organelle with multiple functions. It is comprised of distinct morphological domains. Regulation of this morphology and its dynamics are mediated by several highly conserved families of proteins, namely the reticulon (RTN) proteins responsible for generating high curvature membranes, Lunapark (LNP) proteins mediating cisternae formation, and ROOT HAIR DEFECTIVE 3 (RHD3/Atlastin/Sey1p) which is required for 3-way junction formation. The differential expression of these proteins induces changes in ER morphology, and morphological dysregulation has been associated with disruptions in overall cellular function.

Within the Arabidopsis genome, there are 21 *RTN* genes, across 6 protein clades. Clade 1-4 RTNs have been demonstrated to induce tubule formation, and upon over-expression produce a hyperconstriction phenotype on ER tubules. This function is mediated via the reticulon homology domain (RHD), which contains 4 transmembrane domains (TMDs). The 'W' shaped topology allows the RTNs to induce hydrophobic wedging and subsequent curvature of the ER membrane, and which is stabilised via oligomerisation of RTNs. Clade 5 RTNs, were previously characterised and found to localise distinctly different to clade 1-4 RTNs and are involved in regulation of sterol contents in roots due to the presence of a 3β-hydroxysteroid dehydrogenase domain (3βHSD).

In this body of work, the three members of clade 6 RTNs are characterised for the first time, revealing that RTN17, RTN18 and RTN21 localise to distinct punctate structures across the ER network. Analysis of RTN17.1 interacting partners indicates it could act as a hub protein utilising intrinsically disordered termini to interact with RHD3, and associates with the cytoskeletal network to promote homotypic fusion within the ER. Clade 6 RTNs are functionally distinct from clade 1-5 RTNs, and quantitative analysis of over-expression phenotypes reveal a distinct morphological profile linked to their suggested role in 3-way junction formation.

Glossary

3βHSD - 3β-hydroxysteroid dehydrogenase

ANOVA – Analysis of variance

AP – Acceptor photobleaching

APH – Amphipathic helix

ATL - Atlastin

cDNA – Complementary deoxyribonucleic acid

DM - Desmotubule

EPCS – Endoplasmic reticulum plasma membrane contact site

ER – Endoplasmic reticulum

ERAD – Endoplasmic reticulum associated degradation

FRET - Förster resonance energy transfer

GFP – Green fluorescent protein

IDR/IDP – Intrinsically disordered region/protein

Lat B – Latrunculin B

LNP – Lunapark

PC – Phosphatidylcholine

PCR – Polymerase chain reaction

PD – Plasmodesmata

PE – Phosphatidylethanolamine

PI - Phosphatidylinositol

PM – Plasma membrane

PS – Phosphatidylserine

REEP – Receptor expression enhancing protein

RHD – Reticulon homology domain

RHD3 – ROOT HAIR DEFECTIVE 3

RFP – Red fluorescent protein

mRNA – Messenger ribonucleic acid

RTN – Reticulon

SRP – Signal recognition particle

TMD – transmembrane domain

UPR – Unfolded protein response

Acknowledgments

This project would not have been possible without the support from supervisors, colleagues, friends, and family. I am extremely grateful for the opportunity, guidance and supervision from Verena Kriechbaumer who never failed to have the time for the students despite constant new demands and curveballs across the few years of my PhD. Thank you to Patrick Moreau for all his feedback and incredible knowledge, and for the potential opportunity to be welcomed to your lab briefly, if it were not for the pandemic. Finally, I am grateful and feel extremely fortunate for the time I was supervised by Chris Hawes, who is greatly missed.

Thank you to all of the plant cell biology group; Charlotte Pain especially for all the help getting up to speed early on and continued support and wisdom with the AnalyzER analysis, Tatiana Spatola Rossi, Bisa Andov, Alastair McGinness, and Joe McKenna for all of the great technical help and lab chats. Further thanks to all the annex cell biology group and technical staff, the office environment and social outings were greatly missed during lockdown and beyond.

Finally, I am thankful to the amazing support from my family, girlfriend, and her family, who have always supported me and enabled me to do my best through a challenging few years.

Contents

Figures List

Tables list

Supplementary figure list

Supplementary movie list

Chapter 1 – Introduction

1.1 – Introduction

The work within this thesis describes the localisation and functions of the previously unexplored clade 6 of Arabidopsis reticulon (RTN) proteins, RTN17, RTN18 and RTN21. In brief, RTNs are a family of key proteins involved in regulating the morphology of the endoplasmic reticulum (ER), found across all eukaryotic cell types. Of the 21 Arabidopsis *RTN* genes, the encoded proteins have been found to be implicated in the formation of ER tubules. However, the clade 6 genes code for structurally distinct proteins, compared to other clades. These have not yet been described in terms of their role within the plant ER.

1.1.i – Origins of the Endoplasmic Reticulum (ER)

The Eukarya domain encompasses all organisms in which the cells contain an enclosed nucleus, as well as the presence of other membrane bound organelles (Woese et al., 1990). Eukaryotic cells are typically much larger than prokaryotic cells and found as both unicellular and multi-cellular lifeforms. Besides the presence of endomembranes, another hallmark of eukaryotic cells is the presence of highly conserved cytoskeletal proteins that form filaments as well as motor proteins that work upon these filaments. However, prokaryotic cells do contain some cytoskeletal proteins, but these are more genetically heterogenous and not all capable of forming filaments (Wickstead & Gull). The exact origins of eukaryotes from a previously prokaryotic exclusive world are still being debated, with theories of organelles arising from symbiosis of other specialised cells, being produced by invagination of the plasma membrane (PM), and forming de novo functions, and many other variations (Jékely, 2007; Martin et al., 2015). Each organelle has unique a composition of proteins and lipids, and thus are functionally distinct despite being

interconnected to a variety of cellular components and other organelles. A group of these organelles comprise the secretory pathway and are responsible for transcribing proteins for extracellular and intracellular destinations, via the nuclear envelope to the PM via the ER, Golgi, and intermediary vesicles, as well as the reverse direction at certain stages. This system is thought to have been present as early as the last eukaryotic common ancestor (Schlacht et al., 2014), making these organelles intrinsic and vital to all modern eukaryotic lifeforms.

1.1.ii – ER functions[1]

The ER is comprised of a continuous membrane spanning the outer nuclear envelope and a large distal peripheral network, occupying a tenth of the intracellular space in eukaryotic cells (Alberts et al., 2014). As well as being part of the secretory pathway the ER is host to a variety of functions including synthesis of proteins, calcium homeostasis, mediating cellular stress responses, biosynthesis of lipids, signalling, and is intimately connected with various other cellular components (Goyal & Blackstone, 2013). The ER is the site in which the majority of membrane integral proteins destined for compartments within the secretory pathway, as well as where secreted proteins are produced via co-translation (Jan et al., 2014). This occurs when cytosolic mRNA is received by a ribosome, and upon the recognition of a signal recognition particle (SRP), the complex is attached to the surface of the ER via the SRP receptor (Gilmore et al., 1982; Akopian et al., 2013). From here, signals within the protein sequence will result in either translocation into the ER membrane via the translocon (Walter & Blobel, 1981), or peptidase activity removes the SRP to relinquish the protein product into the lumen of the ER (Evans et al., 1986). A smaller portion of proteins can be post-translationally targeted to the ER and other organelles, following translation by free floating cytosolic ribosomes (Rapoport 2007). Across these two broad categories, around 30% of a cell's proteome will at one point interact with the ER (Akopian et al.,

[1] The information in this section includes evidence from non-plant systems.

2013). From here proteins can be sent to other organelles or secreted based on the presence of other signals and motifs within the protein structure (Wojcik & Kriechbaumer 2021), with many secretory and integral membrane proteins receiving post-translational modifications at the Golgi-apparatus (Stanley, 2011). Initial stages of post-translational modifications such as N-glycosylation occurs at the ER and is performed via a family of proteins called glucosidases which are highly conserved across all Eukarya (Schallus et al., 2008; Strasser, 2016).

As well as hosting a large portion of protein synthetic machinery, the ER is also the major site of membrane lipid biogenesis, with a variety of different enzymes involved in the production of phospholipids being localized in the ER membrane (Fagone & Jackowski, 2009). For example, one pathway for phosphatidylcholine (PC) synthesis, the most common phospholipid found across eukaryotic membranes, requires a diacylglycerol choline/ethanolaminephosphotransferase (CEPT) for the final enzymatic step in synthesis. This enzyme is localised in the ER (Henneberry et al., 2002). Other groups of lipids such as sphingolipids are fully synthesised across both ER and the Golgi apparatus, with the initial steps occurring at the ER (Merrill Jr, 2002). Phospholipids exist asymmetrically across biological membranes, and so the ER also hosts an abundance of proteins effective in establishing lipid asymmetry and leaflet specificity (Bell et al., 1981; Pomorski & Menon, 2006).

Another primary role of the ER is that of an intracellular Ca^{2+} store. Utilising pumps, specifically the sarcoendoplasmic reticular Ca^{2+} ATPases (SERCA), the ER is capable of generating an extreme Ca^{2+} concentration gradient, up to 1 mM compared to the cytosolic concentration of 100 nM (Strehler & Treiman, 2004). The release of Ca^{2+} from the ER is mediated by IP3 and the calcium release channel ryanodine receptor 2 (RyR2) (Kaya et al., 2013). These are activated in response to multiple signalling cascades triggered by extracellular stimuli such as G-protein coupled (GPCR) or Tyrosine-kinase (TKR) receptors (Clapham, 2007). Triggering Ca^{2+} release, as well as general leakage from the ER often means the ATP demand to maintain the concentration gradient alone is insufficient. To combat this, ER-PM contact sites (EPCS) mediate a store-operated Ca^{2+}

entry mechanism. Here, stromal interaction molecule 1 (STIM1), accumulates in the ER at points in which the membrane is within a short distance (<50 μm) from the PM, and interacts with the PM localised Ca^{2+} channel protein called calcium release-activated calcium channel protein 1 (ORA1) (Putney, 2005). The subsequent complex formed that spans both the ER and PM is known as Ca^{2+} release activated channels (CRAC; Zhang et al., 2005). The CRAC pathway gives the ER lumen access to the high extracellular concentration of Ca^{2+} ions. This allows the ER to sufficiently restore the Ca^{2+} gradient, essential for continuing a variety of intracellular signalling pathways via proteins such as Calmodulin and other adaptors that sense changes in Ca^{2+} concentration and in turn activate a multitude of kinases and phosphatases (Burgoyne, 2007). Kinase and phosphatase activity mediate the addition or removal respectively of phosphate groups, which are ubiquitous post-translational modifications in proteins to induce conformational changes and regulate functions throughout the proteome (Westheimer, 1987). Another important role of the ER as a Ca^{2+} store is the regulation of apoptosis. The ER interacts with mitochondria at contact sites called mitochondria associated membranes (MAMs). Here under certain scenarios such as ER stress, the ER is capable of increasing mitochondrial matrix Ca^{2+} concentration via voltage-dependent anion channels (VDAC) on the outer mitochondrial membrane (De Pinto & Palmieri, 1992). This increases causes the mitochondria to initiate the process of apoptosis and is the reason mutations affecting proteins that control the Ca^{2+} regulatory functions of the ER can induce cell death (Marchi et al., 2018).

Another avenue in which the ER is fundamentally linked to overall cellular function and longevity is with the unfolded protein response (UPR). This is a highly conserved set of mechanisms that mediates ER homeostasis in response to multiple stressors (Schwarz & Blower, 2016). If these stressors cause the ER-associated protein degradation (ERAD) pathway to be overwhelmed and the folding demands of the cell cannot be met, the UPR is triggered (Ruggiano et al., 2014). The most conserved and ubiquitous UPR branch is mediated by the endoribonuclease IRE1, however other branches are present in mammalian cells, which are mediated by other proteins such as activating transcription factor 6 (ATF6) and protein kinase RNA-like kinase (PERK; Zeeshan et

al., 2016). In mammalian cells, activation of IRE1 results in unconventional splicing of *Xpb-1* transcript response to an accumulation of misfolded proteins, and the resulting *Xpb-1* mRNA encodes for BZIP that controls transcription of ER chaperones to assist and remedy the presence of misfolded proteins (Lin et al., 2007). IRE1 activation is caused by the accumulation of a free BiP within the ER lumen, a protein chaperone which dissociates from IRE1 and PERK in response to increased misfolding (Bertolotti et al., 2000). Arabidopsis UPR is mediated by two IRE1 homologues IRE1A and IRE1B (Koizumi et al., 2001), as well as bZIP28 which is homologous to mammalian ATF6 (Liu et al., 2007). The interaction between BiP and bZIP28 is similar to that as mammalian ATF6, in which binding of BiP to the c-terminal portion releases bZIP28 to act as a transcription factor promoting protein folding. However, the IRE1/BiP interaction has not been fully elucidated in Arabidopsis, but functions similarly to activate the transcription factor bZIP60, the functional homologue to metazoan Xpb1 (Pastor-Cantizano et al., 2021). Due to the importance of correct protein folding and ER homeostasis, the UPR and ERAD pathways are heavily linked to a variety of diseases across Eukarya (Hetz & Papa, 2017), as well as being vital for responding to a variety of signals or stressors (Park & Park 2019).

1.1.iii - The plant ER

The major functions of the ER are ubiquitous and conserved across all Eukarya as described previously. However, between the main kingdoms of eukaryotic organisms there are the presence or absence of organelles. For example, chloroplasts and other plastids are found within plantae, and some groups of chromita and protozoa (Woese et al., 1990), whilst being absent from Fungi and Animalia kingdoms. Furthermore, plant cells are distinct in having cellulose-based cell walls (Keegstra, 2010), and undergo cell division in a distinct way compared to other Eukaryotes, with the production of the phragmoplast and later cell-plate prior to cytokinesis, in a centriole independent manner (Buschmann & Zachgo, 2016). One specific feature of plant cells that pertains to the ER is the presence of plasmodesmata (PD). These are pores between higher plant

cells that allow intercellular communication to adjacent cells despite being enclosed by a cell wall. Within the PD resides a specialised form of the ER called the desmotubule (DM) allowing continuity of the membrane across cells (Overall & Blackman, 1996; Maule, 2008). These are semi-restrictive in what proteins, and other molecules are permitted to be transported between cells via the DMs. Viral proteins such as tobacco mosaic virus (TMV) replicase and movement proteins are capable of transferring between cells via the DM (Guenoune-Gelbart et al., 2008), allowing the spread of infection to pass through from initial contact site to the rest of the plant. This region of specialised cell wall, PM and ER is integral to the proper intercellular communication required for the development of multicellular organisms (Sager & Lee, 2018). Therefore, in the case of plants especially, the ER is not only functionally relevant for mediating multiple avenues of intracellular signalling but is also implicated in intracellular communication via this specialised region.

1.2 – ER morphology

1.2.i - Static and dynamic features of the ER

Initially, the ER was characterised into two sub-domains, the rough and smooth ER, based on the presence or lack of ribosomes (Shibata et al., 2006). However, based on advances in light and electron microscopy techniques (Hepler et al., 1990; Boevink et al., 1996) the peripheral ER network is now more accurately distinguished between the two main morphologies that constitute the ER network; cisternae (sheets) and tubules (Fig 1.1). Although comprised of a continuous membrane, these compartments each host unique characteristics and properties (Hawes et al., 2015). Cisternae are flattened bilayers that have a higher proportion of ribosomes as well as a greater lumen capacity, relevant for folding, as well as hosting polyribosomes for protein synthesis (Shibata et al., 2006). Tubules, although not completely deficient of ribosomes (West et al., 2011), are highly curved and elongated membranes, offering a greater surface area for membrane-based processes, such as lipid biosynthesis, vesicle formation and budding for ER export to post-ER compartments such as the Golgi (Shibata et al., 2006). The polygonal network is comprised of the negative cytoplasmic space surrounding the labelled ER, and the tubules typically converge at 3-way junctions (Fig 1.1). The ER is extremely pleomorphic through over different time scales and through development. For example, the ER in plant root cells undergoes drastic alterations as they mature and elongate, with expanding cells at the tip having a high proportion of cisternal ER, compared to a largely tubular network with large polygonal regions in mature cells (Ridge et al., 1999). Short-time scale alterations are also frequent in the ER network, and the resulting polygonal network form a Steiner tree-like network, with stable points from which tubules can elongate, shrink, fuse and form branches at high frequencies (Griffing et al., 2017) (Fig 1.1).

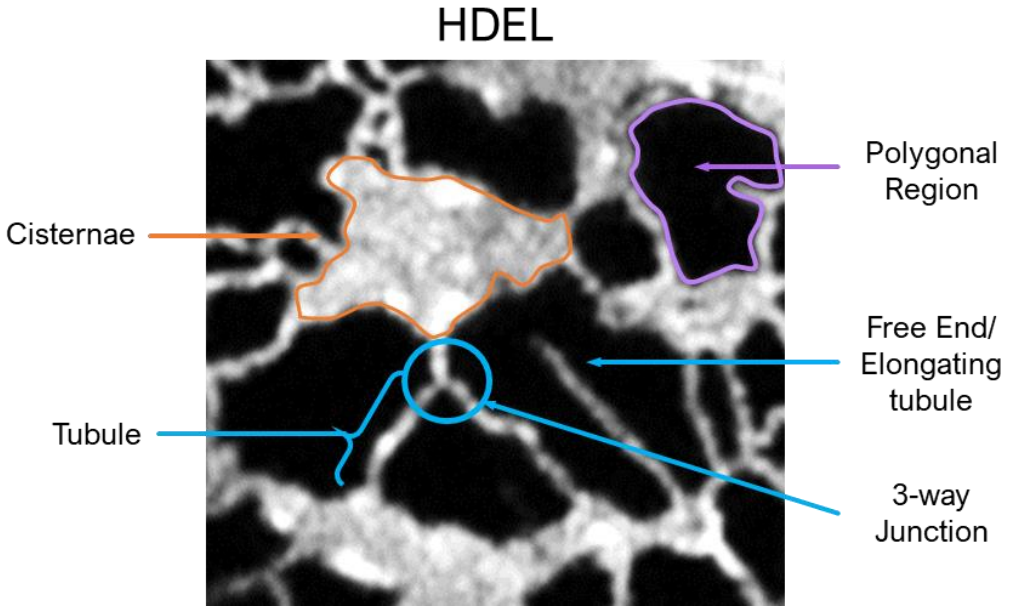

Figure 1.1 - Typical ER morphologies

Confocal microscope image of live cell ER in tobacco leaf epidermal cells. The cells are transiently expressing the fluorescent construct GFP-HDEL, which resides in the ER lumen. ER-features include cisternae (sheets), tubules, 3-way junctions, and polygonal regions which comprise the negative space around the network.

1.2.ii - ER and the cytoskeleton

Conversely to mammalian and yeast systems, in plants the actin cytoskeleton is the primary cytoskeletal component responsible for the generation of the characteristic polygonal ER network (Ueda et al., 2010). Myosin XI proteins are ER associated motors that mediate particular ER dynamics such as bulk flow and streaming. Perturbed myosin XI function results in decreased ER velocities as well as disorganised actin bundles as shown by dominant negative expression studies (Sparkes et al., 2008; Ueda et al., 2010; Griffing et al., 2014). This suggests that actin and the ER are both linked in terms of their respective structures and morphologies. This important interaction is also supported by evidence from studies utilising treatment with drugs such as latrunculin B (LatB) that inhibit the repolymerisation of actin filaments and cytochalasin D which inhibits polymerisation. Multiple studies employing this technique have shown that, like myosin XI disruption, depolymerisation results in disrupted morphology characteristics, as well as reduced dynamics at the network and molecular level (Sheahan et al., 2004; Sparkes et al., 2009a). Candidate proteins for mediating ER-actin cytoskeleton contacts are NET3b proteins (Hawkins et al., 2014; Peng & Hussey, 2017) and a plant specific SNARE protein, SYP73 (Cao et al., 2016). Overexpression of SYP73 creates a perturbed ER network that highly aligns with the actin cytoskeleton (Cao et al., 2016).

Despite this integral link between the two cellular components, *in vitro,* a tubular ER network can form in the absence of a cytoskeleton with the presence of certain morphogenic proteins (Powers et al., 2017). Furthermore, although actin is believed to be the main driver of plant ER dynamics, the extension of slow growing tubules has been associated with microtubules in plant cells and shown to act as an anchor point for ER tubule branching, similar to that in animal cells (Hamada et al., 2014). This suggests that the ER morphology is not fully dependent on actin alone. In mammals a protein called receptor expression-enhancing protein 1 (REEP-1) has been shown to

tether the ER and microtubules together via a microtubule binding domain. This protein is implicated in regulating the formation of the tubular network, and mutations of REEP-1 have been implicated in multiple neurite outgrowth disorders, as a result of a disturbed ER structure (Park et al., 2010). Although the Arabidopsis HVA22 protein is highly homologous to that of REEP, it does not appear to exhibit the same properties as REEP proteins (Lee et al., 2013; Park et al., 2010).

1.2.iii - ER-PM contact sites (EPCS)

Areas in which the ER is within 15-20 nm of the PM without fusing are known as EPCS. These typically act as stable points within the network, in which the ER is effectively anchored. Remodelling can occur around these subdomains of the ER (Sparkes et al., 2009a). In plants, this corresponds to 5-10% of the PM area, in lengths between 50-350 nm, depending on cell stage or type (McFarlane et al., 2017). EPCS are linked to a variety of functions, including maintaining ER stability, lipid regulation, and Ca^{2+} signalling (Bayer et al., 2017). In plants, proteins such as NET3C are localised to EPCS and involved in their formation. It is proposed that NET3C binds filamentous actin via C-terminal mediated dimerization and stabilises the ERs interaction with the PM via a putative mechanism (Wang et al., 2014). In combination with this, the vesicle associated membrane protein (VAMP) - associated proteins (VAP) 27 also localise to EPCS (Wang et al., 2014). Specifically, VAP27-1 and VAP27-3 are capable of interacting with NET3C via the major sperm domain (MSD) and appear to associate with junctions of actin and microtubules at EPCS (Wang et al., 2016).

Distinct from NET3C/VAP27 complexes, there appears to be another population of EPCS which are specific to Arabidopsis synaptotagmin 1 (SYT1; Sia et al., 2016). SYT1 has been shown to act as a tether protein that is integral to the formation of EPCS, with a *sSyt1* knock out resulting in a rescuable depletion of EPCS (Sia et al., 2016). PD are interconnections between neighbouring cells

that allow cell-cell communication. Viral movement proteins traversal through these junctions has been shown to be mediated via interaction and recruitment of SYT1 (Levy et al., 2015), potentially due to the close association with the PM and the desmotubules in the PD. The regulatory roles of EPCS reveal an important role in membrane interaction and overall cellular physiology.

As described earlier, the ER is an important store and regulator of intracellular calcium and much of this regulation is mediated via the EPCS. In mammalian cells for example, PM resident ORA1 proteins, interact with ER resident STIM1. This interaction is is Ca^{2+} sensitive and occurs at EPCSs to mediate store-operated Ca^{2+} entry (SOCE), restoring ER Ca^{2+} concentration after it's depletion in response to a variety extracellular signals and subsequent signalling pathways (Hogan et al., 2010). The EPCS labelled by SYT1 have been shown to be Ca^{2+} dependent, with Syt1 remodelling and increasing both proportion and strength of SYT-EPCS in response to Ca^{2+} activity (McFarlane et al., 2017). This Ca^{2+} responsive nature of SYT-EPCS has broader impacts in plant immunity (Kim et al., 2016) and exogenous stresses (Pérez-Sancho et al., 2015). Other regulatory roles of EPCS and the proteins localised at these subdomains include sterol transport, cytoskeleton arrangement and cell-cell communication, as reviewed by Wang et al (2017) and Bayer et al (2017).

1.2.iv - ER structure and function

The morphology of the ER is closely linked with the functional capacity of a cell. Under native conditions, cells often have a propensity towards one ER morphology based on the functional role of the cell. For example, high secretory cells having an increased proportion of cisternae to allow sufficient polyribosome occupation and increased protein production levels (Stephenson & Hawes, 1986) and other cells such as adrenal cells and muscle cells that require a greater lipid

production capacity and Ca^{2+} store respectively have a greater proportion of tubular structures (Baumann & Walz, 2001; Shibata et al., 2006).

The morphology of the ER also typically changes throughout developmental stages, for example when expanding cells have a higher proportion of perforated cisternae, in contrast to the tubular network of terminally extended cells (Ridge et al., 1999). Aside from typical changes of morphology through development and cell specialisation, the ER morphology is incredibly responsive and dynamic in response to exogenous stressors, or disease states in an organism. For example, upon pathogenic infection in Arabidopsis, actin filaments bundle and subsequent ER aggregation occurs in which the morphology shifts more cisternal at the site of infection (Takemoto et al., 2003). The increase of cisternal content within the network is also present with treatment of drugs such as BFA, as well as changes in abiotic factors such as temperature (Pain et al., 2019). Furthermore, when proteins involved in regulating ER morphology (morphogens) are perturbed, the UPR fails to initiate in the correct manner (Lai et al., 2014). The UPR is typically required to combat the accumulation of toxic aggregates or misfolded protein that can initiate cell death in response to exogenous stressors such as temperature, salinity imbalance, or pathogenic invasion (Deng et al., 2013). Upon induction of the UPR, an increase in ER volume occurs allowing the ER to meet the folding and synthesis demands under the stress conditions, and if it cannot be met the cell will undergo apoptosis (Schuck et al., 2009). Proteins that modify the shape of the ER can also lead to defects in plant growth (Chen et al., 2011) and multiple ER shaping proteins are implicated in various mammalian neurological disorders such as spastic paraplegia, sensory neuropathies (Zhao et al., 2016) as well as neurite outgrowth and plasticity in general (Schwab & Strittmatter, 2014). Together these aspects highlight the fundamental importance of ER shape in relation to its function.

1.3 - ER morphogens

ER morphogens are proteins whose primary function is involved in the regulation of ER morphology. The three primary families of conserved ER shaping proteins are Lunapark (LNP) proteins (Kriechbaumer et al., 2018a; Ueda et al., 2018), root hair defective 3 (RHD3) (Chen et al., 2011) and the reticulon-like protein subfamily B (Tolley et al., 2008; Sparkes et al., 2010), referred to within this work as reticulons (RTNs).

1.3.i - RHD3

RHD3 is a plant homologue of mammalian atlastin (ATL) and yeast Sey1p (Chen et al., 2011). These are ER membrane integral GTPases, which have been shown to mediate *in vivo* homotypic ER fusion in a GTP dependent manner (Moss et al., 2011; Anwar et al., 2012) as well as being sufficient to produce a reconstituted network via tubular fusion *in vitro* (Powers et al., 2017). Utilising CRISPR-Cas9, one group produced a triple knock out mouse cell line for the three mammalian ATL proteins, ATL1, ATL2 and ATL3, which resulted in a perturbed ER morphology (Zhao et al., 2016). The resulting ER network has a distinct lack of 3-way junctions and shows a decreased rate of fusion events, further supporting an important role for these GTPases in the formation of the regular polygonal ER network. This knockout phenotype can be rescued with the expression of both yeast Sey1p and plant RHD3 (Zhao et al., 2016), however an Arabidopsis RHD3 knock out cannot be rescued by overexpression of Sey1p suggesting that divergence in function has occurred evolutionary between these homologous proteins (Zhao et al., 2016). In plants, RHD3 is capable of forming homodimers via interaction between both the GTPase domain, as well as 3-helix bundles in the middle domain (Sun & Zheng, 2018). Both the full homodimerization of RHD3, as well as integration of the C-terminus into the ER membrane via an amphipathic helix (APH) is required to maintain a regular polygonal network (Sun & Zheng, 2018). The APH is capable and required to disturb the lipid bilayer based on hydrophobic interaction allowing

homotypic fusion to ensue and form a 3-way junction (Sun & Zheng, 2018). Not only do *rhd3* mutants exhibit a drastic defect in growth, particularly in root hair cells (Chen et al., 2011), RHD3 has also been shown to mediate the UPR upstream of IRE1, and thus is integral to the proper plant ER stress response (Lai et al., 2014).

1.3.ii - Lunapark proteins

There are two LNP proteins encoded by the Arabidopsis genome AtLNP1, and AtLNP2, which are homologues of mammalian (mLnp1), and yeast Lnp1p. mLnp1 and Lnp1p are ER integral proteins containing two N-terminal transmembrane domains (TMDs) and a zinc finger motif at the C-terminus. This is required for homodimerization and subsequent ER morphogen capabilities (Chen et al., 2012), as well as association with other proteins such as Sey1p to mediate cortical ER morphology (Casey et al., 2015). Specifically, it is postulated that the mammalian ATL, is responsible for formation of 3-way junctions, following which Lnp1 incorporates into the junction to stabilise this structure (Wang et al., 2016). This is exemplified by the fact that overexpression of mLnp1 *in vivo* increases the proportion of 3-way junctions, and subsequent deactivation of a functional mLnp1 either by mutation of the N-myristoylation site or knock-out decreases 3-way junctions (Moriya et al., 201; Zhou et al., 2019). AtLNP1 and AtLNP2 both share the generic LNP structural features but have no prediction for an N-terminal myristoylation site. The proteins share 67% amino acid (aa) identity and localise differentially within the ER but exhibit similar effects on ER morphology (Kriechbaumer et al., 2018b). AtLNP1 is capable of labelling cisternae and some 3-way junctions exclusively whereas AtLNP2 labels the ER as a whole (Kriechbaumer et al., 2018b). However, despite structural similarity, the function of LNP proteins in the plant ER appears to differ to that of Lnp1p and mLnp1 in yeast and mammals respectively (Ueda et al., 2018). Transient expression of the Arabidopsis LNP proteins induces sheet formation in a dose dependent manner, whereas deletion of either AtLNP proteins show decreased cisternal area and

increased polygonal regions of the network compared to wild type plants (Kriechbaumer et al., 2018a). It was also shown that AtLNP1 and 2 are capable of interacting with RTNs, and co-overexpression of RTN1 and LNP proteins supresses the cisternal phenotype of an AtLNP (Kriechbaumer et al., 2018a). RTN proteins localise to the edge of LNP labelled cisternae, and thus may act as a regulator of expansion of cisternae, however the exact interplay and biogenesis of cisternae is yet to be determined.

1.3.iii - Reticulons

Whereas LNP is responsible for the formation and regulation of cisternae, RTNs are responsible for the other major ER subdomain, tubules. Tubules are narrow cylinders that interconnect the network and are areas of high curvature along with the edges of cisternae, which contrast to the flat surfaces of the centre of cisternae. The Arabidopsis genome encodes for 21 *RTN* genes. A key feature of a RTN is the presence of a conserved reticulon homology domain (RHD), which is homologous to those present in mammalian and yeast reticulons. This RHD varies in sequence identity but maintains a similar length across all Arabidopsis RTNs (170-190 aa) (Nziengui et al. 2007) and consists of two hydrophobic regions linked by a cytosolic loop. Each hydrophobic region is comprised of two individual TMDs, which contain an unusually high number of amino acids compared to typical TMDs found in other proteins (Tolley et al., 2010). The RHD across Eukarya is highly conserved, with mammals having four RTNs and yeasts a homolog called Yop1p.

It has been proposed that the RHD allows the RTN to span the ER membrane with a 'W' shaped topology, meaning both the N- and C-termini are cytosol facing. The longer length of the TMDs allows the RHD to induce hydrophobic wedging, resulting in an increase in surface area of the outer bilayer, in turn inducing membrane curvature (Tolley et al., 2010)(Fig 1.2). The 21 RTN proteins can be subdivided into 6 phylogenetically distinct clades. Clade 1-4 are comprised of the first 16 RTNs which all contain a generic structure with short termini aside from the RHD and are between 150-250 aa long (Nziengui et al., 2007; Brooks et al., 2021). Clade 5 reticulons, RTN19 and RTN20 contain an N-terminal extension and are ~550 aa in length. Clade 6 reticulons are comprised of RTN17, RTN18 and RTN21, which contain both N and C-terminal extensions outside of the RHD (Nziengui et al., 2007; Brooks et al., 2021).

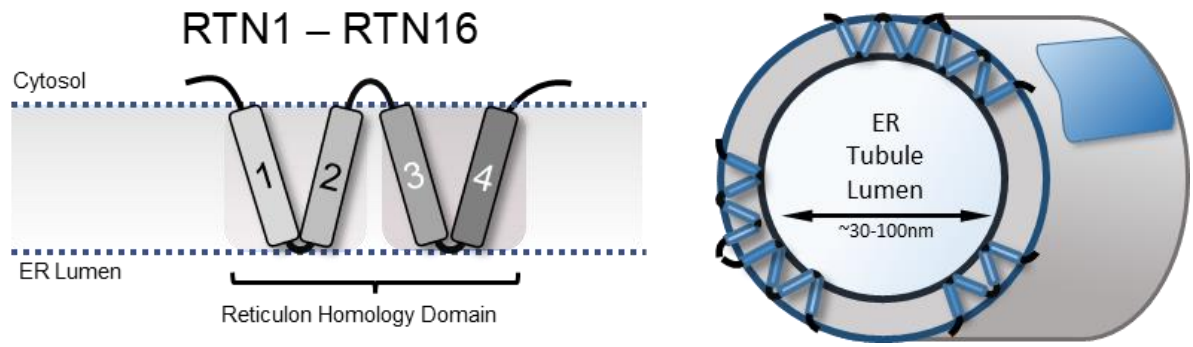

Figure 1.2 – RTN structure and role in the ER

Generic structure of majority of Arabidopsis RTNs. Reticulon homology domain (RHD) contains 4 transmembrane domains, with the two hydrophobic groups being linked by a cytosolic facing loop and bookmarked by cytosolic facing termini. These oligomerise to induce and stabilise curvature and form ER tubules of 30-100 nm in diameter. Blue square = RTN oligomer

RTNs localise exclusively to high curvature membranes such as tubules and the edges of cisternae, and overexpression of clade 1-4 RTNs results in the hyperconstriction of tubules where the lumen is constricted beyond the physiological norm. Overexpression also decreases the proportion of cisternae within the ER network (Sparkes et al., 2010). The majority of RTNs have a di-lysine signalling motif at the C-terminus, which is typically implicated in ER localisation of other proteins, however this is not consistent nor necessary for ER localisation in all RTNs (Sparkes et al., 2010). RTNs such as RTN13, which is a seed specific isoform, contain an APH that is implicated in its curvature inducing capabilities (Breeze et al., 2016). Of the 21 Arabidopsis RTNs, there are 2 configurations for APH containing RTNs. Either the APH is located immediately after the RHD, such as RTN13 and the other RTNs of clade 2, 3 and 4, or the APH and RHD are intersected by a ~20 aa long linker, such as the case for clade 1 RTNs. Clade 5 and clade 6 RTNs do not contain an APH (Brooks et al., 2021). RTNs are capable of homo- and hetero-oligomerisation, which is another integral factor in the tubule forming capabilities of RTNs (Tolley et al., 2010; Sparkes et al., 2010). As well as the hydrophobic wedging induced by the RHD, protein crowding from oligomerisation also contributes to promoting membrane curvature (Zimmerberg & Kozlov, 2006), and the protein-protein interaction between the monomers stabilises the resulting structure and leads to the formation of a tubule or cisternae edge (Shibata et al., 2008, Kriechbaumer et al., 2015)(Fig 1.2).

Consistently across Eukarya, overexpression of RTN induces both an increased proportion of tubular membrane components within the ER network, and depletes the proportion of cisternae (Voeltz et al., 2006; Tolley et al., 2008). Conversely, deletion of mammalian RTN4a or Yeast Yop1p increases proportion of cisternae (Voeltz et al., 2006). This vital role of RTN regulating ER morphology has also highlighted important impacts on cell physiology. For example, mammalian RTN3 has roles in trafficking, where it mediates non-clathrin-dependent endocytosis of EGFR at EPCS in response to local Ca^{2+} signalling, and in yeasts the generation of high curvature has implications in vesicle formation and budding as revealed by tracking defects in Yop1p overexpression experiments (Calero et al., 2001). Furthermore, as previously mentioned, RTN

dysfunction exhibits drastic effect on neurite outgrowth in neurons, potentially through RTNs impact on other cellular structures such as the cytoskeleton (Schwab & Strittmatter, 2014; Voeltz et al., 2006).

Of the 21 plant RTNs, the majority have been shown to be involved in regulating the tubular network of the ER (Tolley et al., 2008; Sparkes et al., 2010; Breeze et al., 2016). However, amongst the large group, different functional niches are being revealed, that go beyond just inducing membrane curvature. For example, RTN3 and 6 are unique in their capability of localising to the desmotubule within the PD, and co-localise with viral movement proteins, suggesting a potential role in regulating cell-cell communication and plant immunity via these specialised sub-domains (Knox et al., 2015; Kriechbaumer et al., 2015). Clade 5 and 6 RTNs, comprised of RTN17-21 are structurally distinct due to the presence of elongated termini outside of the RHD (Nziengui et al 2007; Brooks et al., 2021). Of this subgroup, RTN19 and RTN20 from clade 5 have recently been identified and show distinct functions beyond that of generating curvature (Kriechbaumer et al., 2018). Clade 5 RTNs have a unique role in lipid regulation, based on the presence of the extended N-terminus which shares homology with a 3β-hydroxysteroid dehydrogenase (3βHSD) protein, an enzyme involved in sterol synthesis (Kriechbaumer et al., 2018b). These 3βHSD homologues localise differentially with RTN20 labelling discrete puncta within the ER membrane, whereas RTN19 labels the entirety of the network. Both RTNs do not share a role in constricting the ER into tubules as with other RTNs, instead, RTN19 and RTN20 appear to be a novel group of proteins capable of regulating bulk sterol synthesis within Arabidopsis roots. The other 3βHSD homologue (3βHSD/D1) is comprised of 2 splice variants, which also occupy distinct locations: one localising to ER-exit sites, the other one to Golgi bodies (Kriechbaumer et al., 2018b). Amongst this subgroup of RTNs with terminal extensions, are RTN17, 18 and 21 which contain elongated N- and C-termini, making them distinct from the rest of the RTN family. The function of these proteins and their impact on the plant ER is undetermined as of yet.

1.4 – Aims and objectives

The plant ER is of great interest for many fields such as biotechnology and agriculture as it is the cornerstone organelle in regard to secretory protein production, as well as being vital for overall cellular physiology and response to stressors such as drought. The RTN family of proteins are of great importance across Eukarya, as ER shaping proteins have implications in several human neurological disorders and evidence from multiple studies indicate the function of the ER is dependent on its dynamic morphology (Yang & Strittmatter, 2007). There are still many questions around the functionality of certain proteins and how these morphologies are derived, especially in plant cells in which studies have shown some diverging results when comparing Arabidopsis proteins to mammalian and yeast homologues, which have typically garnered greater attention and studied more regularly.

To better understand the mechanisms underlying the regulation of ER morphology, this work aims to characterise the previously unstudied clade 6 Arabidopsis RTNs, RTN17, RTN18 and RTN21. The primary objective of this work is to compare and contrast clade 6 RTNs structure, localisation and function against the other clade of RTNs and classes of plant ER morphogens. In doing so this will progress the wider understanding of ER morphology and dynamics and bolster the growing population of proteins that have been shown to implicated in the complex organisation of ER sub structures. Firstly, genes of interest shall be isolated from cDNA prior to cloning into fluorescent fusion protein constructs and assessing transcript levels in Arabidopsis tissues. Subsequently, the Clade 6 RTNs shall be cloned not fluorescent fusion constructs and will be primarily interrogated by live-cell confocal microscopy experiments. This will be done to determine localisation of full-length proteins, transiently in tobacco and stable in Arabidopsis, co-expressed with other proteins of interest, mainly other ER morphogens, and interactions tested via Förster resonance energy transfer (FRET) based experiment. Beyond assessing the full-length proteins, these experiments aim to investigate specific aspects of the protein structure by

examining the splice variants of the clade 6 RTNs, as well as generate truncations and chimeric proteins to identify and probe functional domains present within the protein structure.

There will be a strong focus on quantified data from imaging experiments. Network modifications that arise from co-expression of the proteins of interest will be analysed via the software, AnalyzER (Pain et al., 2019). AnalyzER provides extensive quantitative analysis of ER strcture and dynamics. Alongside this, identification and assessment of knock out mutants will be carried out, including lipidomic analysis to explore potential phenotypes relevant to the proteins. Taken together, the functionality of the previously uncharacterised Arabidopsis clade 6 RTNs and their role within the plant ER will be unveiled.

Chapter 2 – Clade 6 Reticulons: Bioinformatics analysis

2.1 – Introduction

2.1.i – Organisation of Arabidopsis RTNs

The Arabidopsis genome codes for 21 Arabidopsis genes, divided into 6 clades (Fig 2.1A)(Brooks et al., 2021). Despite their significant role in the regulation of ER morphology the clade 1-4 RTNs, comprised of the first 16 RTNs, are relatively small and simple proteins between 150 and 250 residues long. This contrasts with other RTNs across Eukarya which contain larger terminal *-segments, often 1000+ aa long (Yang & Strittmatter, 2007). Clade 1-4 RTN function is largely a consequence of their structural domains, namely the TMDs within the RHD (Tolley et al., 2010), as well as the presence of the APH (Brooks et al., 2021). These domains allow recognition and insertion at curved membranes and subsequent stabilisation of this curvature via hydrophobic wedging of the TMDs and oligomerisation (Shibata et al., 2008; Sparkes et al., 2010). With the large variety of RTN genes present in the Arabidopsis genome, simply examining the protein sequence in greater detail with the variety of bioinformatics tools available can allow identification of the potential differences between the RTNs of each clade. For example, clade 5 and 6 RTNs were initially identified as distinct proteins due to their greater length (>400 aa) compared to clade the more compact structures of the clade 1-4 RTNs. Furthermore, clade 6 containing a putative extra TMD in the c-terminal portion of the protein sequence (Nziengui et al., 2007). Despite this, the RHD components including the cytosolic loop remain similar in length and are the most conserved regions when aligning the sequence of all RTNs (Nziengui et al.,

2007). This suggests that the difference with clade 5-6 RTNs, and the potential unique functionality lies in the terminal extensions of the protein.

The N-terminal extensions of the clade 5 RTNs 19 and 20 contain a 3βHSD domain (Fig 2.1B), and RTN19 was previously studied as an isoform of 3βHSD/D1, known as 3βHSD/D2 (Rahier et al., 2006). 3βHSD/D1 is similarly involved in sterol biosynthesis, however unlike RTN19 and RTN20, does not contain transmembrane domains. Protein BLAST reveals a high amino acid identity between these 3βHSD/D1 and RTN19, (82%) and less so with RTN20 (46%), suggesting that RTN19 and RTN20 are derived from a clade 104 RTN but had the functional domain of 3βHSD/D1 fused to the N-terminus (Kriechbaumer et al., 2018b). Evolutionarily this may have been utilised as a method to ensure localisation of the 3βHSD to the ER for its use in regulating sterol composition in Arabidopsis root tissue.

2.1.ii – Aims and objectives

The aim of this chapter is to interrogate the available DNA and protein sequences *in silico* to inform future *in vivo* experimentation. This will be achieved by utilising various bioinformatics platforms including UniProt, TAIR, SMART to determine phylogeny of the genes, identify potential homologous functional domains and other insights into the protein structure. The information derived from this analysis gave an initial indication as to whether the clade 6 RTNs are functionally distinct from other clades, and suggestions as to what interactions or functions to explore when looking to characterise RTN17, RTN18 and RTN21.

2.2 – Results

2.2.i - Phylogeny of RTNs, splice variants and sequence comparison

The Arabidopsis genome codes for 21 RTN genes (Fig 2.1A), of which RTN17, 18 and 21 reside within clade 6 (Fig 1A; Nziengui et al, 2007; Brooks et al., 2021). These 3 genes code for 6 proteins, which are structurally distinct from that of the rest of the RTN family, due to the presence of elongated termini either side of the RHD. RTN17 codes for 3 potential splice variants (Fig. 2.1B): RTN17.1, the full-length protein (431 aa), RTN17.2, a natural truncation of the 108 C-terminal residues (323 aa), and RTN17.3 which has a 13 aa deletion in the N-terminal region, between Q141-N155. RTN18 does not code for any splice variants and the full-length protein is 457 aa long. RTN21 codes for two splice variants, of which RTN21.2 is the full-length protein (593 aa), and RTN21.1 which has a truncation of the first 106 aa of the N-terminus (Fig 2.1B). A multiple sequence alignment (MSA) of the three full length proteins reveals that the main area of sequence conservation occurs within the RHD (Fig 2.1C), whereas the termini have a lower proportion of conserved residues (Fig 2.1C). Looking at the percentage identity matrix of the full structure of for RTN17.1, RTN18 and RTN21.1, we see that RTN17.1 and RTN18 share 62% sequence similarity, RTN17.1 and RTN21.1 share 31%, and RTN18 and RTN21.1 share 27% (Fig 2.1D). As suggested by the MSA, when comparing just the RHD of the clade 6 RTNs the sequence similarity is much more conserved and therefore have higher identity scores. The RHD of RTN17 and RTN18 share 76% sequence identity, 42% between RTN17 and RTN18, and RTN18 and RTN21.1 share 39%. Together with the phylogeny, this indicates that RTN18 is closer related to RTN17 than RTN21, which has greater sequence divergence and longer N-terminus than the other clade 6 RTNs (Fig. 2.1A).

A

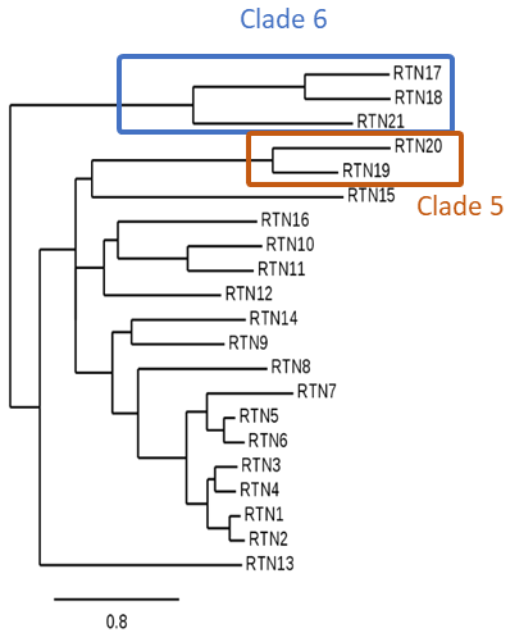

B

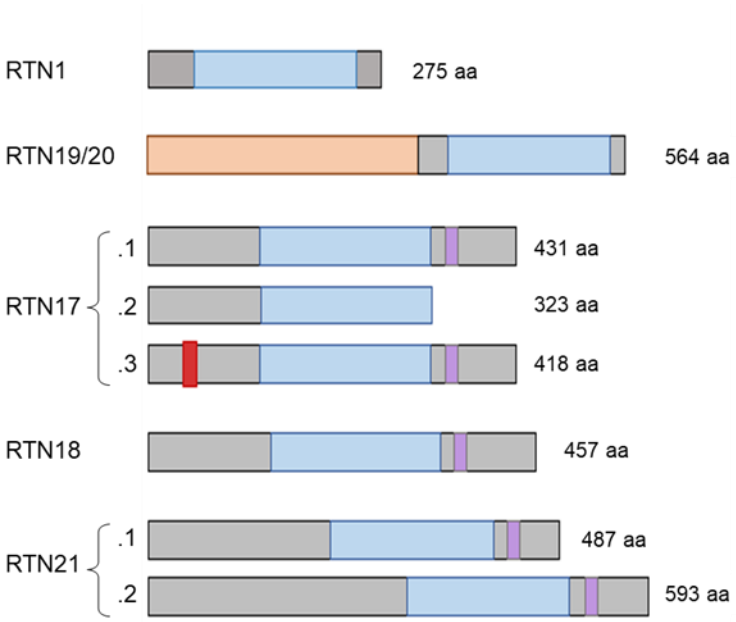

C

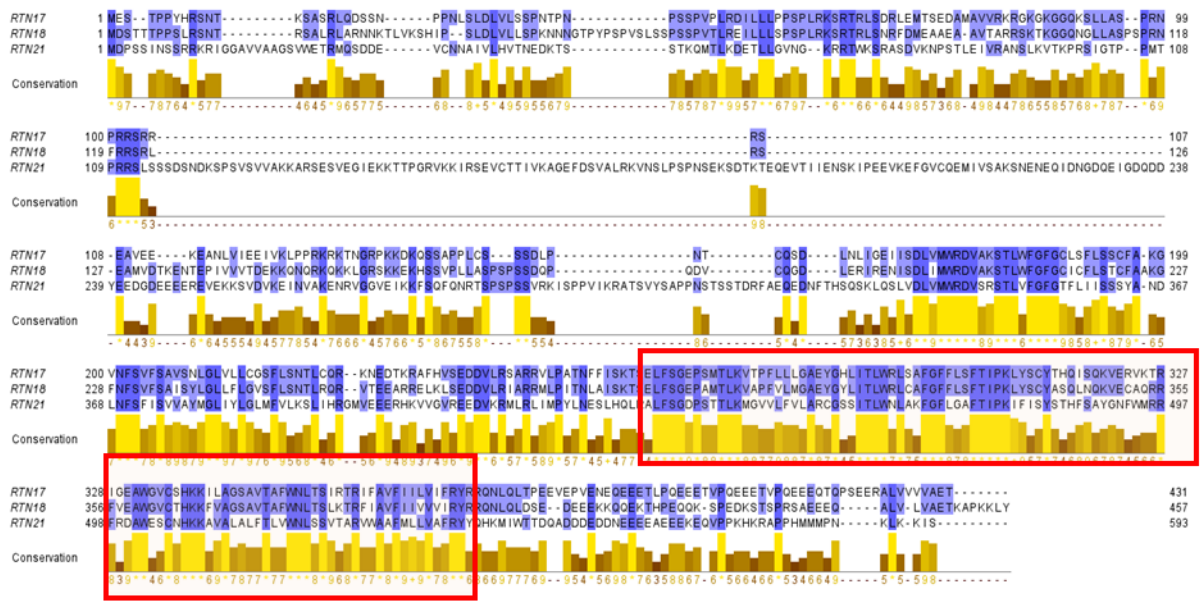

D

Full Structure

Percentage Identity Matrix (%)

X	RTN17.1	RTN18	RTN21.1
RTN17.1	100	62	62
RTN18	62	100	27
RTN21.1	32	27	100

RHD Only

Percentage Identity Matrix (%)

X	RTN17	RTN18	RTN21
RTN17	100	76	42
RTN18	76	100	39
RTN21	42	39	100

Figure 2.1 – Bioinformatic summary of Arabidopsis RTNs

A. Phylogeny of Arabidopsis RTN's. Clade 6 highlighted in blue, and clade 5 highlighted in orange. **B**. Schematic diagram of Clade 6 reticulons compared to Clade 1. Grey boxes indicate terminal extensions, blue is the reticulon homology domain (RHD), purple the putative TMD in clade 6 C termini, orange the 3βHSD homology domain. The red box identifies the deleted segment in RTN17.3. **C**. Multiple sequence alignment of clade 6 RTN's. Blue highlights indicate conserved residues, light blue low conservation, dark blue high conservation, and yellow bars represent conservation score. **D.** Percentage identity matrices of clade 6 RTNs compared against each other, as either the full proteins or just the RHD sequences.

2.2.ii – Gene transcription analysis

Data available from the Arabidopsis EFP browser (Schmid et al., 2005; Winter et al., 2007; Waese et al., 2017) was used to identify potential gene transcription levels of clade 6 *RTNs* across various tissues. RTN17 is expressed at low levels throughout Arabidopsis tissues (<4 absolute value (AV), as defined by Winter et al., 2007) with slight enrichment in the bud at 15 AV. RTN18 was minimally transcribed in all chosen tissues, at no greater than 5 AV. RTN21 was shown to be expressed at low levels throughout the assessed tissues (<4 AV), with enrichment in mature siliques and 10-day old root and shoot, at 17 AV, 12 AV and 10 AV respectively (Fig 2.2A). These contrast greatly to the highest transcribed RTN in Arabidopsis, RTN13, which scores 250 AV in silique (Winter et al., 2007).

To confirm this, qualitative analysis of the cDNA levels via reverse transcriptase polymerase chain reaction (RT-PCR) was assessed and compared intensity of labelled bands with an actin control. To distinguish between splice variants, a different reverse primer was used between RNT17.1 and RTN17.2, and a different forward primer for RTN21.2 and RNT21.1 during cDNA synthesis. Following the RT-PCR, isolated bands were purified and sequenced to confirm the transcripts where correct. Sequencing was also necessary to distinguish between RTN17.1 and RTN17.3 which have identical sequences except a 69 base pair, inter-sequence deletion meaning they could not be separated by using different primers. The qualitative assessment compared to actin showed relatively high signal intensity ratios for RTN21.2 in whole siliques as well as flowers and siliques, and lower intensity bands in other tissues. RTN21.1 was also observed at lower levels with a similar distribution. RTN17.1 had a low signal intensity ratio across all tissues compared to actin, with RTN17.2 had a slight enrichment in 35-day old leaves (Fig 2.2C). These results do not align perfectly with the data from the EFP browser which may come down to the specific tissue isolated for each analysis. Overall clade 6 reticulons seem to be broadly expressed at very low levels compared to other proteins and RTNs such as RTN13, with some tissue specificity for RTN17 in mature siliques and flowers based on cDNA, and RTN21 appears to be

higher expressed than RTN17. Clade 6 RTNs have a distinct expression pattern compared to that observed in Clade 5 RTNs which are specifically enriched roots where they are implicated in bulk sterol regulation (Kriechbaumer et al., 2018b) (Fig 2.2B). RTN18 as well as having low transcription levels as indicated by the EFP browser, could not be detected using RT-PCR across any of the assessed tissue.

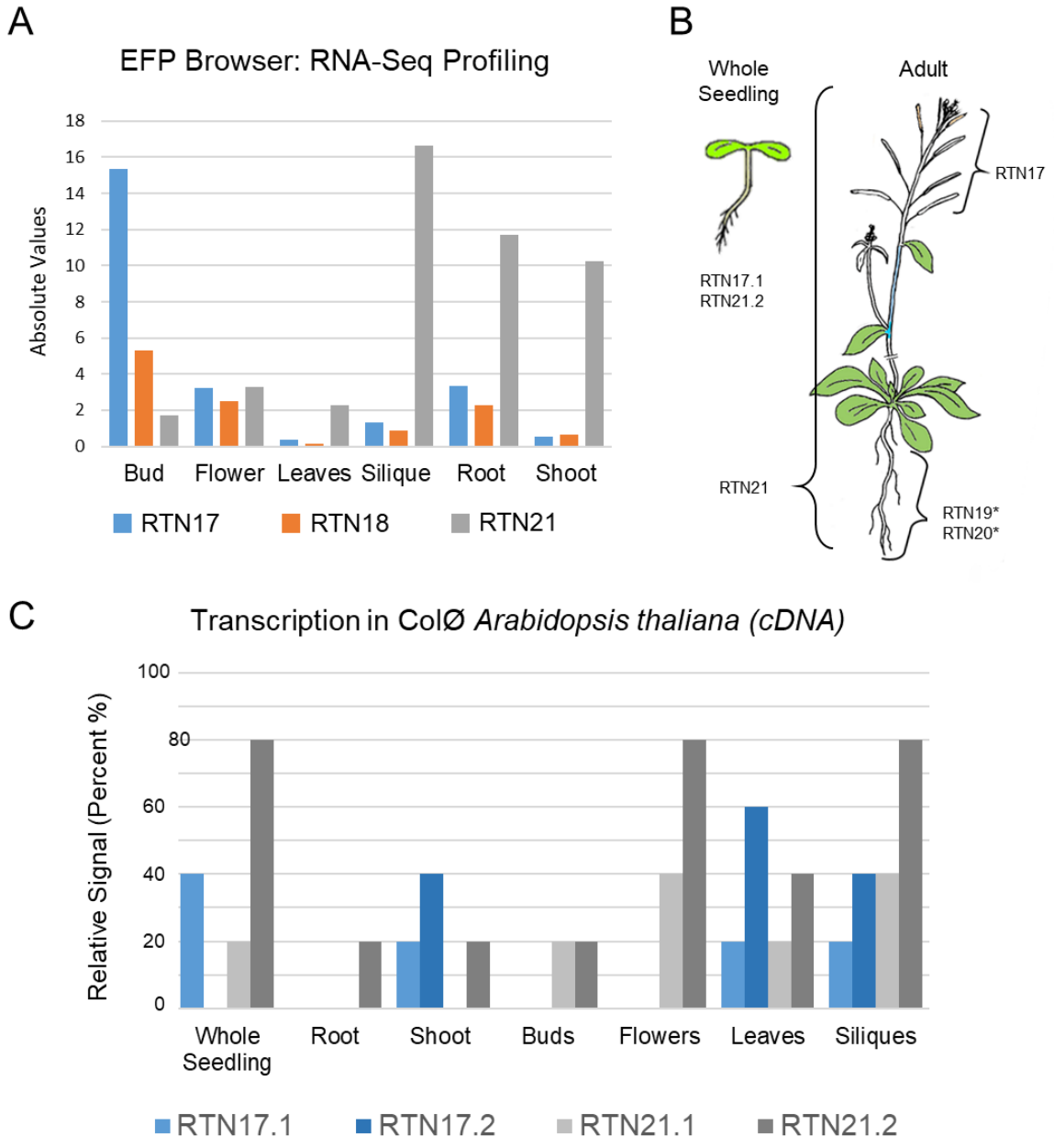

Figure 2.2 – Assessment of clade 6 RTN expression

A. EFP browser data (Winter et al., 2007) of transcription levels from RNA-Seq data (absolute value). Bud, flower, leave, siliques all from adult (35 day+) tissue, root and shoot from 10-day old seedling. **B**. Schematic diagram of regions of expression enrichment. Figure derived from EFP browser output. *Clade 5 transcription based on Kriechbaumer at al. (2018). **C**. Transcription levels from RT-PCR data, qualitative signal ratio compared to actin control. Bud, flower, leaves, siliques from adult tissue, whole seedling, root and shoot from 10-day old.

2.2.iii – Protein structure overview

Exploring the protein structure of the clade 6 RTNs in more detail reveals only a few discreet motifs within the sequence. Protein BLAST analysis reveals no specific protein homology outside of other RTNs, nor functional domains. SMART (Letunic et al., 2020) and Uniprot databases suggest the RHD resides between residues 168 and 324, with two hydrophobic regions of 42 and 39 aa long within, as well as a further TMD within the C-terminal extension (Fig 2.3A). Other features include areas of low complexity, such as 380aa-410aa which contain a high proportion of glutamine residues predicted to potentially to fold as a coiled-coil (Fig 2.3A; Sapay et al., 2006). The main feature of interest is the high degree of intrinsic disorder throughout the terminal extensions, as indicated by IUPRED (Mészáros et al., 2018; Erdos & Dosztányi, 2020) and DISOPRED (Ward et al., 2004) tools.

With the use of IUPRED, each residue in the sequence is scored between 0-1 indicating probability of being part of an intrinsically disordered region (IDR). ANCHOR2, an extension of IUPRED, is used to to determining whether a residue is both disordered and within a sequence that undergoes context-dependent binding, again scored between 0 and 1. Context-dependent binding is whereby a sequence forms an interaction based on the presence of other interacting partners or factors in the environment surrounding the IDR, that induce a conformational change(Mészáros et al., 2018). A score of 0.5 indicates the residues have a 50% likelihood of being part of an IDR or binding region. The first 150 amino acids of RTN17.1 are above the threshold for being considered intrinsically disordered, as were the last 60. Regions such as the RHD have a rigid tertiary structure scored low indicating they are not disordered (Fig 2.3B). Features such as the cytosolic facing loop can also be identified within the RHD, as they reach a score of 0.3 due to their less hydrophobic nature compared to the TMDs. The Anchor2 plot shows that the majority of the disordered region also scores highly for potentially undergoing conformation changes and subsequent binding when introduced to a binding partner. These context-dependent

changes are implicated in protein-protein and protein-lipid interactions (Mészáros et al., 2018). Similar to RTN17.1, both RTN18 and RTN21.2 share similar patterns of disorder distribution, with the termini having high scores for both intrinsic disorder and context-dependent binding (Fig 2.3D,F). Other features such as the predicted coiled-coil domain and polyglutamine region are absent from RTN18 and RTN21 (Fig 2.3C,E).

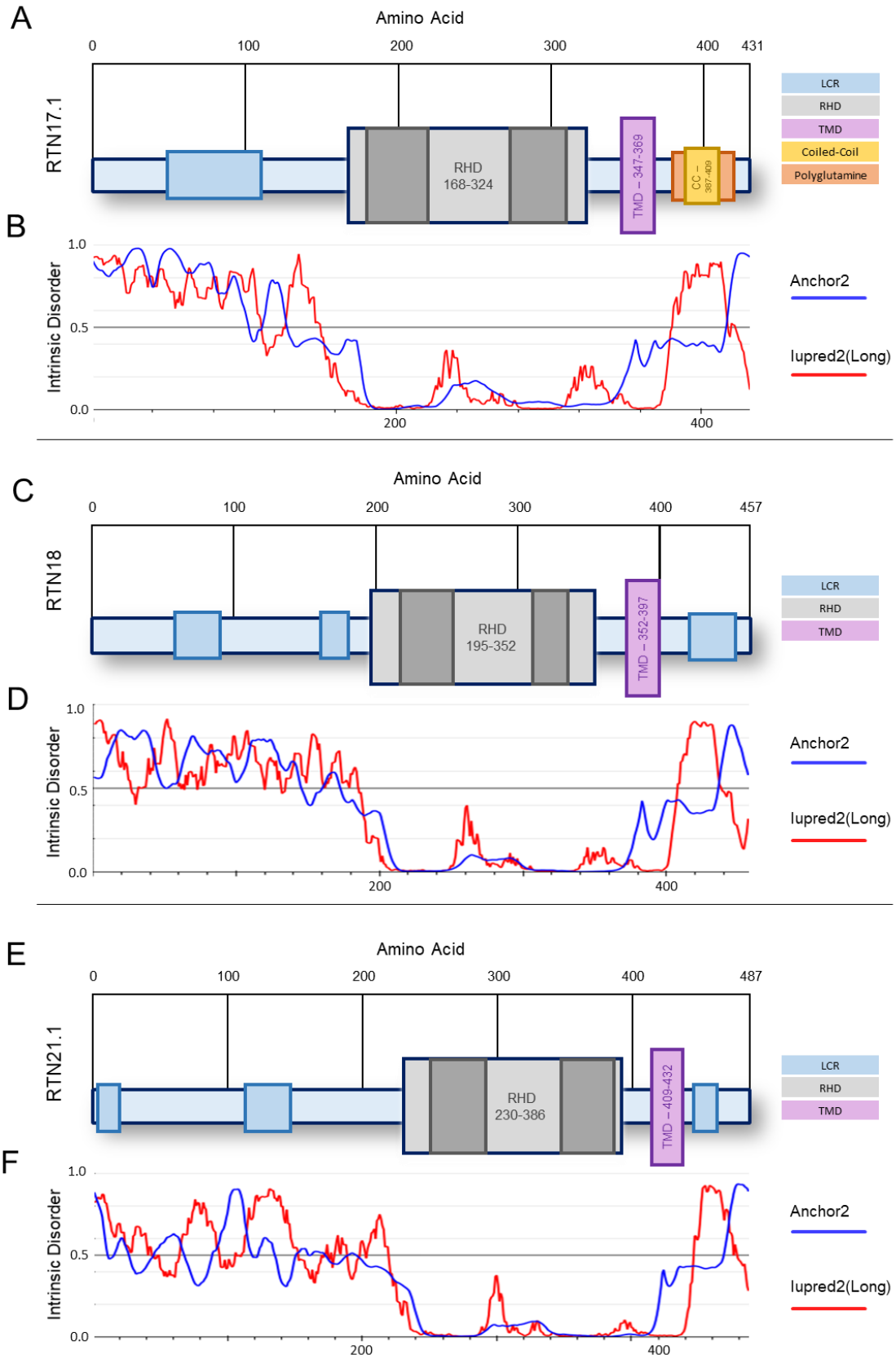
A
Amino Acid
0
100
200
300
400
431
RTN17.1
RHD
168-324
TMD – 347-369
CC – 367-409
LCR
RHD
TMD
Coiled-Coil
Polyglutamine
B
Intrinsic Disorder
1.0
0.5
0.0
200
400
Anchor2
Iupred2(Long)
C
Amino Acid
0
100
200
300
400
457
RTN18
RHD
195-352
TMD – 352-397
LCR
RHD
TMD
D
Intrinsic Disorder
1.0
0.5
0.0
200
400
Anchor2
Iupred2(Long)
E
Amino Acid
0
100
200
300
400
487
RTN21.1
RHD
230-386
TMD – 409-432
LCR
RHD
TMD
F
Intrinsic Disorder
1.0
0.5
0.0
200
400
Anchor2
Iupred2(Long)

Figure 2.3 – Clade 6 RTN structure and disorder profile

Structural overview of **A)** RTN17.1, **C**) RTN18, **E**) RTN21.1. Sequence to scale with boxes representing structural features. Light blue box = Low complexity region, dark grey = hydrophobic regions, grey = RHD, purple = putative extra TMD, yellow = coiled-coil, orange = polyglutamine region. Intrinsic disorder plot of **B)** RTN17.1, **D**) RTN18, **F**) RTN21.1. Iupred2 Red line indicating degree of disorder, and Anchor 2 blue line indicates potential binding regions. Plot from Iupred2 (Mészáros et al., 2018; Erdos & Dosztányi, 2020).

2.2.iv – Topology

Of the previously studied clade 1-5 reticulons, namely RTN1-4 and RTN13, each feature 4 TMDs within the RHD, with both termini facing the cytosol as indicated by roGFP assays (Sparkes et al., 2010) (Fig 2.4A). This structure and "W" shaped topology is integral to its localisation and function (Tolley et al., 2010). TOPCONS, a transmembrane prediction software based on consensus of other algorithms (Tsirigos et al., 2015), successfully predicts the same topology for RTN1 that was experimentally confirmed (Fig 2.4A)(Sparkes et al., 2010). Assessing the amino acid sequence for the clade 6 RTNs via multiple transmembrane domain prediction databases reveals that the c-terminal extension of clade 6 RTNs is predicted to contain an a TMD outside of the RHD. This in turn produces 2 possible topologies. Clade 6 RTNs could either contain a 5 TMD topology with a luminal facing c-terminal extension (Fig 2.4B), or as a 4 TMD topology with both termini in the cytosol (Fig 2.4B).

TOPCONS, which is a consensus of multiple databases predicts the 4 TMD topology to be most likely, which means the RHD does not assume a regular "W" shape as Clade 1-4 RTNs, with the last 2 TMDs being further apart as opposed to being within close succession. Prediction software also predicts that some other Clade 1-5 RTNs are predicted to have 3 TMDs, such as RTN 10-14 (Nziengui et al., 2007), with the C-terminal hydrophobic region of the RHD perhaps being one elongated transmembrane domain or sitting in the membrane as a hairpin. Similarly, in regard to the mammalian RTNs, the exact topology of all isoforms have not been concretely assessed (Yang & Strittmatter, 2007), with the possibility for each hydrophobic domain to assume multiple configurations.

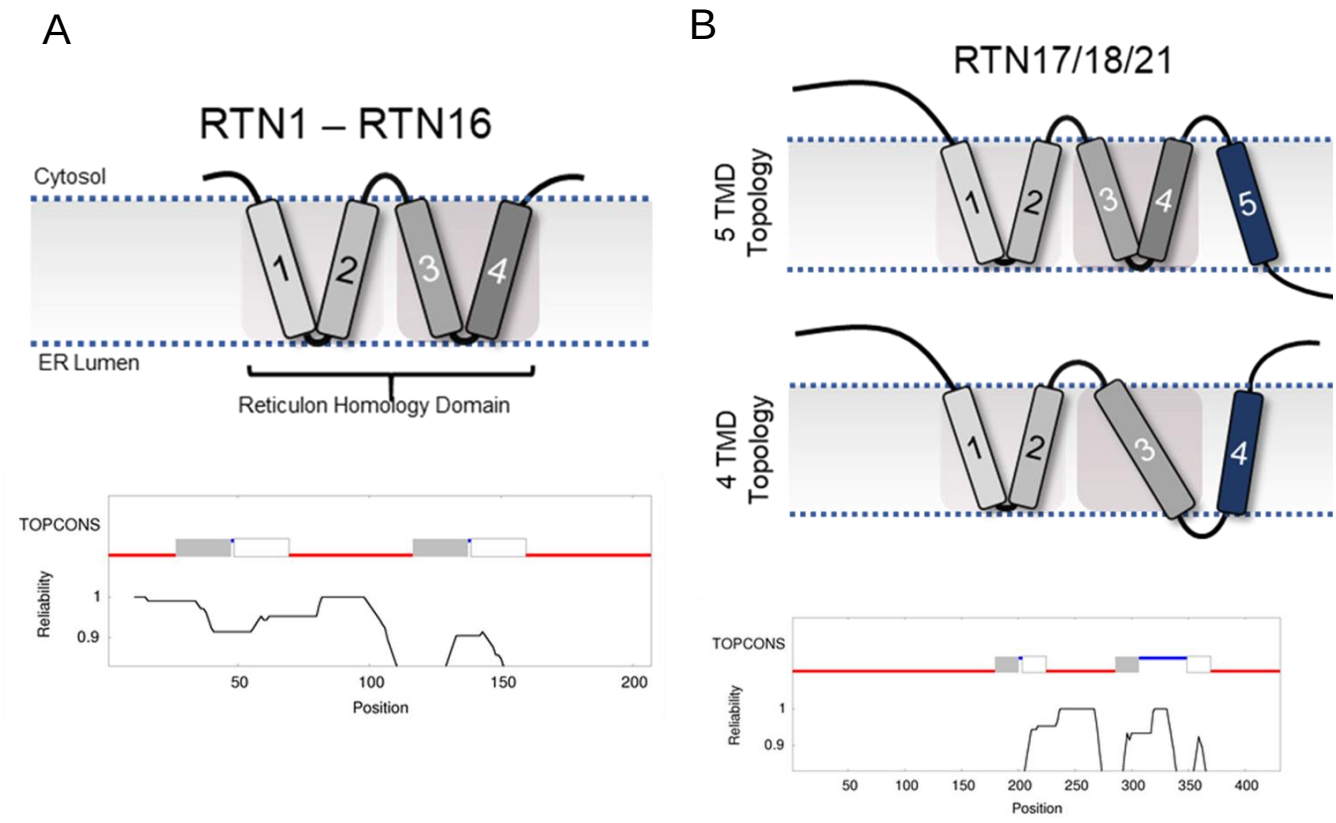

Figure 2.4 – Topology of RTNs

A. Topology of Clade 1-5 reticulons, with 4 TMDs spanning the ER membrane. **B**. Clade 6 RTN potential topologies (5TMD vs 4TMD) depending on number of TMDs. TOPCONS prediction show 4 TMD topology.

2.3 – Discussion

2.3.i - Clade 6 RTNs are structurally distinct

Besides this assessment of the proteins, information about these proteins is extremely sparse. Our analysis reveals that the clade 6 RTNs are comprised of an RHD with extended N- and C-termini (Fig 2.1B). The C-terminal extension is predicted to contain a TMD outside of the RHD, which produces 2 possible topologies (Fig 2.4B). Previously, the general length of the proteins as well as the number of transmembrane domains was described. For clade 6 RTNs, RTN17.1, RTN18 and RTN21.1 were predicted to have 4 TMDs within the RHD, and a putative 5 TMD in the C-terminus, according to a consensus of multiple bioinformatics databases (Nziengui et al., 2007). These results align with our analysis, and subsequently it was discovered that these terminal extensions are classified as IDRs (Fig 2.3). Aside from this, the only other prior studies including details of clade 6 RTNs was from analysis of the APH presence and distribution within the 21 Arabidopsis RTNs. In this study, biophysical assessment of putative APH peptides confirmed that clade 5-6 RTNs do not contain a C-terminal APH, unlike those involved in the curvature induction such as RTN13 (Brooks et al., 2021).

The first step to potentially understand the function of these proteins is to utilise the wide variety of bioinformatic tools and databases for *in silico* analysis of both nucleotide and amino acid sequences. RTN17, 18 and 21 reside in clade 6 of the Arabidopsis RTN family of proteins (Brooks et al., 2021). Not only phylogenetically distinct, but the generic structure of this clade also differs to clade 1-5 RTNs, with the presence of elongated termini and a 3rd hydrophobic region outside of the RHD. Although the 3 full length proteins share a common structural outline, there is relatively low sequence homology within the Clade, especially between RTN21 and the others. Multiple sequence alignments reveal that within the N-terminal extension of RTN21.2 there is large sequence between 110aa-240aa with no homology to RTN17.1 and RTN18 (Fig 2.1C).

Conversely the RHD across all three are much closer related with larger proportions of conserved residues, consistent with all RTNs across Eukarya, which have largely divergent sequences outside of the conserved RHD (Yang & Strittmatter, 2007). Typically, longer disordered residues are less evolutionarily conserved (Chen et al., 2006), and protein BLAST does not show sequence homology for the terminal extensions outside of clade 6. This contrasts to clade 5 RTNs which simply contain a domain homologous to 3βHSD, which may have fused to the RHD domain throughout evolution as a means of ER targeting (Kriechbaumer et al., 2018b). Phylogenetic analysis of eukaryotic RTNs across multiple branches of eukaryotic organisms found that the N-terminal residues were hypervariable, and the RHD highly conserved. RTNs with extended amino termini appear to me more common, and shorter RTNs as found in Arabidopsis usually arise from splice variation from longer genes (Oertle et al., 2003). It is interesting to consider whether clade 6 are evolutionary predecessors to the other clades of RTN which lost these variable extensions, or rather they are descendants after receiving the extensions through various recombination and other genetic events.

Interrogating the protein structure in more detail reveals that unlike the clade 5 RTNs (Kriechbaumer et al., 2018b), clade 6 RTNs terminal extensions are not homologous for other functional domains or proteins. The extensions for RTN17.1 are predicted to be disordered according to IUPRED (Mészáros et al., 2018) and DISOPRED (Ward et al., 2004) databases. Intrinsically disordered proteins (IDPs) are classified as proteins comprised with greater than 50% of the total residues scoring high for intrinsic disorder, and IDRs are regions of more than 30 aa that do not establish a rigid tertiary structure in their native state (Ward et al., 2004). Initially, these regions and proteins were once thought to be unimportant with no function, until later found to be both present extensively throughout the genome and relevant to a host of different functions (Wright & Dyson, 1999). IDP/IDRs are identified via long stretches of charged and polar amino acids, with glutamic acid, proline and glutamine scoring highest of the disorder promoting amino acids (Radivojac et al., 2007). Disorder is a feature in 33% of eukaryotic proteins, and can provide certain characteristics to a full-length protein, and are therefore

implicated in multiple functions (Ward et al., 2004). The major uses of IDRs are to act as a flexible linker between globular regions that may aid in positioning of each region, involvement in signalling, mediating protein-protein and protein-lipid interactions, and subsequently are involved in the formation of multi-protein complexes (Dyson & Wright, 2005; Dunker et al., 2005; Xie et al., 2007).

The Arabidopsis genome contains 29.5% IDPs, with a higher proportion of proteins with at least one IDR than the Human genome. Although found in almost all categories of protein function, plants have a higher proportion of IDP/IDRs in hormonal and non-hormonal signalling and PTM regulation proteins. It is suggested that the rapid evolution capabilities of IDPs compared to structural proteins is capable of meeting the need for plants to have phenotypic plasticity via signalling networks, as sessile creatures in changing environments they must be able to adapt to stressors differently to mobile species (Pietrosemoli et al., 2013). The disorder profile is similar for all three full length proteins of clade 6 RTNs (Fig 2.3), with the terminal extensions being highly disordered. Understanding which role, the IDRs have within the clade 6 RTNs will require further investigation of the protein in vivo, and it is likely that any protein-protein interactions that are revealed are mediated via the context dependent binding of the IDRs. Furthermore, interactions with lipids and therefore other biological membranes or the ER may be facilitated by the presence of these IDR domains.

2.3.ii - Clade 6 RTNs are expressed at low levels in Arabidopsis tissues

The mRNA transcription data of these from the EFP browser (Winter et al., 2007) indicates that clade 6 RTNs in general are expressed at low levels throughout Arabidopsis tissues. RTN21 appears to have a slight enrichment in adult silique tissue, and in seedling root and shoot, whilst RTN17 an enrichment in buds (Fig 2.2A). mRNA was isolated and transcribed to cDNA to compare

gene transcription levels to the database. Here transcription is similarly sparse when semi-qualitatively assessing signal ratios of cDNA compared to an actin control. RTN21.2 appears to be the higher expressed of the two potential transcripts, with some enrichment in seedling and siliques as seen with the mRNA data. RTN17.1 and RTN17.2 were both found at low levels throughout, however RTN17.3 could not be currently identified due to the small difference between the full-length protein (Fig 2.2C). RTN18 transcript was not identified, indicating either a lack of transcription or at levels too low to be detected. Arabidopsis RTNs from other clades have not been assessed in terms of their transcription levels, aside from RTN13 being identified as the highest expressed and specifically in the seeds (Tolley et al., 2008), and clade 5 RTNs being root specific (Kriechbaumer et al., 2018b). Due to the large number of individual genes, and the apparent distinction between the structures of clade 1-4 and clade 5-6 RNTs, it would be interesting to identify what developmental or cell specificity exists across the number of RTNs, and whether those like RTN18 which are expressed at extremely low levels in the assessed tissues are functionally relevant, or simply arise through duplication events and became redundant.

2.3.iii - Topology of Clade 6 RTNs deviates from the rest of the Arabidopsis family

The topology of RTN1-4, and RTN13 have been experimentally resolved via FRET-FLIM, protease protection and BiFC assays (Sparkes et al., 2010). These revealed they all contained a "W" shaped topology, with 2 pairs of TMDs, leaving a cytosolic facing loop and cytosolic facing termini (Fig 2.4A) (Sparkes et al., 2010). This agrees with the consensus prediction shown with TOPCONS, although some individual programs suggest the possibility of the second hydrophobic region of the RHD only consisting of one TMDs, indicating some discrepancy in the predictions (Tsirigos et al., 2015). There are two likely conformations for the clade 6 reticulons to undergo. If the consensus prediction is correct, the second hydrophobic region is likely to form a single TMD. Following this, the extra TMD in the C-terminal extension will result in 4 TMD topology with both

termini facing the cytosol, one cytosolic facing loop and one luminal loop. However, as some programs predict, and considering the 4 TMD nature of the other clade of RTNs, it may instead exist as a 5 TMD topology with opposing termini (Fig 2.4B).

The topology of RTNs across Eukarya has been tricky to pinpoint, with the exact topology of human RHDs still being experimentally unconfirmed, and debate between whether the hydrophobic regions consist of hairpin TMDs, or single spanning or a combination of the two (Yang & Strittmatter, 2007). The most concrete evidence for the exact nature of mammalian RTN topology comes from a study utilising protease protection experiments, in which human RTN3 has been shown to consist of 2 hairpin loop TMDs with cytosolic facing termini via (He et al., 2007), consistent with the Arabidopsis RTN topology (Sparkes et al., 2009b). This suggests that the RHDs across eukaryotic RTNs have a preference to assume the "W" shaped topology. It will be important to confirm the current consensus prediction with experimental evidence, as this will surely impact the nature of the terminal extensions and their functions depending on which compartment, whether cytosol, or luminal they localise to.

2.3.iv - Conclusion

The utilisation of multiple bioinformatic tools aided in gathering available information in regard to the structure of clade 6 RTNs. This reveals that the three full length-proteins and their splice variants share a generic structure of an RHD with extended n- and c-termini which are regions of high intrinsic disorder. The c-terminal extensions are all predicted to have a TMD, which may result in a distinct topology compared to that of the other Arabidopsis RTN. Aside from this, the proteins do not contain any particular sequence homology to functional domains or motifs. Furthermore, the transcription levels from current databases have been assessed, and compared with our RT-PCR data, and found that all of the genes are expressed at low-levels, with some very slight tissue specificity as discussed earlier. The structural differences as well as the functional

nature of IDRs already suggest that the clade 6 RTNs may be functionally distinct. Later *in vivo* experimentation will consider whether these features will be of particular importance when identifying potential interacting partners, as well as the localisation and dynamics of the proteins in live cell imaging experiments.

Chapter 3 – Subcellular localisation of clade 6 RTNs

3.1 – Introduction

3.1.i – RHDs of RTNs allows ER localisation

As reticulons across Eukarya localise exclusively to the ER (Nziengui et al, 2007; Voeltz et al.,2006), it is expected that clade 6 RTNs similarly localise to the ER. 18 of the 21 Arabidopsis RTNs contain a dilysine (KKXX) motif, which from other proteins and studies of targeting signals, is thought to act as an ER retention signal (Nilsson et al., 1989), hence required for RTNs ER localisation. However, this motif has been experimentally shown for RTN13 to not be required for ER localisation (Sparkes et al., 2010). Similarly, in human RTN1-A, each hydrophobic segment of the RHD is sufficient alone to target a GFP marker to the ER (Iwahashi et al., 2007). Shortening of the hydrophobic regions can result in Golgi body localisation, and complete removal of the TMDs causes cytosolic localisation, due to lack of hydrophobic domain to allow membrane anchoring (Iwahashi et al., 2007). This suggests that the nature of the TMDs themselves is responsible for localisation in the majority of RTNs across phyla, and the major influence on ER localisation is aspects such as length, hydrophobicity, and flanking charge of the TMDs, which are well documented as determinants in protein localisation (Singh et al., 2016; Manu et al., 2018; Cosson et al., 2013). Therefore, the RHD being the primary conserved structure within RTNs across divergent organisms has allowed the proteins to remain localised to the ER without necessitating specific targeting signals.

Arabidopsis RTN proteins have been experimentally shown to localise to the ER, mainly from experiments with clade 1 proteins such as RTN1 – RTN4 and RTN13 (Nziengui et al., 2007;

Sparkes et al 2010). These studies showed clade 1 RTNs localised exclusively at areas of high membrane curvature within the ER network, namely the tubules and edges of cisternae, due to their role in generating these substructures within the ER (Sparkes et al., 2010). A marked feature of clade 1 RTN over expression is the induction of hyper-constricted tubules. This is whereby the ER lumen marker GFP-HDEL, when co-expressed, is unable to label tubules evenly and is instead squeezed into pockets throughout the network making the signals mutually exclusive from each other (Tolley et al., 2008).

This phenotype is thought to arise due to the narrowing of the ER lumen, due to the elevated levels of RTN and subsequently greater degrees of tubule curvature. Other studies have also demonstrated a localisation of RTN3, 4 and 6 at the cell plate during cytokinesis, as well as RTN3 and 6 being found in the desmotubule of PD and Hechtian strands in tobacco BY2 cells (Knox et al., 2015). This suggests even within a clade of Arabidopsis RTNs, some specific roles and localisations may be divided between the different clades and individual RTNs. RTN3 and RTN6 specifically may be involved in the formation of the desmotubule, a highly specialised form of ER that requires an extremely narrow lumen, and consequently may be involved in cell-cell communication and viral transport, as these processes are mediated via the PD in plants (Knox et al., 2015).

3.1.ii – Clade 5 RTNs localise uniquely within the ER

Clade 5 Arabidopsis RTNs, RTN19 and RTN20, are structurally distinct from the rest of the Arabidopsis RTNs. They contain an N-terminal extension of 378 or 383 aa, for RTN19 and RTN20 respectively, beyond the regular 4 TMD RHD (Nziengui et al., 2007). This N-terminal extension is homologous to an enzymatic protein 3βHSD /D1 (Rahier et al., 2006). Although localised to the ER as with clade1-4 RTNs, neither RTN19 nor RTN20 are capable of inducing hyperconstricted tubules upon over-expression. Instead, RTN19 labels the entirety of the ER network as a diffuse

signal similar to an ER marker, whereas RTN20 expression results in a punctate distribution. This distribution of RTN20 is an exclusive property of the C-terminal region, shown via the generation of a chimeric protein, in which the N-terminus and RHD of RTN19 with the C-termini of RTN20 is similarly localised to puncta. Both of these proteins have implications in the overall regulation of sterol composition in Arabidopsis roots (Kriechbaumer et al., 2018b). This makes for interesting speculation as to whether throughout the evolution of this family of proteins, the RHD was utilised to target enzymes such as 3βHSD to the ER.

3.1.iii – Aims and Objectives

In this chapter the localisation of clade 6 reticulons was explored (RTN17, 18, 21), to describe their subcellular localisation and sub-domain distribution. This shall be achieved through the use of confocal based live-cell imaging of transient and stable expression of fluorescent conjugated proteins. It is important to distinguish whether this clade of RTNs shares similar localisations with other clades, and if it is capable of inducing hyper-constriction, as this so far has been a large distinguishing feature between clade 1-4 RTNs and clade 5 RTNs (Kriechbaumer et al., 2018b). Based on the bioinformatic information available, clade 6 being uniquely structured suggests a likelihood of unique localisation, although the presence of the RHD dictates it should localise to the ER regardless of terminal extensions. This resulting localisation may offer insight into their potential function based on the sub domain localisation, distribution, or dynamics of the protein at subcellular level.

3.2 – Results

3.2.i - RTN17.1 localises to discreet puncta across the network.

Transiently expressed RTN17.1 in tobacco leaf epidermal cells under a constitutive promoter control results in localisation to discrete puncta across the ER network, with no expression detected in other cellular compartments (Fig 3.1A). These puncta vary in size, ranging from 0.2-0.4 μm, and an average of 0.33 μm in circular equivalent diameter (Supplementary figure 1), although a population may exist of smaller diameter puncta that are unaccounted for, as they may not pass the signal detection threshold, or are under the diffraction limit of light. These puncta are highly motile, with an average mean track speed of 1.08 μm s^{-1}, and no distinct trend between speed and diameter (Fig 3.1B; Supplementary movie 1A). ER dynamics have previously been calculated with speeds of up to 1.35 μm s^{-1} for bulk flow compared to ER remodelling that is described to occur at a rate of about 0.3 μm s^{-1} (Ueda et al., 2010; Pain and Kriechbaumer, 2020) suggesting that these puncta move with the ER. Consistent with transient expression, constitutively, stably expressed RTN17.1 in Arabidopsis also reveals a punctate localisation, with a similar distribution and size as in transient (Fig 3.1C). These puncta are also similarly motile and are free to move as the ER remodels over short time scales (Supplementary movie 1B). Stable expression of RTN17.1-Clover does not appear to create any visible physiological abnormalities or growth defects compared to wild type Col-0.

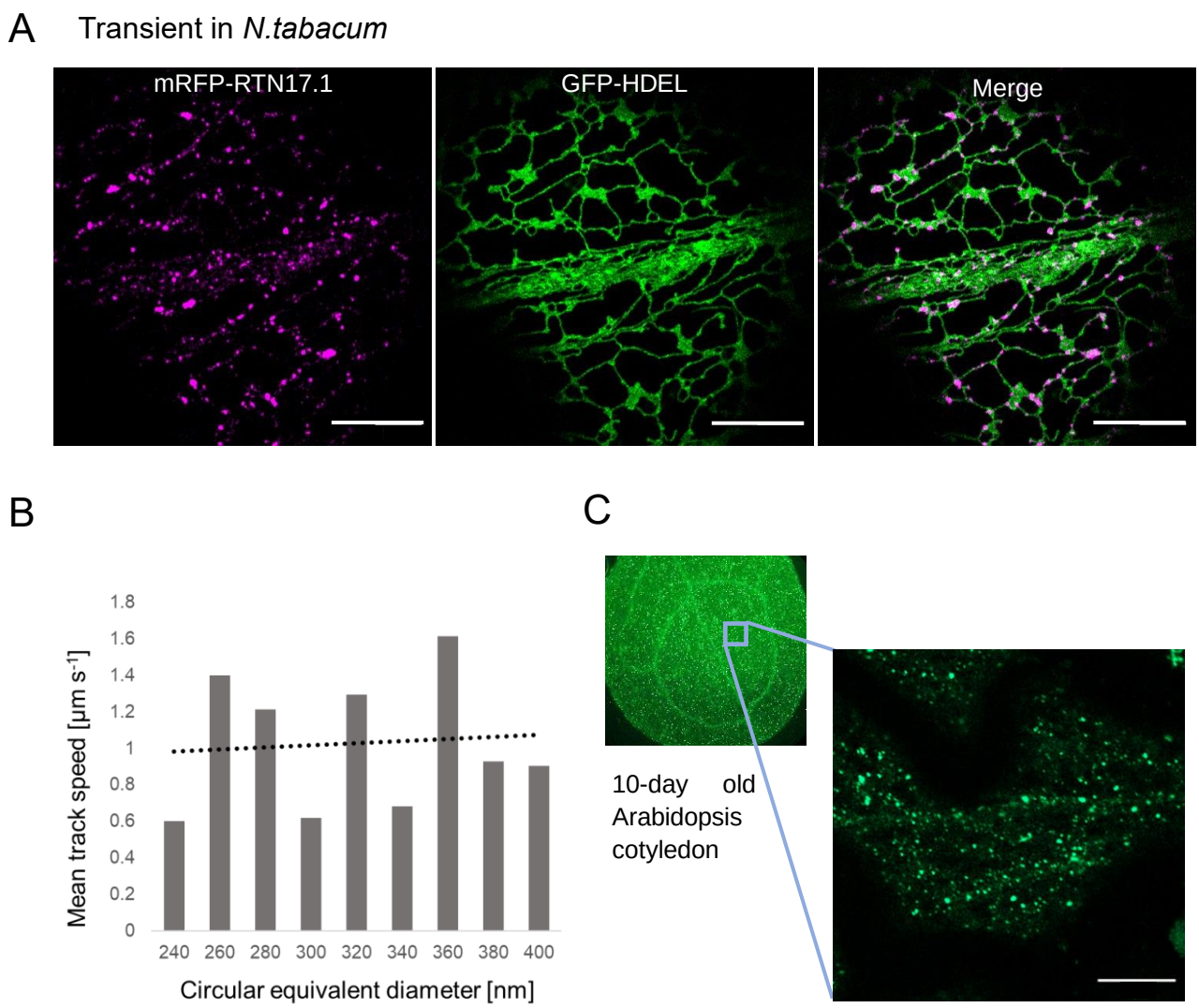

Figure 3.1 – RTN17.1 localisation

A. mRFP-RTN17.1 transient expression in tobacco leaf epidermal cells, co-expressed with the ER marker GFP-HDEL. **B**. Histogram of circular equivalent diameter of puncta [nm] vs mean track speed of puncta [µm s^{-1}]. Grouped by 20 nm data intervals. Black dotted line indicates trend. N = 4 biological repeats with, 22 experimental repeats. **C**. RTN17.1-Clover stable expression in Arabidopsis, shown here in 10 day old cotyledon cells. Scale bars = 10 µm.

3.2.ii – RTN18 overexpression localises to puncta

RTN18 cDNA could not be amplified from cDNA, and so for the generation of fluorescent conjugate proteins for live cell imaging, the coding sequence was instead synthesised. Expression of the RTN18-Clover construct results in a similarly distributed and localised protein to that of RTN17.1 (Fig 3.2A). Puncta of an average diameter of 0.31 μm are found throughout the ER (Fig 3.2A; Supplementary figure 1), with no tubular labelling as seen in a clade 1-4 RTN. Similar to RTN17.1, these puncta are reasonably motile as revealed by the temporal colour coded hyperstack (Supplementary movie 2). Here the majority of puncta can be seen moving within the short 8 second time frame. The general signal-to-noise ratio, as well as percentage of expressing cells utilising transient infiltration in tobacco was not as optimal as with the RTN17.1 constructs, and so effective tracking of puncta speed could not be carried out.

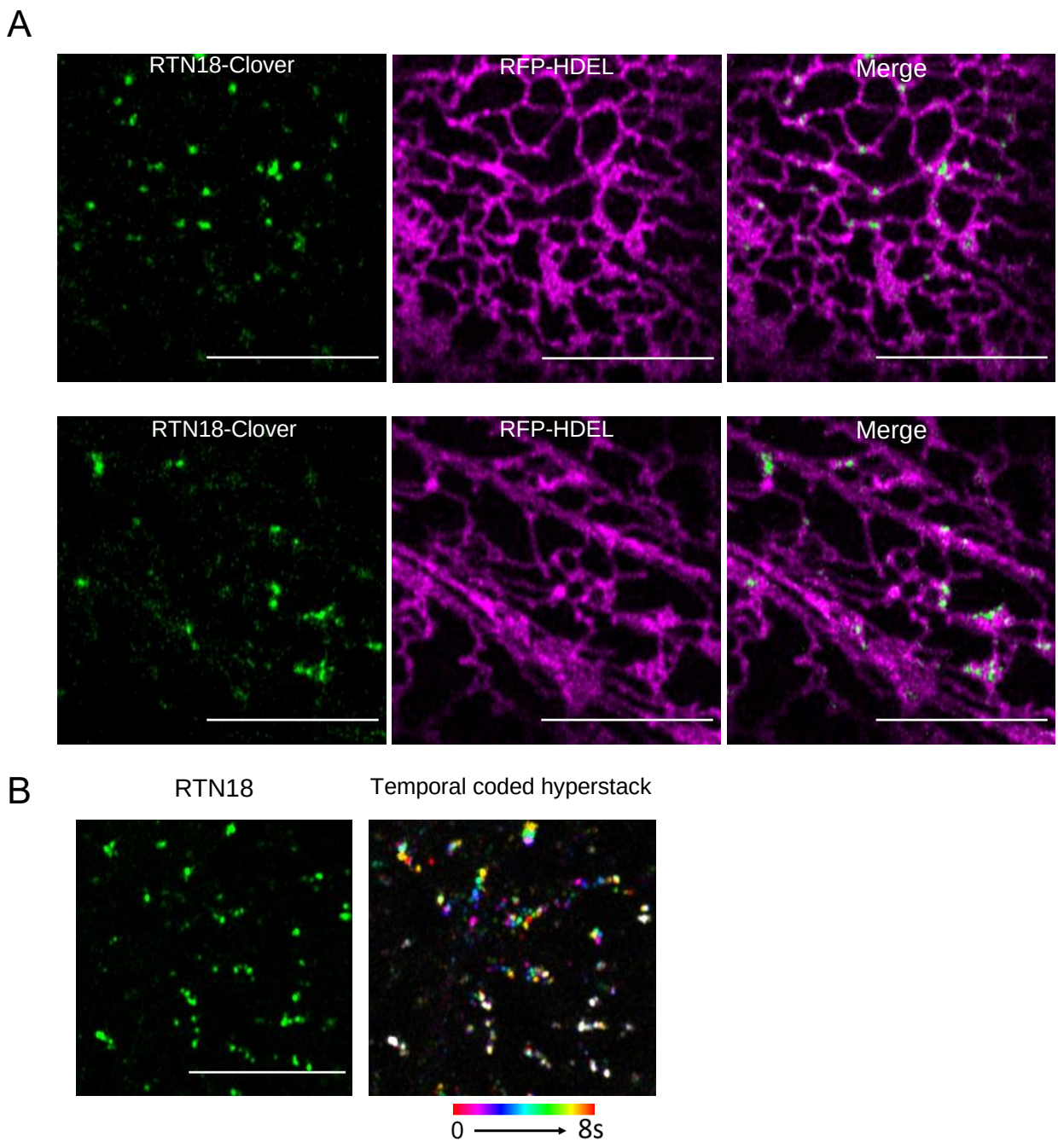

Figure 3.2 – RTN18 localisation

A. Representative images of RTN18-Clover overexpression transient in tobacco leaf epidermal cells, co-expressed with ER marker RFP-HDEL **B**. Singular expression of RTN18-Clover, with a temporal colour coded image. 8 frames at 1 s intervals, white areas represent stability. Scale bars = 10 µm.

3.2.iii - RTN21.2 overexpression shares similar punctate localisation with higher stability.

The splice variant RTN21.2 encodes the longest variant of the protein at 593 aa. This full-length protein under transient constitutive overexpression in tobacco similarly to RTN17.1 localises to discreet puncta exclusively in the ER (Fig 3.3A; Supplementary movie 3). These puncta appear to be larger, with an average diameter of 0.60 μm (Supplementary figure 1), and temporal colour coded hyperstacks demonstrate that the majority of puncta, excluding those in certain areas of the ER network such as streams, are less mobile over time scales upwards of 20 seconds (Fig 3.3B). This contrasts to the smaller and motile RTN17.1 and RTN18 puncta. Closer examination of specific puncta reveals that the puncta correspond with static areas of the network. These points within the network show are whereby the network remodels around. This can be seen from the presence of a unique arrangement of tubules at each time point within the temporal colour coded hyperstack of the HDEL channel (Fig 3.3B, Red insert).

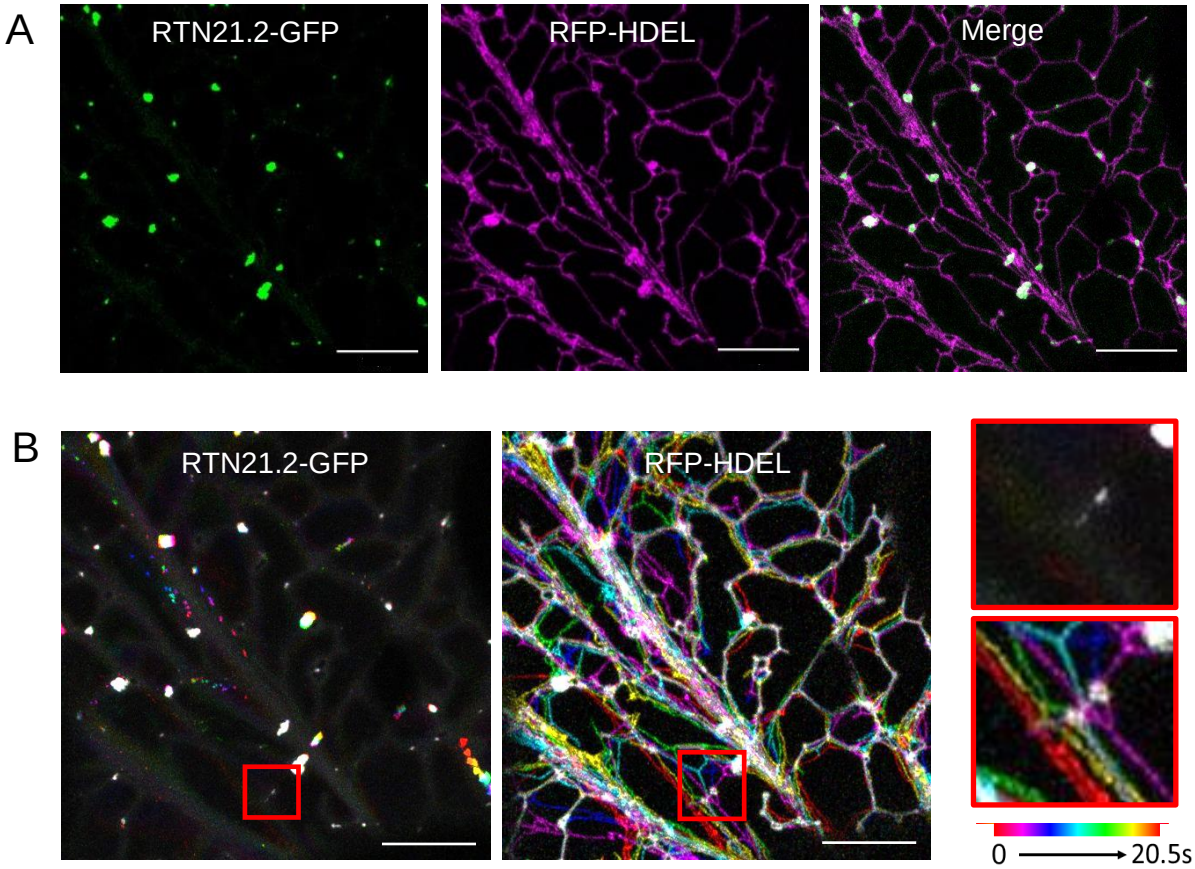

Figure 3.3 – RTN21.2 localisation

A. Representative image of RTN21.2-GFP co-expression with RFP-HDEL. **B**. Temporal colour coded hyperstacks of above image representing a 20.5 second time series, consisting of 6 Frames 3.42 s apart. Red insert showing close up on specific puncta and the network. White represents areas of overlapping signals across all images in the stack. Scale Bars = 10 µm

3.2.iv - RTN17.1 puncta localise with a preference to 3-way junctions and areas involved with fusion.

RTN17.1 puncta are localised across multiple subdomains of the ER, with the majority (55%) being associated with or within the range of less than 1 μm of stable 3-way junctions (Fig. 3.4A, F). RTN17.1 also localises to the tip of elongating tubules (4%; Fig. 3.4B, F), at the target point in which an elongating tubule forms a stable 3-way junction (5%; Fig. 3.4C, F), or mid-way along tubules (13%; Fig. 3.4E, F) where no remodelling is occurring. 25% of puncta are associated with dense clusters of polygonal regions, which are comprised of multiple small rings (Fig. 3.4D, F); these puncta are frequently involved with the remodelling and closure of these rings at these sites. Although only a relatively small proportion of the puncta can be seen at the tip or target of elongating tubules at a given time, this is due to elongating tubules only representing a small proportion of the ER. However, within the network the majority of either the elongating tip or the target points of tubules undergoing fusion events are labelled by a RTN17.1 punctum. After crossing a polygonal region, an elongating tubule can often be seen moving laterally after reaching the opposing tubule. Generally, the tubules will only form a static 3-way-junction after a short duration of scanning, and when labelled RTN17.1 is present this scanning appears to finish and commence "locking" after coming into contact with a RTN17.1 punctum (Fig. 3.4C yellow arrows). Taken together, this localisation data indicates a link between RTN17.1 and ER fusion events.

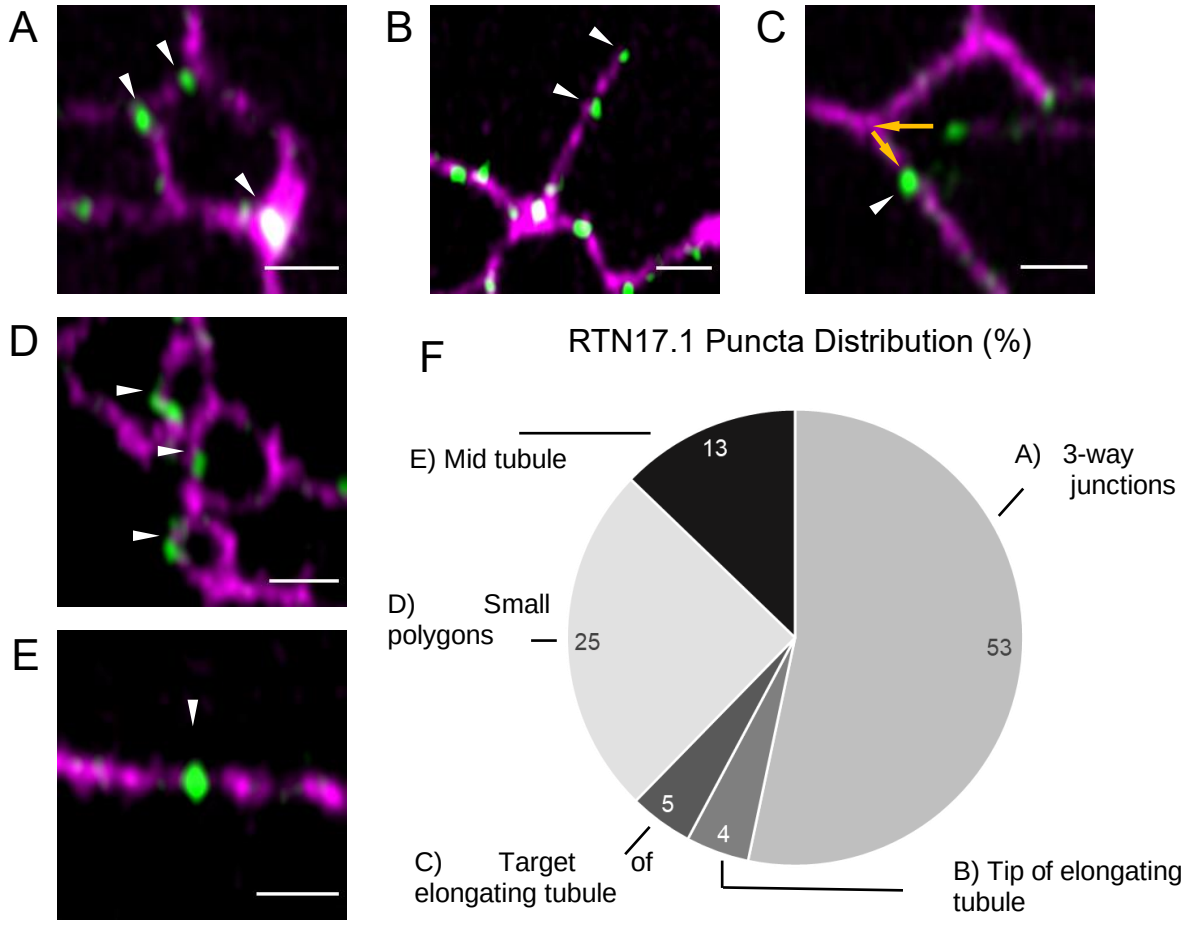

Figure 3.4 – RTN17.1 puncta distribution

A. RTN17.1 puncta localised to 3-way junctions. **B**. Puncta localised at the end of elongating tubules. **C**. Puncta localised to the tip of elongating tubule, and the target puncta in which the tubule slides towards prior to forming a stable connection. **D**. Puncta localised in denser areas with small polygonal regions. **E**. Puncta localised mid-way along tubules. White arrowheads mark puncta of relevance. Yellow arrows depict the path of tubule movement, sliding down the opposing tubule. Scale bars = 1 µm. **F**. Percentage of puncta across these localisations; n = 4 biological repeats, 365 puncta counted.

3.2.v - RTN17.1 does not induce hyperconstriction

Due to this unique localisation and distribution of RTN17.1, and a qualitative lack of hyperconstriction observed, closer inspection of the tubule profiles and comparison to clade 1 RTNs was required. For this, a subset of the AnalyzER software (Pain et al., 2019) was utilised. AnalyzER is capable of quantitatively assessing ER morphological aspects across a variety of parameters and will be utilised extensively later within the thesis for full characterisation of clade 6 RTNs (Chapter 6). Overexpression of RTN proteins from clade 1 results in hyperconstriction of the ER network (Fig. 3.5A), with the RTNs localising exclusively to regions of high membrane curvature and the lumenal marker GFP-HDEL being restricted to small pockets (Tolley et al., 2008; Tolley et al., 2010; Sparkes et al., 2010; Breeze et al., 2016). This is reflected in the trace plot of a 4 μm distance across several tubules and nodes. Here we see as the intensity of RTN1-mRFP reaches a peak, it corresponds directly with a trough in GFP-HDEL intensity as a result of the hyperconstriction (Fig 3.5A). In comparison, GFP-HDEL when colocalised with an ER membrane marker, Calnexin (CXN-RFP), have trace profiles of each marker that align, and show the typical degrees of signal fluctuation observed in a non-constricted tubule (Fig 3.5B). The trace plot of GFP-HDEL co-localised with RTN17.1-mRFP co-expression shows that RTN17.1 overexpression does not induce a hyperconstriction phenotype, with the GFP-HDEL intensity still remaining above 0.4 AU within the troughs, and not 0.1 as seen with RTN1 co-expression. Furthermore, the peaks of RTN17.1-mRFP signal are not aligned with the troughs of HDEL, however there may be some fluctuations caused by the presence of the puncta, and potential bleed through or quenching occurring between fluorophores. Of particular note is the strong peak of RTN17.1-mRFP from the puncta at the beginning of the trace is co-localised with a GFP-HDEL signal of 0.6, indicating that the puncta do not induce localised constriction (Fig 3.5C).

This observation is supported by examining certain parameters in greater detail such as the mean trough co-variance. Trough covariance is a comparison of trough intensities from each channel, with positive scores resulting from the two channels following the same trends, whereas a

negative value suggests the channel intensities follow opposing trends. As such, the RTN1-mRFP co-expression, and induced hyperconstriction results in a mean trough co-variance of -0.0097 (Fig 3.5D). For HDEL and CXN co-expression, the mean trough co-variance is 0.0091, indicating the signals correspond in their intensity profiles, as seen in the example tubule profile trace (Fig 3.5D). For RTN17.1 co-expression with GFP-HDEL, and their seemingly unrelated signal profiles from the trace, we would expect to see a co-variance near 0. The average trough co-variance was -0.0028, which is closer to a neutral signal profile than seen with the hyperconstriction but does indicate that some of the signal profiles from each channel show a degree of opposing signal profiles. However, this again may be due to puncta causing some alteration to the local tubule morphology, or potential impact on fluorophores due to the concentration at the puncta.

Examining the trough and peak widths of the different co-expressions also reinforce that RTN17.1 does not result in hyperconstriction. RTN1 co-expression results in wider troughs and peaks of the GFP-HDEL, of 0.079 μm and 0.087 μm respectively, which is consistent with larger portions of the network being squeezed into discontinuous pockets of HDEL labelled ER as a result of hyperconstriction (Fig 3.5E). This contrasts to the non-constricted trough widths of 0.052 and 0.057 μm as observed with co-expression of CXN and RTN17.1 respectively. Furthermore, the peak widths of 0.0523 μm and 0.0569 μm (Fig 3.5E), are indicative of the typical signal troughs and peak widths observed from fluctuations within the tubules. These quantitative aspects reinforce the observed qualitative observations and confirm that RTN17.1 does not induce hyperconstriction as clade 1 RTNs are capable of doing upon over-expression.

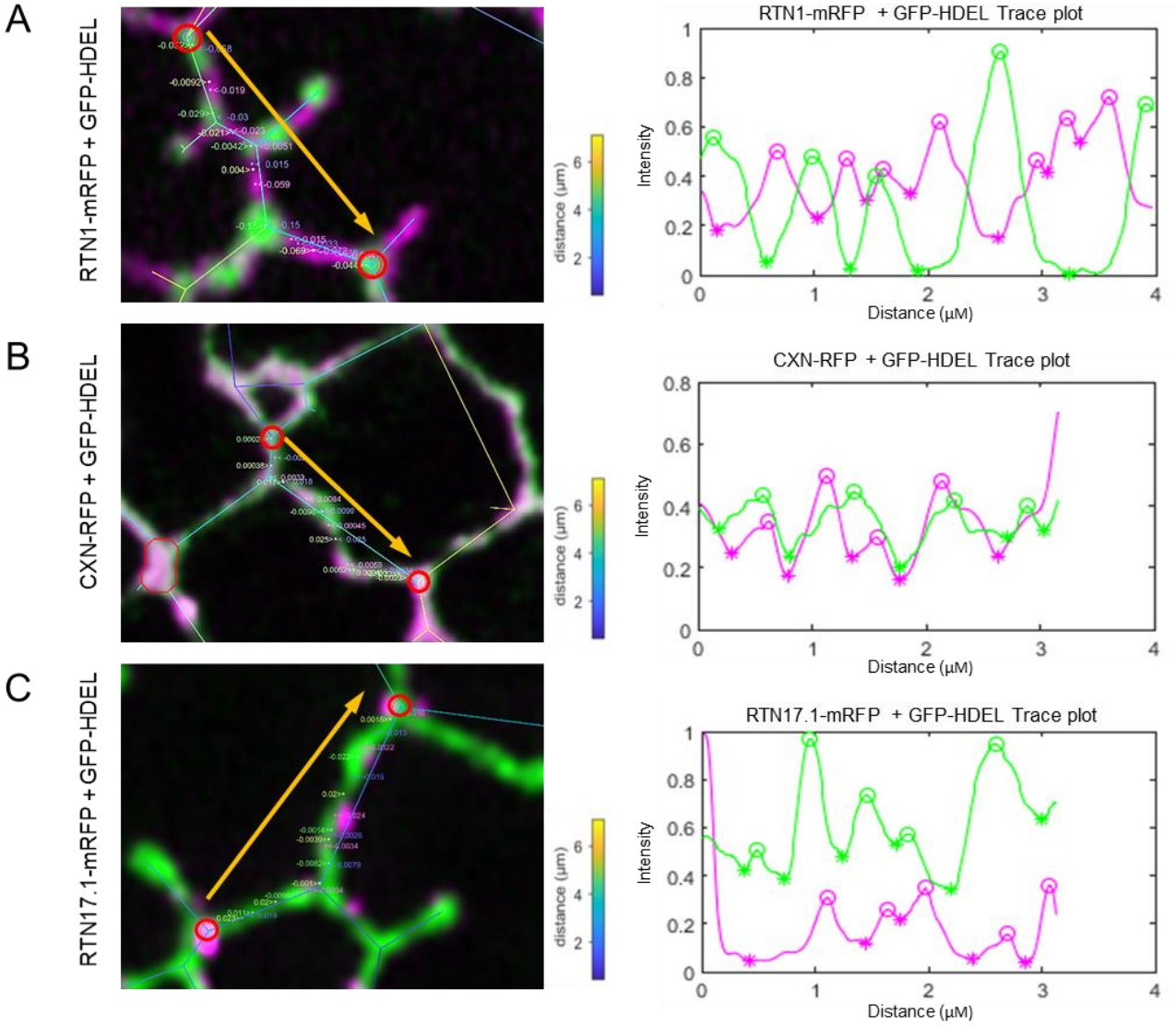
A
RTN1-mRFP + GFP-HDEL
RTN1-mRFP + GFP-HDEL Trace plot
Intensity
Distance (µM)
distance (µm)
B
CXN-RFP + GFP-HDEL
CXN-RFP + GFP-HDEL Trace plot
Intensity
Distance (µM)
distance (µm)
C
RTN17.1-mRFP + GFP-HDEL
RTN17.1-mRFP + GFP-HDEL Trace plot
Intensity
Distance (µM)
distance (µm)

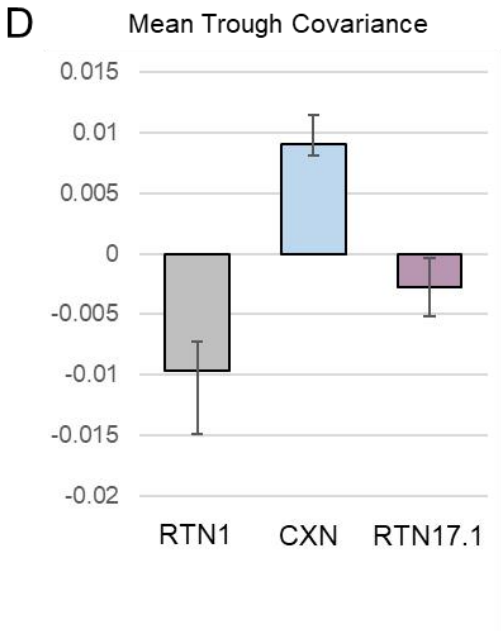
D
Mean Trough Covariance
RTN1
CXN
RTN17.1

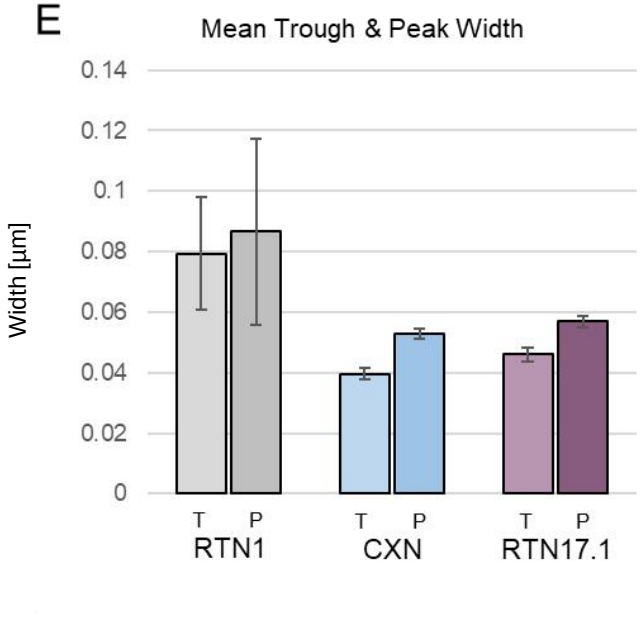
E
Mean Trough & Peak Width
Width [µm]
T P
RTN1
CXN
RTN17.1

Figure 3.5 – Hyperconstriction analysis

A. Tubule trace analysis of RTN1-mRFP co-expressed with GFP HDEL. Original merge image with tubule length skeleton overlay and trough co-variance annotations. **B**. Tubule trace analysis of CXN-RFP co-expressed with GFP HDEL. Original merge image overlayed with tubule length graphed skeleton and trough co-variance annotations. **C**. Tubule trace analysis of RTN17.1-mRFP co-expressed with GFP HDEL. Original merge image overlayed with tubule length graphed skeleton and trough co-variance annotations. Red circles = node start and finish, yellow arrow = direction of tubule trace. Magenta plot line = mRFP/RFP construct signal profile, green plot line = GFP-HDEL signal profile. Circle on plot line represents signal peak, star represents signal trough. **D**. Bar graph plot of average mean trough co-variance, error bars represent standard deviation. **E**. Bar graph of average mean trough and peak widths, error bars represent standard deviation. N=3 per treatment.

3.3 – Discussion

3.3.i – Clade 6 RTNs are ER localised proteins

As demonstrated, clades 1-4 RTNs are intrinsically capable of localising to the ER due to their topology and properties of the TMDs within the RHD (Sparkes et al, 2010; Tolley al., 2010). With the majority of the 21 Arabidopsis RTN genes containing the "W" shaped topology, they have been shown to be involved in the formation of tubules and stabilising curved edges of cisternae, and their localisation within the ER is strictly along these ER sub domains (Sparkes et al., 2010). However, despite the presence of the conserved RHD within clade 5 RTNs, they showed distinct localisations, with RTN19 labelling the entirety of the ER and as puncta for RTN20 (Kriechbaumer et al., 2018b).

Based on the closer phylogeny between clade 5 and clade 6 RTNs, as well as the presence of extended termini unique to these clades (Chapter 2), which clade 6 have a predicted extra TMD in which may affect the traditional "W" shaped topology of the RHD, it was hypothesised that clade 6 RTNs will be similarly distinct from clade 1-4 RTN localisations whilst still residing in the ER. This was confirmed from over-expression of all three clade 6 RTNs, with each of them localising as discrete puncta across the ER (Fig 3.1, 3.2, 3.3). Although robust analysis of RTN20 puncta distribution, size and speed is required, assessment of the distribution and dynamics of RTN17.1 suggest that the punctate distribution is distinct compared to that of RTN20, due to its propensity to localise areas involved with tubular fusion, which was not noted in regard to RTN20 (Kriechbaumer et al., 2018b). Specifically, RTN17 is localised adjacent or within stable 3-way junctions, as well as being located at the tips and areas in which elongating tubules form nascent 3-way junctions. This localisation may suggest some involvement in 3-way junction formation, among other proteins such as RHD3 (Chen et al., 2011). This distinct localisation paired with the differences in structures between clade 5 and clade 6 RTNs, and lack of specific homologous

domains with other proteins aside from the conserved RHD (Chapter 2) suggests that these two clades are distributed differently, to potentially serve different functions within the plant ER.

One key difference as a result of this punctate localisation is that RTN17.1 appears to be incapable of inducing hyperconstriction of ER tubules (Fig 3.5). There may be a degree of lumenal displacement as shown by the slight variations in HDEL signal along the tubule, however as RTN17.1 is not labelling the entirety of the ER, we do not see apparent pockets of HDEL (Fig 3.5) as a result of hyperconstriction typically seen with clade 1 RTN over-expression (Tolley et al., 2008). This provides a further distinction compared to clade 1 reticulons, and suggests that the terminal extensions, and potentially the presence of extra TMDs in the C-terminal extensions may alter the ability to constrict tubules beyond the normal physiological degree. As the oligomerisation capabilities of RTNs RHD are also a key aspect of RTN function in the generation of high curvature sub domains (Shibata et al., 2008; Sparkes et al., 2010), it will be important to determine whether the clade 6 RHD is similarly responsible for oligomerisation capabilities within the clade. Previous studies utilising the same methods of generating and expressing fluorescent constructs have shown fusion proteins to be fully functional despite fluorophore addition. For example, leaf curling is induced in tissues over-expressing fluorescent auxin biosynthetic YUCCA proteins (Kriechbaumer et al., 2016). This provides evidence that this technique is a robust in producing functional proteins that can be visualised by fluorescence microscopy. Some doubt may arise as there is no clear physiologically impact of over-expression of the clade 6 RTN fusion proteins that can be attributed to a functioning protein. However, considering their distinct localisation and properties compared to other RTNs expressed in a similar fashion, this may suggest that these features are not artifacts of RTN fusion proteins. Furthermore, the distinct localisation is independent of which termini of the protein is tagged, and by what fluorophore. Further assays to support their correctness may be required as more about the physiological impacts of clade 6 RTN expression are uncovered.

3.3.ii – Puncta properties

Between the three proteins of interest there are differing puncta properties and dynamics. The puncta are highly motile and vary in size and speed, but on average move at similar speeds to that of which the ER remodelling occurs at (Ueda et al., 2010; Pain and Kriechbaumer, 2020). The association with 3-way junctions, and the direct observations of puncta at free ends of tubules, as well as the target point in which elongating tubules make a new 3-way junction with, suggest an involvement with the formation of 3-way junctions. Puncta can also be seen at regions which contain a denser array of polygons with frequent ring closure events (Sparkes et al., 2009a). This may also indicate a degree of fusion occurring in these processes that sees RTN17.1 involvement. RHD3 is thought to mediate homo-typic fusion of ER tubules, and although is thought to have some enrichment at 3-way junctions, however, primarily labels the entirety of the ER (Chen et al., 2011). Priority for future experiments will be comparing the localisation of RTN17.1 and RHD3 as well as probing for a potential protein-protein interaction, based on this association with 3-way junctions. Furthermore, it will be interesting to determine, what impacts clade 6 RTNs and RHD3 have on the modulation of fusion and its impact on the ER morphology.

The presence of puncta suggests the capability of homo-oligomerisation, with average diameters ranging from 200-600nm across the 3 full-length proteins (Supplementary Figure S1). The typical range of puncta sizes observed vary greatly, from puncta smaller than the diffraction limit of Airyscan resolution acquisition (<150 nm) up to 1 μm in some cases of RTN21.2 puncta for example. RTN17.1 and RTN21.2 as well as having differing sizes of puncta from over-expression, have different mobility characteristics, with RTN17.1 freely moving within the ER, whereas RTN21.2 puncta localise to more stable regions of the ER (Fig 3.1, 3.3, supplementary movie 1 & 3). These stable junctions, as well as the larger puncta diameter coincide with the static nature of EPCSs, in which NET3Clabelled EPCSs are similarly immobile and show occupy areas of 0.25-1μm (Wang et al., 2014). Identifying interacting partners that support this suggestion will further determine whether this is indeed a specific localisation for RTN21.2. RTN18 on the other hand

has more motile puncta of a similar size to that of RTN17.1 (supplementary movie 2), and as the phylogeny suggests they are likely to have arisen from ma gene duplication event, the functional role of the protein is likely to be closer than between RTN17.1 and RTN21.2

3.3.iii - Summary and Conclusion

Within this chapter the subcellular localisation of the clade 6 RTNs and their distribution within the ER has been described and characterised for the first time. The full length-proteins, RTN17.1, RTN18 and RTN21.2 all share a punctate localisation, with RTN17.1 and RTN18 showing smaller and more motile puncta associated with 3-way junctions, compared to RTN21.2 which localises to more stable junctions that correspond with potential EPCS within the network. Going forward it will be important to characterise the protein-protein interactions of these proteins and relate them to this localisation, as well as determine which aspect of the proteins structure are responsible for this distinct localisation and divergence from clade 1-4 RTNs localisation and function.

Chapter 4 – RTN17.1 protein-protein interactions

4.1 – Introduction

4.1.i - Homotypic protein-protein interactions

Cellular proteins do not exist in isolation. Protein function is often defined by their interaction with other proteins, lipids, and small molecules (Pawson & Nash, 2000), and for example in yeast each protein is estimated to form an average of 5 protein-protein interactions (PPI) (Grigoriev, 2003). Identifying and understanding PPI and other interactions is an essential step to understanding the functionality of previously uncharacterised proteins. One key characteristic discovered in Mammalian and yeast RTNs, and Yop1/p was their ability to form oligomers. This was shown via cross-linking assays and subsequent FRAP of ER tubules that revealed that large immobile 'rafts' form within the ER tubule membranes based on homo-oligomerising capability of RTN and Yop1P (Shibata et al., 2008). Mutant isoforms of Rtn1p that had localisation defects where also shown to have higher degrees of mobility, showing that the RHD structure is integral to both ER localisation, and oligomerisation capabilities, and as a result these mutants are incapable of inducing tubules as effectively. Furthermore, the oligomerisation appears to occur in an ATP dependent manner, suggesting that the formation of these protein-protein interactions may be a dynamic process and the size and abundance of the immobile RTN/Yop1p rafts, and as such the degree of ER tubulation can change in response to other cellular events (Shibata et al., 2008).

Similarly, to yeast and mammalian homologues, Arabidopsis clade 1 reticulons have been shown to form hetero- and homo-typic interactions via yeast-two hybrid assays (Hwnag & Gelvin, 2004)

as well as FRET-FLIM (Sparkes et al., 2010), with RTNs of across clades 1-4 being capable of interacting. This interaction can occur despite truncation of the second hydrophobic region of the RHD, although this does impact the curvature-inducing capability of both RTN1 and RTN13 (Sparkes et al., 2010).

4.1.ii - RTN protein-protein interactions

Due to their relevance in human neurological disorders and being the first and most extensively studied RTNs, a large number of interactions for Human RTN1-4 have been identified. Human RTNs have been shown to interact with other ER shaping proteins such as spastin (Connell et al., 2009; Mannan et al.,2006), REEP1, and ATL-1, of which the latter are thought to form a complex mediating the formation of 3-way junctions in the ER (Park et al., 2010). Other interactions across a broad scope of ER functions include RTN1 and RTN2 with the AP-2 adaptor complex medium chain, involved in endocytosis (Iwahashi & Hamada 2003), Sec61β translocon subunit (Zhao & Jäntti, 2009), the calcium release channel RyR2 (Kaya et al., 2013). Though, the most comprehensively studied interaction is that between RTN4A (described initially as Nogo), and its receptor NogoR, which mediates inhibition of dendrite outgrowth and is thus a target of interest for therapies promoting neuronal regeneration for multiple diseases (Fournier et al., 2001). In general mammalian and yeast RTNs have a wide variety of interactions including homo-typic and those across multiple functional categories such as regulation of ER morphology, trafficking, vesicle formation and more (Yang & Strittmatter, 2007).

As well as RTNs capability of and seeming dependence on interacting with other RTNs as part of its tubule inducing function, other PPI have been identified regarding Arabidopsis RTNs. RTN3 and RTN6 are both clade 1 RTNs but with a unique enrichment within the PD compared to other RTNs (Knox et al., 2015). These proteins have been interrogated by a combination of co-immunoprecipitation (Co-IP), mass spectroscopy (MS) and FRET-FLIM to identify interacting

partners. Co-IP combined with MS identified 42 interactors for RTN3 and 57 for RTN6, of which 17 were tested via FRET-FLIM to confirm interactions and test false positives from the initial run (Kriechbaumer et al., 2015). The interacting partners are <95% distributed across the PD, ER and PM. This corresponds with their specific activity at the desmotubule, and the fact most membrane bound PM proteins are synthesised initially in the ER such as PIP3 which was identified as an interactor across all methods. Of particular significance was RTN3 and RTN6 being positive for both homo- and heterotypic interaction, as well as RTN1 and RTN5 present in the Co-IP results, confirming previous data of RTN1-4 and RTN13 and their ability to interact (Kriechbaumer et al., 2015). Other proteins potentially relevant to ER morphology that were identified as interacting partners were VAP27 and SYT1. Both proteins involved in EPCS formation and ER-cytoskeletal interaction (Wang et al., 2016) and RHD3 (Kriechbaumer et al., 2015). Another study also revealed RHD3-like 2 (RL2), the seed specific isoform of RHD3 to interact with RTN13 via Co-IP, which is preserved despite mutations in the GTP-ase domain, suggesting the interaction Is mediated by the transmembrane domains or C-terminal portion of RHD3 (Lee et al., 2012).

4.1.iii – Interactions between other ER morphogens

Other ER morphogens such as AtLNP1 and AtLNP2 have been shown to interact with RTN1 with FRET-FLIM, which likely suggests interaction with another clade 1 RTNs (Kriechbaumer et al., 2018a). More recently AtLNP1 and 2 were shown to interact with RHD3 via split-ubiquitin assays, and AtLNP1 interaction further confirmed with Co-IP (Sun et al., 2020). This interaction is proposed to be required for the ubiquitin ligase activity of AtLNP1 and AtLNP2 and its role in degrading RHD3 at 3-way junctions (Sun et al., 2020). Mammalian LNP proteins were similarly shown to function as a ubiquitin ligase directed against ATL, as well as to interact with gp78, a ubiquitin ligase part of the mammalian ERAD complex (Zhao et al., 2016). These studies suggest a LNP and RHD3 interaction across Eukarya is a conserved mechanism essential for the generation of 3-way junctions. RHD3 function is also dependent on dimerization of the C-terminal

tail of the protein in mediating homotypic tubular fusion (Sun et al., 2018), and has been shown to interact with proteins such as ARK1 mediating a link between the ER and the plus-end of microtubules promoting ER tubule extension subsequent to 3-way junction formation (Sun et al., 2020). Although not typically described as ER morphogens in the strict sense, EPCS and proteins localised at these sub-domains often have implications in certain aspects of ER morphology due to the link to the cytoskeleton. At these hubs multiple proteins localise and have confirmed protein-protein interactions with each other. Aside from the interaction between VAP27 and RTN3 and 6 (Kriechbaumer et al., 2015), VAP27 also interacts with NET3C, which in turn interacts with the Actin cyto-skeleton and are involved in the regulation of EPCS formation and activity (Wang et al., 2014).

4.1.iv - Aims and objectives

The diverse array of interactions between RTNs, RHD3, LNPs and other ER resident proteins, suggests that ER morphology is a product of a complex interplay between many of these partners and their regulatory impacts upon each other. RTNs across Eukarya have many identified interactions, not just with themselves and other ER morphogenic proteins, but partners functional in multiple roles within the ER, and even those that occupy other organelles. RTNs in general appear to be capable of forming many protein-protein interactions, especially in mammalian and yeast systems where many interactions have been identified. Here the potential interactions between clade 6 RTNs, RHD3 and LNP will be interrogated through the imaging of co-expressions of multiple proteins of interest. Following this, candidate proteins will be interrogated by FRET experiments, to quantify and confirm interaction capability. These results will further elucidate the potential functional role of clade of Arabidopsis RTNs and their already seemingly distinct properties compared to other RTNs.

4.2 – Results

4.2.i – RTN17.1 co-localisation with ER morphogens

To identify potential protein-protein interactions and to compare whether interaction properties are similar to that of the other clades of RTN, co-localisation of the proteins of interest were first assessed. Tobacco leaf epidermal cells co-expressing both RTN17.1-Clover and another ER morphogen were imaged, and their co-localisations were quantified utilising Pearson's correlation co-efficients (PCC). A PCC score of 1 suggests 100% of the signal from both channels are co-localised, and a PCC score of 0 implies 0% of the signal from either channel is co-localised. RTN17.1 as shown previously localises to discreet puncta across the ER network. However, due to the lack of hyperconstriction and RTN17.1 puncta residing within the ER, most of if not all of signals of RTN17.1 overlap with the signal from HDEL (Fig 4.1A). However, this co-localised area only represents a small portion of the total HDEL signal, and as such RTN17.1-Clover and RFP-HDEL expression gives a PCC score of 0.45 (Fig 4.1G).

RTN17.1-Clover co expressed with mCherry-RTN17.1 results in near complete colocalization of the fluorophores in these puncta consistent with expression of a singular construct (Fig 4.1B). This corresponds with a high PCC score of 0.84, as the majority of the signals of each fluorophore are highly co-localised (Fig 4.1G). RTN17.1-Clover co-expressed with RTN1-mRFP reveals that the two proteins do not co-localise, with RTN1 distributing across high curvature membranes of the ER network as typical for clade 1 RTNs, with RTN17.1 remaining in its puncta (Fig 4.1C). This is reflected in the PCC score of 0.60, similar to that of the HDEL co-localisation, again representative of RTN17.1s signal only occupying a portion of the total area of RTN1 signal (Fig 4.1G). Similar distributions are seen with both LNP1-RFP (Fig 4.1D) and LNP2-RFP (Fig 4.1E) which have median PPC scores of 0.60 and 0.61 respectively (Fig 4.1G) suggesting no co-localisation between RTN17.1 and LNP proteins.

RTN17.1 when co-expressed with RHD3-RFP both localise to puncta similar to that of RTN17.1 expressed alone. This results in a high PCC score of 0.90, showing the majority of the signal from both channels are highly co-localised.

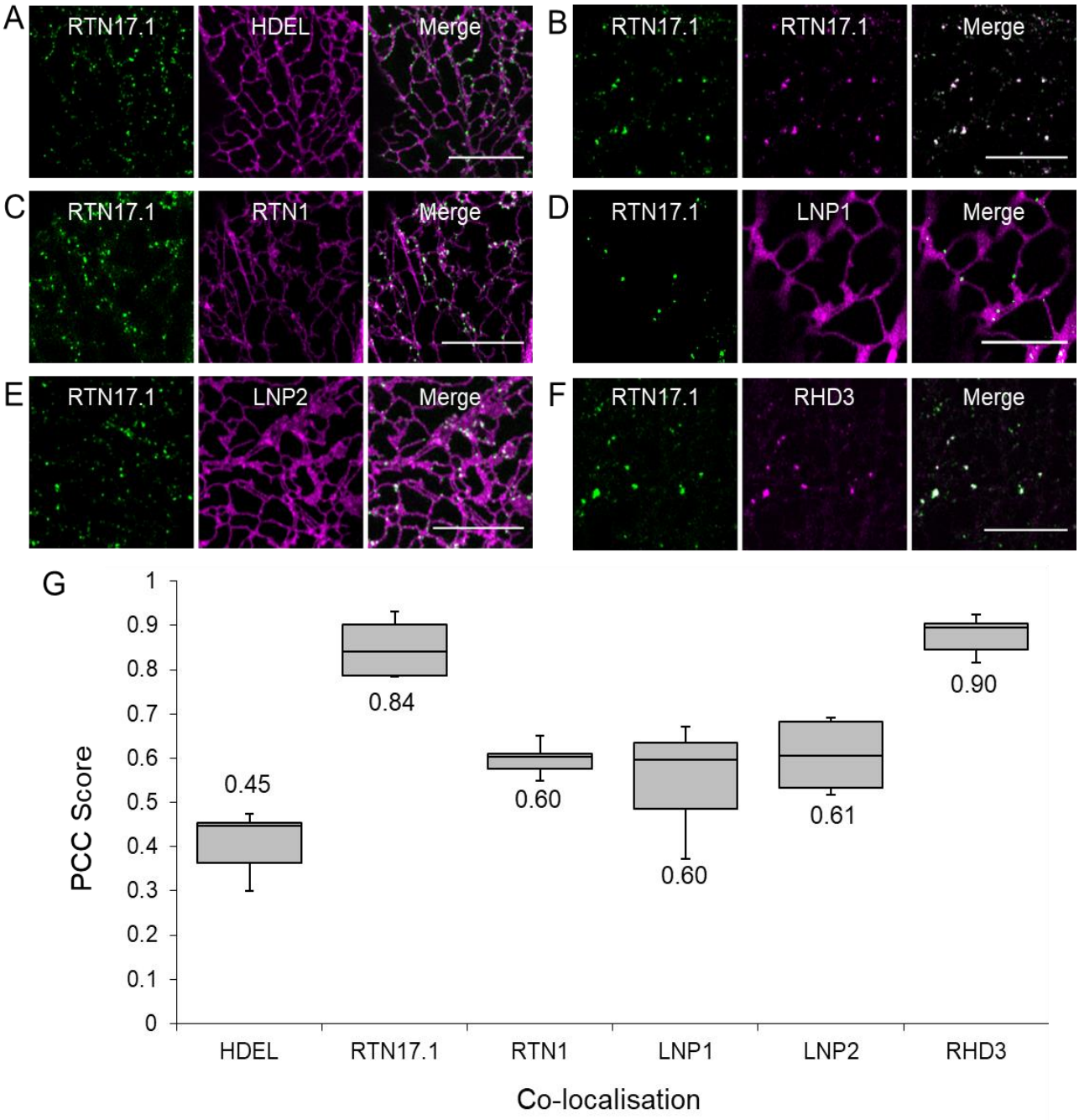

Figure 4.1 – Co-localisation of RTN17.1 with ER morphogens

Co-localisation between A) RTN17.1-Clover and RFP-DHEL. B) RTN17.1-Clover and mCherry-RTN17.1. C) RTN17.1-Clover and RTN1-mRFP. D) RTN17.1-Clover and LNP1-RFP. E) RTN17.1-Clover and LNP2-RFP. F) RTN17.1-Clover and RHD3-RFP. G) Pearson's correlation coefficient scores of each co-localisation. Numbers represent median. HDEL n=11, RTN17.1 n=4, RTN1 n=5, LNP1 n=3, LNP2 n=5, RHD3 n=9, where n = individual frames from co-expression experiments. HDEL and RHD3 are comprised of 3 biological experimental repeats, and the remainder from 1.

4.2.ii – RTN17.1 & RHD3 interaction

To investigate the co-localisation of RTN17.1 and RHD3 further we first compared the distribution of RHD3 when expressed alone. Previous experiments describe and show GFP-RHD3 expression in tobacco and Arabidopsis as labelling the entirety of the ER with apparent mobile puncta usually at 3-way junctions (Chen et al., 2011). This is consistent with our images of RHD3-Clover expression, although punctate structures are not very apparent or abundant, with the majority of the signal being universally distributed throughout the ER and consistent with HDEL's labelling of the network (Fig 4.2A). Conversely, when RHD3-Clover and RTN17.1-mRFP are co-expressed in the same tissue, RHD3 is seemingly pulled into puncta with RTN17.1. The puncta are less consistent in their size, with some visible background labelling of a network structure that appears to be comprised of smaller puncta. This network labelling also consists of more non-continuous parallel strands, indicative of a more cytoskeleton pattern compared to that of the ER (Fig 4.2B).

FRET in various forms has the ability to determine whether two fluorophores are within 1-10 nm of each other, with increased FRET efficiencies inversely proportional to the distance between the two molecules (Sekar & Periasamy, 2003). This proximity is indicative of protein-protein interaction and is a useful technique to utilise fluorescence microscopy to infer interactions, where co-localisation is hindered by the lack of resolution (Day et al., 2001). AP-FRET utilises the photo-bleaching of the acceptor fluorophore to generate an increase in donor fluorescence signal if a FRET response occurs (Kenworthy, 2001). Here we see that RTN17.1 and RHD3 have a median fret efficiency of 10.19%. This is significantly increased compared to the negative control of RTN17.1 and GFP-HDEL which also do not share a specific co-localisation, with a fret efficiency of 1.42%. RTN1-GFP and RTN1-RFP, known to form hetero-interaction has a FRET efficient of 7.39%, which is significantly increased compared to the negative control (Fig 4.2C). This indicates that RTN17.1 and RHD3 as well as having a strong co-localisation have a confirmed strong degree of interaction.

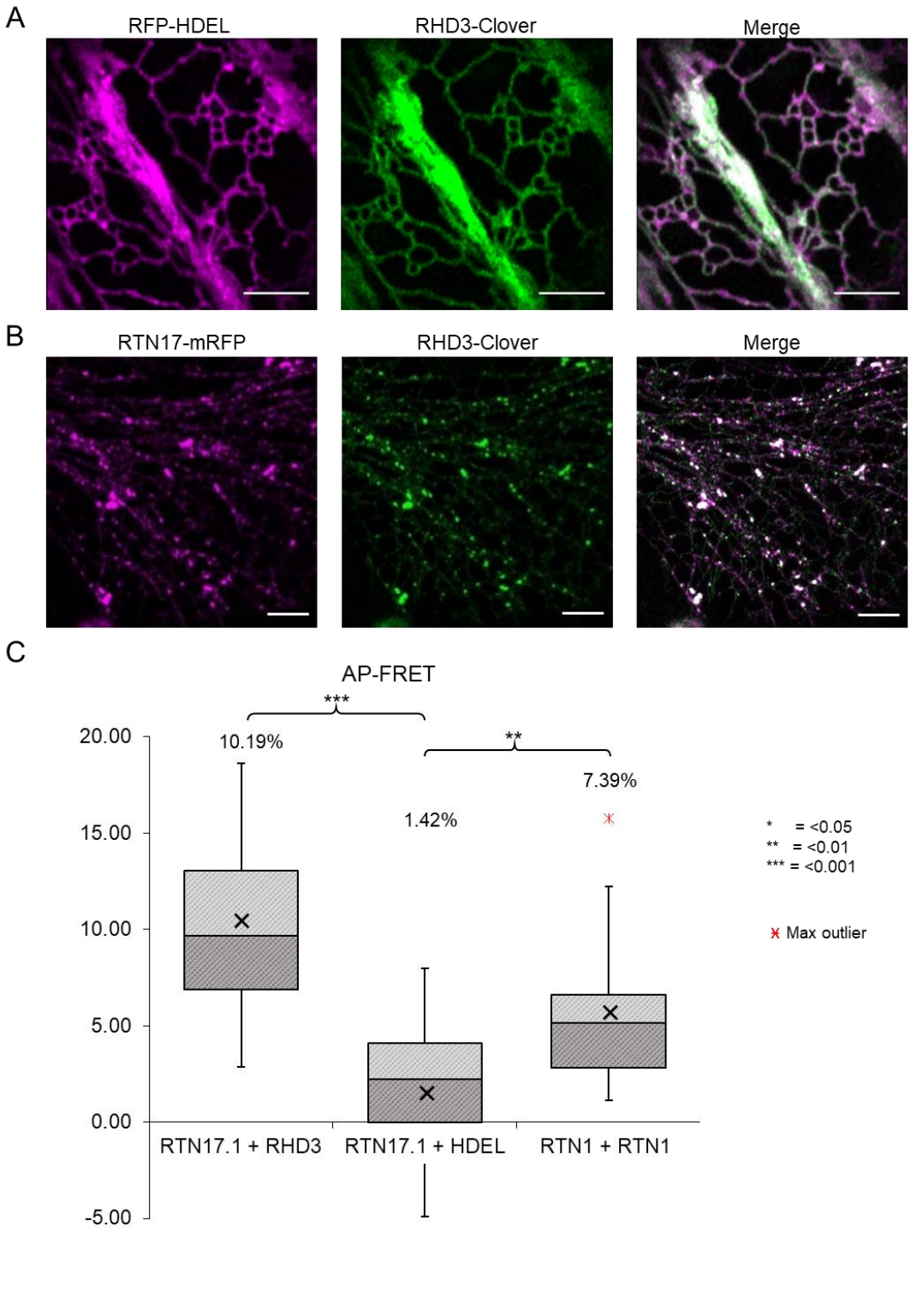

Figure 4.2 – AP-FRET analysis

A) Comparison of RFP-HDEL and RHD3-Clover localisation (left), versus RTN17.1-RFP and RHD3-Clover co-localization (Right). Pale blue arrows represent RHD3 puncta. B) AP-FRET efficiencies of RTN17.1-mRFP & RHD3-Clover puncta, compared to negative (RTN17.1-mRFP + GFP-HDEL) and positive controls (RTN1-RFP + RTN1-GFP). X = average FRET efficiency. Confidence intervals * = <0.05, ** = <0.01, *** = < 0.001. Scale bars = 10 μm.

4.2.iii – RTN17.1 potentially links with cytoskeletal components

Upon co-expression of RTN117.1 and RHD3, a large proportion of cells displayed puncta aligned in a more cytoskeletal appearance, with a more parallel strands and fewer near circular polygons seen in normally labelled ER (Fig 4.3A). Similar distribution can be observed in rare cases of RTN17.1 overexpression alone, with puncta being spread across more linear and parallel strands of the network (<5% of cells) (Fig 4.3B). To determine whether this does correlate with a cytoskeletal component, and whether RTN17.1 is localised in association with either the actin or microtubule cytoskeleton, RTN17.1 constructs were co-expressed with different markers. RTN17.1-Clover co-expressed with actin marker, Lifeact-RFP (Riedl et al., 200), reveals that some puncta align strongly with the actin cytoskeleton. This is to be expected as the ER has direct contacts with actin, however of interest is that these puncta aligned with actin are much less motile, with no movement seen within 30 seconds compared to other puncta which move between each 5 second frame of the hyperstack (Fig 4.3C). A similar observation occurs when mCherry-RTN17.1 is co-expressed with Tua6-GFP, a microtubule marker (Ueda et al., 1999). Here again puncta align with the microtubular cytoskeleton are less motile than those that are not (Fig 4.3D). This suggests there is a possible association between both actin and microtubule cytoskeletons, at least to the point in which puncta reduce their motility when in close proximity of cytoskeletal components.

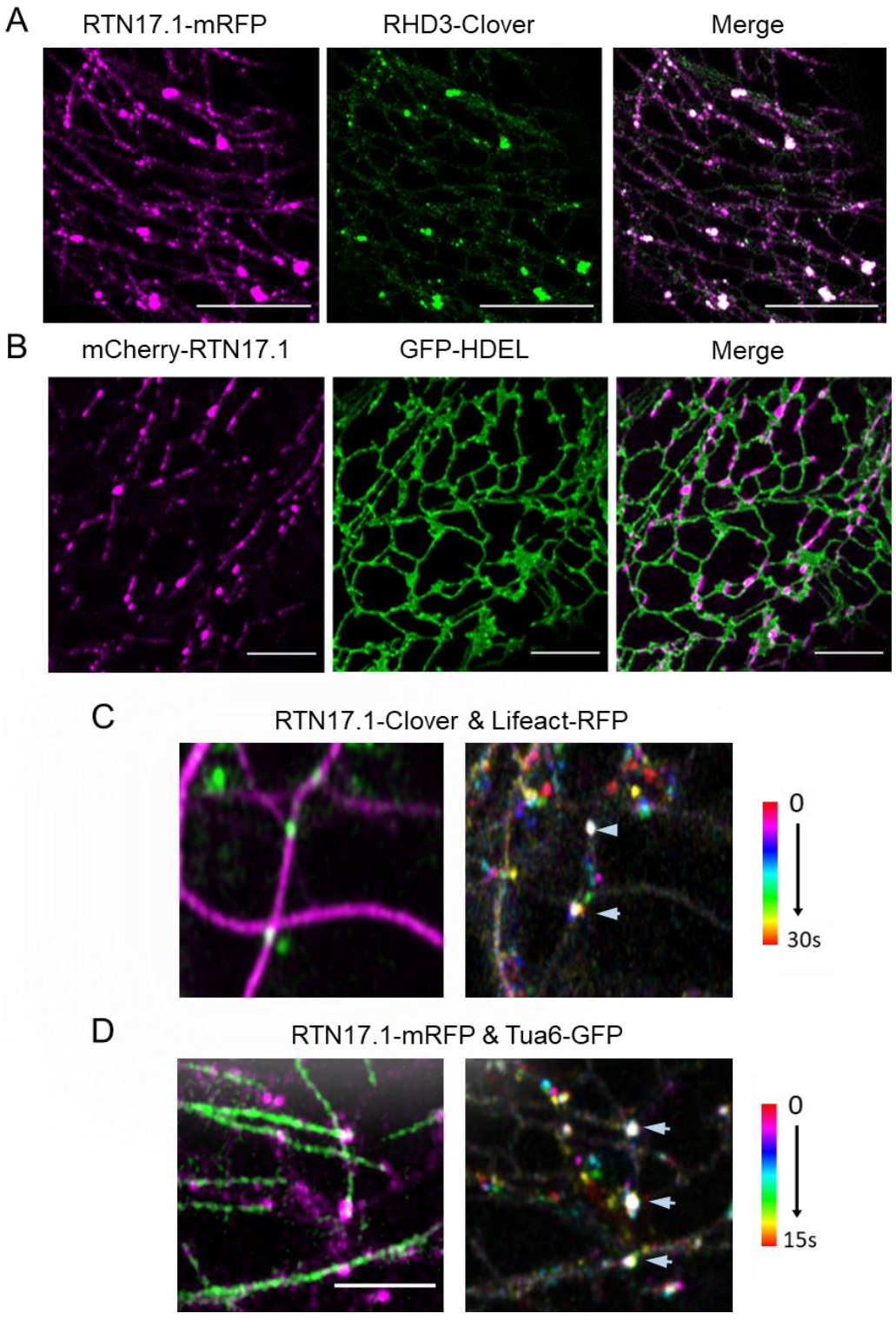

Figure 4.3 – Cytoskeletal association of RTN17.1

A. Representative images of expression of RTN17.1-RFP and RHD3-Clover exhibiting a slight cytoskeletal distribution. B. Example of mCherry-RTN17.1 expression occasionally revealing more linear strands similar to cytoskeletal patterns. **C**. Co-localisation with Lifeact-RFP and **D**. Tua6-GFP, with corresponding 6 frame hyperstacks. Stationary puncta highlighted with pale blue arrows. A & B Scale bars = 10 µm, C = 2.5 µm, D = 5 µm

4.3 – Discussion

4.3.i – RTN17.1 has unique interactions compared to clade 1 RTNs

Multiple investigations have revealed a vast array of interacting partners for clade 1 RTNs, as well as mammalian and yeast RTNs/Yop1p (Yang & Strittmatter, 2007). For clade 1 RTNs and RTN13, a key aspect of their functionality is the ability to form hetero- and homo-oligomers, as these allow the stabilisation of tubules and sheet edges, after the hydrophobic wedging induces the initial membrane curvature. RTNs also interact with other ER morphogens, namely RHD3 and LNP proteins, as well as VAP27 and SYT proteins involved in EPCS formation (Kriechbaumer et al., 2015). So far it has been revealed that the clade 6 RTNs are phylogenetically distinct, as well as have a unique distribution and localisation within the ER compared to other RTNs. Therefore, identifying potential interacting partners is key in understanding just how distinct this clade is from the rest of the RTN family of proteins.

Firstly, due to the specific and unique distribution of RTN17.1 compared to clade 1 RTNs, observing co-localisation of proteins when co-expressed transiently in tobacco may be the first indicator of interaction. Of key interest, was the discovery that RTN17.1 does not share any distinct co-localisation with RTN1 (Fig 4.1C), with similar PCC scores to that of HDEL (Fig 4.1A), LNP1(Fig 4.1D) and LNP2 (Fig 4.1E). This is distinct to that of clade 1 RTNs, which are both capable of homo-typic interactions with other clades of RTN, as well as with LNP. This suggests that although containing the highly conserved RHD which is typically responsible for oligomerisation (Sparkes et al., 2010), clade 6 RTNs are structurally distinct either in the RHD or due to the presence of the termini are incapable of interacting with classical RTNs.

4.3.ii – RTN17.1 interacts with RHD3

When co-expressing RTN17.1 with two different fluorophores we observe a strong co-localisation of the signals, suggesting that the puncta are comprised of both constructs and this PCC score is effective as a positive control for co-localisation (Fig 4.1B). RTN17.1 co-expressed with RHD3 has a PCC similar to RTN17.1 with itself, and visually it is clear RHD3s signal is almost completely co-localised with that of RTN17.1 (Fig 4.1F). This is of great importance when looking at the distribution of RHD3 alone, whereby it labels the ER entirely with slight enrichment at certain 3-way junctions (Chen et al., 2011). This stark change in distribution of RHD3 when co-expressed with RTN17.1 (Fig 4.2) is a strong indicator that these proteins are interacting. Furthermore, this interaction is confirmed by the strong FRET efficiency when probing these puncta with AP-FRET, with a stronger fret-efficiency than the positive control of co-expressed of RTN1-RFP with RTN1-GFP, which have been previously shown to interact via FRET-FLIM (Sparkes et al., 2010). Other co-localisations not shown due to lack of biological repeats include RTN17.1 and RTN21.2, which did co-localise, as well as RTN17.1 with NET3C, another EPCS marker (Wang et al., 2014) which did not co-localise. This suggests that within RTNs within clade 6 can interact and potentially form oligomers, however whether interaction between clade 6 RTNs and EPCS proteins such as NET3C and VAP27 is possible cannot be confirmed, as co-localisation attempts were unsuccessful when co-expressing the constructs together.

One observation that consistently occurred upon co-expression of both RTN17.1 and RHD3, aside from the change in localisation of RHD3, is that the co-localised puncta also appeared to have a more cytoskeletal patterning with more parallel strands compared to ER labelled by HDEL. This could also be seen occasionally with cases of RTN17.1 overexpression alone, but was not predictable or common, and unaffected by controllable factors such as optical density (OD) of agrobacteria used in infiltration. To assess whether there was a relation to the cytoskeleton, and which component, RTN17.1 was co-localised with Tua6 to label microtubules, and Lifeact to label actin filaments. Here similar outcomes are reached, with RTN17.1 puncta labelling relatively

normal and free flowing, besides puncta which align perfectly with a labelled filament. Here the puncta are stationary for periods of time greater than 15 seconds (Fig 4.3). The plant ER is intrinsically linked and driven by both the actin (Sparkes et al., 2009a) and the microtubule cytoskeleton (Hamada et al., 2014). This involves the linkage of proteins such as myosin (Sparkes et al., 2008), Net3B (Wang & Hussey 2017) and SYP73 (Cao et al., 2016) to actin filaments, whilst ARK1 has been shown to link the ER to microtubules in association with RHD3 (Sun et al., 2020). This means that the ER is directly attached to both cytoskeletons at certain points in the network, and so whether this persistent puncta co-localisation at these points are a by-product of other interactions, or from RTN17.1 itself is not clear. However due to the apparent interaction with RHD3, it may be part of this ARK1 complex that is linked to the microtubule cytoskeleton. A more thorough investigation of a larger variety of proteins via other methods such as Co-IP may reveal more into the nature of clade 6 RTNs and their interactions, as well as confirm the current data with positive interactions within the clade and RHD3. Unfortunately, FRET-FLIM attempts with RTN17.1 were unsuccessful due to the speed of the puncta, and the heterogeneity of the signal within the puncta that were immobile enough for FRET-FLIM acquisition. As such, attempts to compare RTN17.1 with previous RTN FRET-FLIM datasets did not produce useable or analysable data (Supplementary figure 2). Aside from FRET based techniques, this could be further confirmed by assays such as membrane-based yeast two-hybrid system (Lentze & Auerbach, 2008), and Co-IP (Lin & Lai, 2017). Co-IP in particular may also allow for identification of a wider array of proteins currently not investigated, as was done for other Arabidopsis RTNs (Kriechbaumer et al., 2015).

4.3.iii - Summary and conclusions

Despite the presence of the conserved RHD, RTN17.1 is incapable of interacting with clade1 RTNs and shows distinct interactions such as that with RHD3 which may be implicated in its punctate localisation associated with 3-way junctions. It also appears that RTN17.1 has a degree of

interaction with cytoskeletal components. Further experimentation identifying the effects of these interactions as well as how they are mediated will be key in understanding the functionality of the clade 6 RTNs.

Chapter 5 – Functional Domains

5.1 – Introduction

Function of Arabidopsis clade 1-4 RTNs as well as mammalian and yeast RTNs is derived exclusively from the structural nature of the RHD and the physical effects this has in terms of embedding into the ER membrane, and subsequent induction of curvature (Chou et al., 2001; Voeltz et al., 2006, Sparkes et al., 2009b). Maintenance of these high-curved regions then relies on the oligomerization capabilities of the RTNs. Both homotypic and heterotypic interactions between different RTNs are prevalent in mammalian, yeast and Arabidopsis RTNs (Shibata et al., 2008; Sparkes et al., 2010). The exact domain within the RTN structure that mediates these interaction and oligomerisation capabilities has so far been unidentified. However, although the capability to induce hyperconstriction observed in clade 1 RTNs requires the full length RHD to be present, deletion of different TMDs within the RHD still allows interaction to occur between clade 1 RTNs (Sparkes et al., 2010), and as the hydrophobic regions are stable within the membrane it is likely to be a portion of the RHD itself that mediates the interaction.

In previous chapters it has been shown that clade 6 RTNs have a unique localisation and functional characteristics to that of the rest of the Arabidopsis RTN family of proteins (Figure 3.1, 3.2, 3.3). Furthermore, it has been have identified that clade 6 RTNs can interact with other clade 6 RTNs, but do not fully co-localise with RTN1, suggesting heterotypic interactions between clade 6 and other clades 1-4 are unlikely (Fig 4.1). As well as this, an interaction between RTN17 and

RHD3 has been identified, that appears to be significant in the localisation of the two proteins and may have implications for both proteins being involved in the formation of 3-way junctions (Fig 4.2). In this chapter, to understand this interaction better, as well as the other unique features of RTN17 such as the distinct localisation and dynamics, we shall interrogate the effect of multiple truncations and expression of different RTN17.1 splice variants. This will allow us to isolate and understand each of the major components of RTN17 structure and understand which domain is functionally responsible for the localisation, distribution, and interactions of the protein.

5.1.i - Functional domains of RTNs

For Arabidopsis RTNs, the only other functional domains aside from the RHD that have been identified are that of the APH in clade 1-4 RTNs (Brooks et al., 2021), as well as the 3βHSD homologues region in clade 5 RTNs (Kriechbaumer et al., 2019). Representatives from clade 1-4 were assessed for the presence and function of the APH (Brooks et al., 2021), and clade1-4 examples were all found to have an APH present responsible for curvature sensing, previously shown to be relevant to the function of Arabidopsis RTN13 (Breeze et al., 2016) and mammalian Yop1p (Brady et al., 2015). Clade 1 RTNs contain a linker region of more than 20 residues long between the RHD and APH, whereas clade 2-4 RTNs only have a few intermediate residues between the RHD and APH (Brooks et al., 2021). However, as only one or two RTNs from each clade were experimentally assessed it may be possible others either do not contain an APH as predicted, or it may not require its presence for function. Clade 5 and 6 RTNs on the other hand contain no APH (Brooks et al., 2021). Clade 5 RTNs contain a functional domain N-terminal to the RHD that is homologous to 3βHSD (Kriechbaumer et al., 2018b). This provides a unique functional role for RTN19 and RTN20 in the plant ER, as they do not appear to be involved in tubule formation nor capable of hyperconstricting tubules upon over-expression, and instead have a role in lipid regulation specifically affecting sterol composition (Kriechbaumer et al., 2018b).

Despite this presence of a different functional domain, homologous to 3βHSD, and lack of APH, clade 5 RTNs have shown to still be capable of interactions with representatives of clade 1 RTNs such as RTN1-RTN3 (Kriechbaumer et al., 2015). This appears to be inconsistent with clade 6 RTNs. Although it was not possible to confirm interactions between clade 6 RTNs and clade 1 RTNs, previous co-localisation attempts show they result in mutually exclusive signals (Figure 4.1) and therefore unlikely to interact considering the strong co-localisation observed in the confirmed interaction of RHD3 (Figure 4.3). Generation of chimeric proteins between RTN19 and 20 show that the punctate labelling observed in RTN20 is generated by the C-terminus alone. Fusion of the last 30 residues to the N-terminus and RHD of RTN19 caused the diffuse labelling of RTN19 to change to punctate localisation (Kriechbaumer et al., 2018b). Although RTN17, 18 and 21 all share a punctate localisation (Fig 3.1, Fig 3.2, Fig 3.3) that is distinct of that to that of RTN19 and RTN20, it will be interesting to determine whether this localisation can be assigned to a specific portion of the sequence or functional domain as is the case for RTN20.

5.1.ii - Mammalian RTN functional domains

Mammalian RTNs, although containing the highly conserved RHD required for its role in shaping the ER (Iwahashi et al., 2007), are structurally different to that of Arabidopsis clade 1-4 RTNs. All the 4 human full length RTNs feature a long N-terminal extension that is highly disordered, with the RHD occupying the final 150-200 amino acids (Li & Song, 2007; Yang & Strittmater, 2007). Although full-length human RTNs contain long N-terminal IDRs, each gene expresses splice variants that do not contain the N-terminal IDR and are comprised of just the RHD, for example *Hs*RTN1C (Fazi et al., 2006). Studies have identified *Hs*RTN1C to be implicated in multiple interactions with proteins involved in various cellular functions such as interactions with Bcl-XL and Bcl-2 (Tagami et al., 2000) as well as Syntaxin and VAMP2 proteins at SNARE complexes (Steiner et al., 2004). *Hs*RTN1C shares the classical functionality of most RTNs, being implicated

in the formation of ER tubules, however over-expression results in ER stress and subsequent cell death and is suggested to act as a modulator of ER stress sensitivity mediated by Ca^{2+} changes (Di Sano et al., 2007). Due to this link between *Hs*RTN1C and ER stress, it has subsequently been shown to be impacted in autophagosome production and autophagy (D'Eletto et al., 2019) and broader implications in disease states such as cerebral ischemia (Gong et al., 2017). Again, these activities all appear to be mediated by the truncated structure comprised of just the *Hs*RTN1 RHD, and no other functional domains. *Hs*RTN4a is the longest isoform of *Hs*RTN4 and has been implicated in inhibition of neurite outgrowth via interaction between the 66 amino acid long cytosolic facing loop (Nogo-66) with Nogo Receptor (NogoR; Fournier et al., 2001; Li et al., 2005). However, later studies revealed that interaction between *Hs*RTN4 and NogoR also occurs independently through a portion of the N-terminus called Δ20 (Oertle et al., 2003). Other mammalian ER morphogens such as REEP-1 are structurally analogous to that of clade 6 RTNs, with a hydrophobic RHD-like domain anchoring the protein to the ER, REEP-1 has been shown to contain a microtubule binding domain that is within a portion of the N-terminal IDR, although not specified as to which residues are involved in this function (Park et al., 2010). REEP-1 is also implicated in multiple other interactions with proteins such as ATL (the mammalian RHD3 homologue), the microtubule-severing spastin protein and mammalian RTNs (Park et al., 2010).

5.1.iii - Aims and objectives

These mammalian RTNs and other ER morphogens such as REEP-1 offer valuable insight in to how both the disordered termini and hydrophobic domains can be responsible or sufficient to mediate certain protein-protein interactions. As similarities can be observed with clade 6 RTNs and REEP-1 structures, it will of interest to determine whether the RTN17 interaction with RHD3 is similarly mediated through the hydrophobic domain, or whether the disordered termini are involved in mediating interactions with other binding partners. To assess the presence of

functional domains within RTN17.1s structure, how the splice variants which encode natural truncations and deletions differ in localisation and characteristics to that of RTN17.1 shall be investigated. Furthermore, the generation of other deletions and chimeric proteins will allow us to identify which domain of RTN17 is potentially responsible for interaction with RHD3. By understanding these facets of RTN17 structure, it shall allow us to determine overall which aspects of the sequences and structural features may be responsible in producing the unique properties of RTN17.1 previously identified in chapters 3 and 4.

5.2 – Results

5.2.i - RTN17.2 and RTN17.3 localise to puncta consistent with the full-length protein RTN17.1

The Arabidopsis *RTN17* gene codes for 3 splice variants, namely RTN17.1, RTN17.2 and RTN17.3. RTN17.2 is a natural deletion compared to the full-length protein (Fig 5.1A), losing the full C-terminal residues beyond that of the RHD, from aa323-431 (Fig 5.1B). The C-terminal portion is predicted to feature a hydrophobic region (Fig 2.3), which is subsequently deleted in RTN17.2 (Fig 5.2B). Transient expression of RTN17.2-Clover in tobacco epidermal leaf cells under a 35S promoter reveals a punctate localisation with similar characteristics to that of RTN17.1 (Fig 5.2C; Supplementary Movie 4). On average, RTN17.2 puncta were around 0.29µm in diameter, slightly smaller than the 3.32µm diameter of RTN17.1 puncta, but within the range of observed diameters for RTN17.1 (Supplementary figure 1). However, the RTN17.2-Clover construct was much more difficult to express than RTN17.1 constructs typically are and displayed a greater variety in morphological impacts. Closer inspection of different representative images from different experiments reveals that there is a potential for RTN17.2 to induce a qualitative hyperconstriction (Fig 5.2D). An equal proportion of cells exhibit either no visible constriction effects, some with slight variations in tubule properties with a portion of dilations and constrictions seen adjacent to RTN17.2 puncta, as well as more extreme cases with very visible hyperconstriction, and less punctate structures. This is shown with the RFP-HDEL labelled ER being discontinuous and heterogenous in terms of signal intensity and width across the length of the networks, indicative of constriction (Fig 5.2D).

RTN17.3 is a 13 amino acid deletion of aa142-154 within the N-terminus of the full-length protein (Fig 5.1D). This deletion exists within the highly disordered region, mainly consisting of low-

complexity residue repeats, with no specific motifs detected (Chapter 2). RTN17.3-Clover expression results in punctate distribution sharing comparable localisation and dynamic properties to that of RTN17.1 and RTN17.2, with an average diameter at 0.31μm, very similar to the puncta diameters of RTN17.1 (Supplementary figure 1; Supplementary movie 5). Consistent across all imaging experiments there appeared to be proportionally less puncta visible within an individual frame as compared to RTN17.1, however this may be related to expression inconsistencies or size differences with smaller puncta being outside of the signal threshold when observing larger brighter puncta (Fig 5.1B, E).

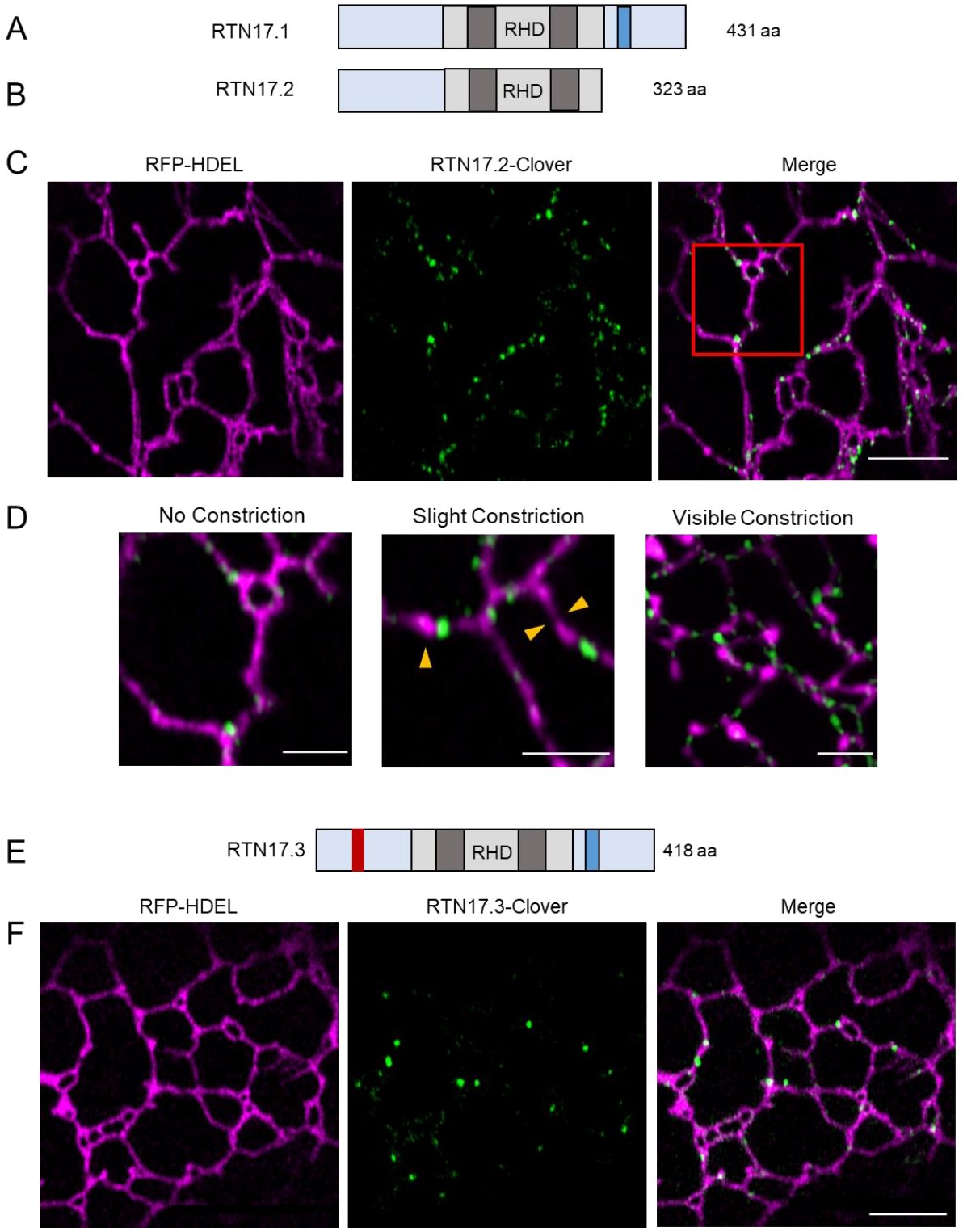
A
RTN17.1
RHD
431 aa
B
RTN17.2
RHD
323 aa
C
RFP-HDEL
RTN17.2-Clover
Merge
D
No Constriction
Slight Constriction
Visible Constriction
E
RTN17.3
RHD
418 aa
F
RFP-HDEL
RTN17.3-Clover
Merge

Figure 5.1 – Transient expression of RTN17.2 and RTN17.3 in tobacco epidermal leaf cells.

Graphical representation of **A**. RTN17.1, and **B**. RTN17.2 with regions to scale are shown. Light blue = terminal extensions, light grey = RHD, dark grey = RHD hydrophobic domains, Blue = C-terminal hydrophobic domain. **C**. Representative image of RTN17.2-Clover co-expressed with the ER lumenal marker RFP-HDEL. **D**. Magnified section showing degrees of constriction across the variable impacts of RTN17.2-Clover expression. Orange inward arrows indicating areas of slight constriction and dilation. **E**. Schematic representation of RTN17.1, using same key as **A**. Red box indicates location of deletion compared to RTN17.1. **F**. Representative image of RTN17.3-Clover co-expressed with RFP-HDEL. Scale bars = 5 μm for **C** and **F**, 2 μm for **D**.

5.2.ii - N-terminal truncation of RTN17.1 eliminates the interaction between RTN17.1 and RHD3

As RTN17.2 encodes for a truncation of the C-terminus, a synthetic construct was to be generated to determine the effect of truncating the N-terminal extension. For this we generated RTN17Δ1-168, which contains the RHD and C-terminal extension of RTN17.1 but has had the N-terminal amino acids 1-168 deleted (Fig 5.2A). Full length RTN17.1-Clover when co-expressed with RHD3-mRFP results in RHD3 transitioning from a diffuse ER labelling to strongly co-localised puncta across the ER network (Fig 5.2B) and has been confirmed to interact via AP-FRET previously (Fig 4.4). RTN17Δ1-168-Clover when expressed transiently in tobacco retains its punctate distribution across the ER, however the co-localisation between RTN17Δ1-168-Clover and RHD3 is lost. This is shown with RHD3-mRFP labelling the entirety of the ER as a diffuse signal when co-expressed with RTN17Δ1-168 (Fig 5.2B). This labelling of RHD3-mRFP is consistent with distribution seen when the protein is expressed individually or with an ER label (Fig 4.4)(Chen et al., 2011). These signals are no longer strongly co-localised (as with the full-length protein) suggesting that the deletion of the N-terminal IDR of RTN17.1 results in a loss of interaction between the RTN17 and RHD3.

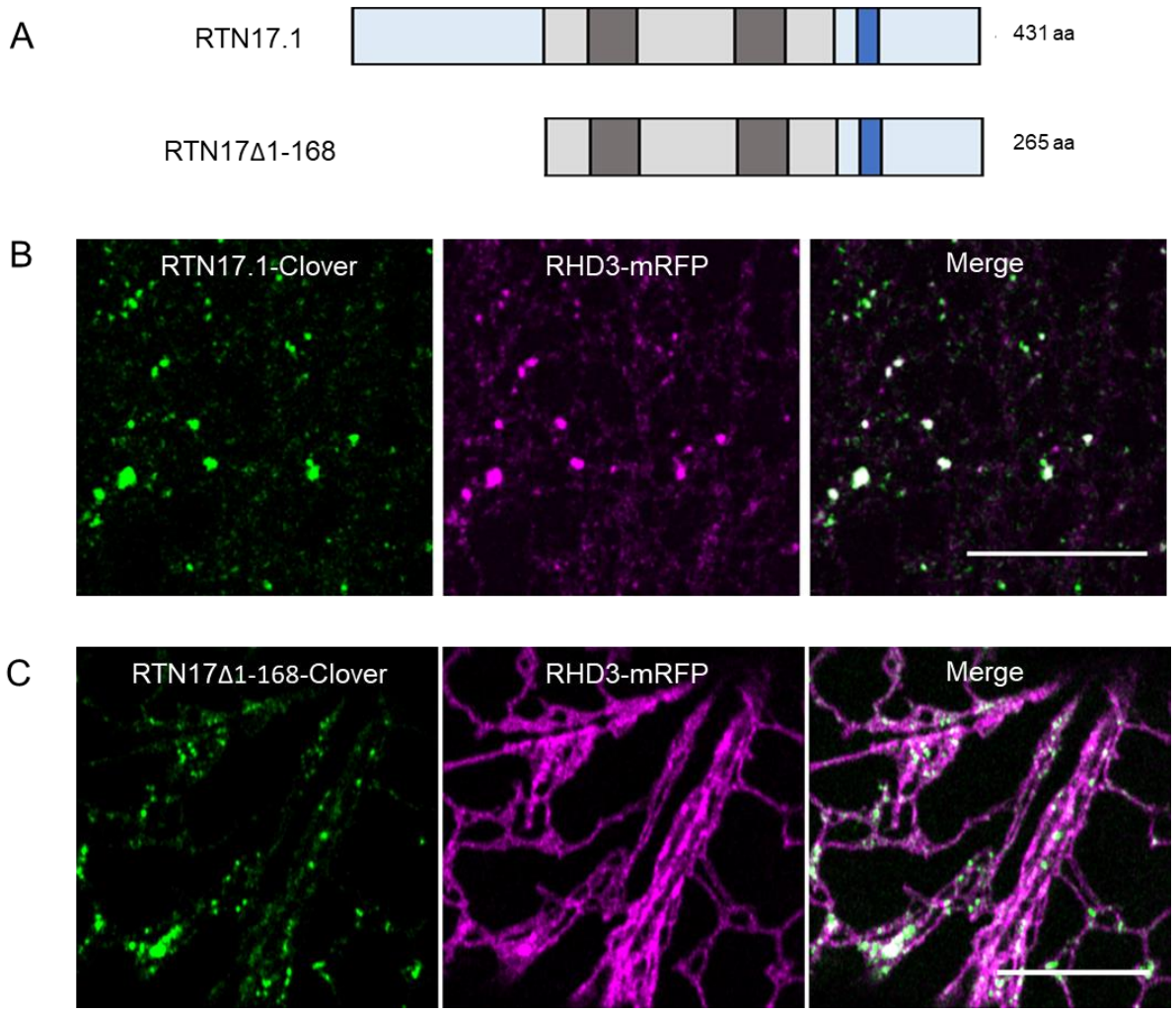

Figure 5.2 – N-terminal deletion of RTN17.1 prevents interaction with RHD3

A. Graphical representation of each protein with protein domains/regions to scale. Light blue = terminal extensions, light grey = RHD, dark grey = RHD hydrophobic domains, Blue = terminal hydrophobic domain. **B**. Representative image of RTN17.1-Clover co-expressed with RHD3-mRFP. **C**. Representative image of RTN17Δ1-168-Clover co-expressed with RHD3-mRFP. Scale bars = 10μm.

5.2.iii - Punctate distribution changes with deletion of N- and C-termini

So far, the localisation of both N- and C-terminal deletions have been assessed independently via expression of RTN17T1 and RTN17.2 constructs, respectively. Both of these proteins maintain a punctate distribution throughout the ER, with some identified changes in characteristics compared to the full-length protein. To develop our understanding of the termini function, a construct consisting of just the RTN17.1 RHD was generated, RTN17ΔTermini. This involves truncating aa 1-168 from the N-terminus as well as aa 324-431 at the C-terminus of RTN17.1. This produces a protein more analogous to the rest of the clades of reticulons, retaining the aa 169-322 of the RHD with its 2 hydrophobic domains, short termini and a cytosolic facing loop (Fig 5.3A). This 156 amino acid long protein was fused at the C-terminus to a Clover fluorescent protein. RTN17ΔTermini-Clover reveals a more diffuse distribution across the ER, with the presence of some puncta, suggesting that the RHD alone is capable of still producing punctate structures, but preferentially labels the entirety of the ER (Fig 5.3B). For RTN17.1 to localise exclusively to puncta, it requires one or both extended termini.

When co-expressing RTN17ΔTermini-Clover with the actin marker Lifeact-RFP, the majority of punctate structures appear to localise largely at points in which the ER is overlapping with the actin cytoskeleton (Fig 5.3C). When RTN17.1-Clover is co-expressed with Lifeact-RFP, also it is also possible to observe puncta aligning with the cytoskeleton, and those that do are often much more stable over time compared to other puncta (Fig 5.3D). RTN17ΔTermini-Clover puncta are similarly much more stable at points in which the ER is overlapping with the actin cytoskeleton and nearby puncta that are more motile over time (Fig 5.3D). This was shown by generating a colour coded hyperstack from a time series of a co-expression experiment. Here white puncta overlapping areas of the actin cytoskeleton can be seen, representing the puncta being stationary for the total sampled duration. This contrasts to other puncta which are represented by an

individual colour per frame of the hyperstack, indicating movement between the frame intervals (Fig 5.3E). This suggests that there is an intrinsic property of the RTN17.1 RHD that is capable of mediating a link with the cytoskeleton, and this in turn is partially responsible for the formation of RTN17.1 puncta. However, to exclusively localise to puncta, RTN17.1 requires the terminal extensions and potentially the interactions they mediate such as with RHD3.

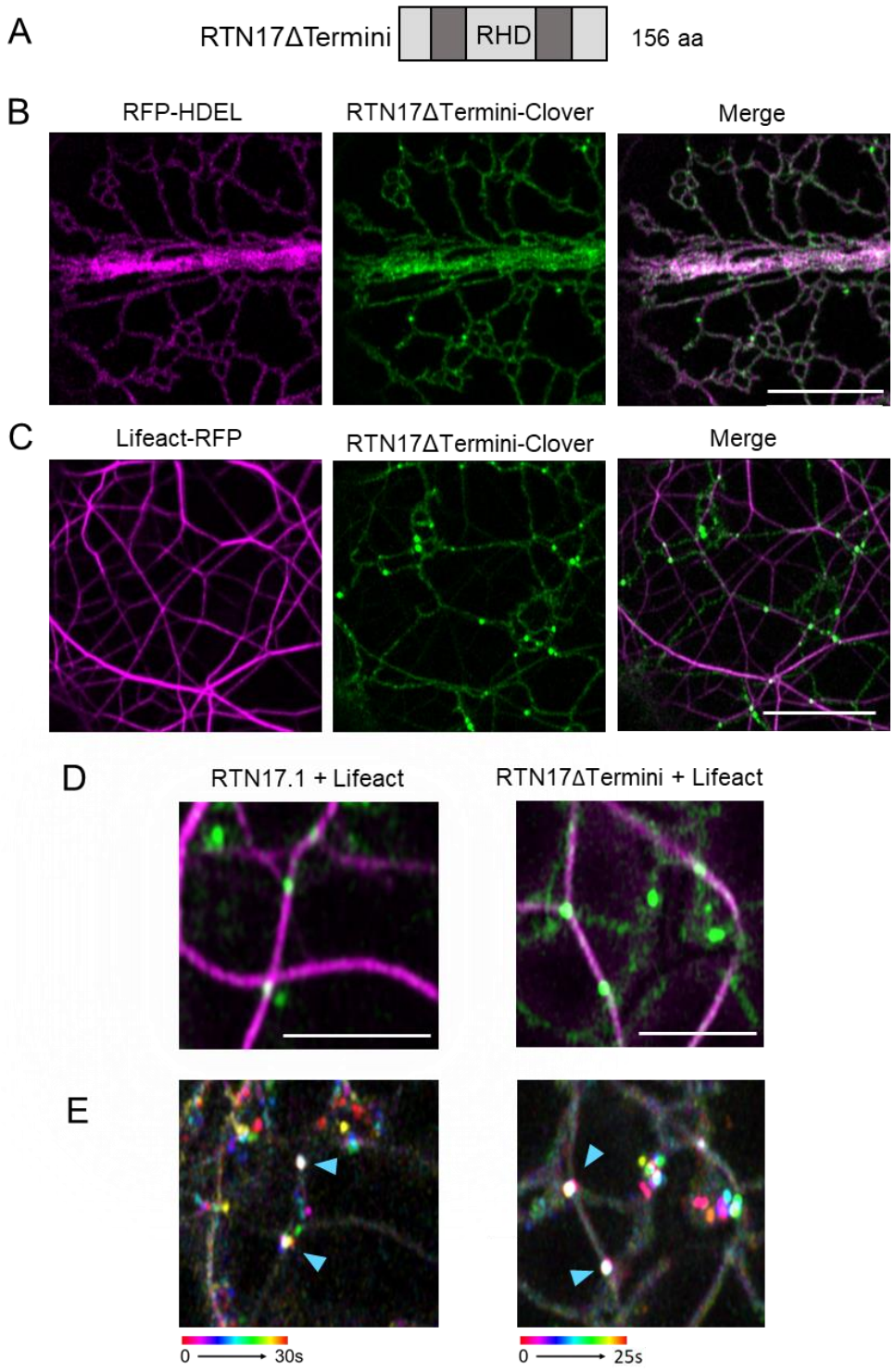

Figure 5.3 – RTN17 RHD alone changes distribution and can align with actin

A. Graphical representation of RTN17ΔTermini with regions to scale. light grey = RHD, dark grey = RHD hydrophobic domains. **B**. Representative image of RTN17ΔTermini-Clover co-expressed with RFP-HDEL and **C**. RTN17ΔTermini-Clover co-expressed with Lifeact-RFP. **D**. Merge images of RTN17.1-Clover co-expressed with Lifeact-RFP, and RTN17ΔTermini-Clover co-expressed with Lifeact-RFP. **E**. Movies used for images in D after persistency analysis using the green channel only in a colour coded hyperstack with 10 frames across 30 s and 25 s, respectively. Scale bars = 10µm for **B**. and **C**. and 2µm for **D**.

5.2.iv – A Chimera construct shows that termini are integral to punctate distribution

The RTN17 termini appear to be responsible for exclusive localisation in puncta, but some punctate structures can still be observed with RTN17ΔTermini. To further investigate the role of the RHD in terms of localisation and characteristics of the full-length protein, a chimeric protein consisting of RTN17.1 termini with the RHD of RTN1 was produced. This chimera was designed to include the N-terminal aa 1-169 and the C-terminal aa 324-431, fused to aa 89-249 from the RTN1 RHD (Fig 5.4A). This RTN1 section was chosen to maintain a consistent length of the protein between the chimera and RTN17.1, as well as this portion containing all of RTN1s hydrophobic regions close to the where RTN17.1 features its TMDs. This exact 156 aa length was also indicated by the SMART database (Letunic et al., 2020) to encompass the full RTN1 RHD. Other studies state the RTN1 RHD to be from amino acid 89-272, however this also includes the APH and linker region C-terminal to the RHD, which do not contribute to the "W" shaped topology (Brooks et al., 2021). The resulting chimeric protein when transiently expressed in tobacco epidermal leaf cells is capable of localising to puncta as observed with RTN17.1. Despite the addition of the RHD from RTN1, which has been shown to mediate tubular hyperconstriction (Tolley et al., 2010), no hyperconstriction or other effects can be observed on the ER, with consistent HDEL labelling throughout the network (Fig 5.4B).

When co-expressed with RTN17.1-mRFP, the proteins show a strong co-localisation, and occupy much more of a cytoskeletal distribution (Fig 5.4C) as seen in some cases of extreme RTN17.1 expression and co-expression with RHD3 (Fig 4.3). This suggests that the oligomerisation capabilities of RTN17.1 are not mediated by the RHD, as previously it has been shown RTN17.1 does not co-localise in puncta with RTN1 (Fig 4.1). The co-localised signals of Chimera-Clover and RTN17.1-mRFP label larger puncta as well as filaments that are longer, straighter, and not always contiguous as an ER tubule would be (Fig 5.4C). As this could indicate a more cytoskeletal alignment, the directionality of these labelled filaments and puncta was assessed (Fig 5.4D, E).

Network skeletons were generated by manually thresholding images featuring co-expression of Chimera-Clover and RFP-HDEL, or Chimera-Clover with RTN17.1-mRFP. The resulting networks were assessed using the inbuilt directionality analysis plugin within ImageJ. The Chimera-Clover construct co-expressed with RFP-HDEL results in a typical polygonal network with HDEL-labelled tubules that occupy an equal distribution of angles, with some slight directionality preference at 40° (Fig 5.4D). In contrast, the cytoskeletal-like labelling of Chimera-Clover and RTN17.1-mRFP shows a much more polar orientation of filaments, with the directionality histogram being skewed towards -90° and +90°, showing that the filaments are horizontally aligned (Fig 5.4E). This difference in alignment suggests that the co-expression of the chimeric protein with RTN17.1 induces cytoskeletal-like labelling and may be a result of greater interaction of RTN17.1 with cytoskeletal components or stronger alignment between ER and cytoskeleton.

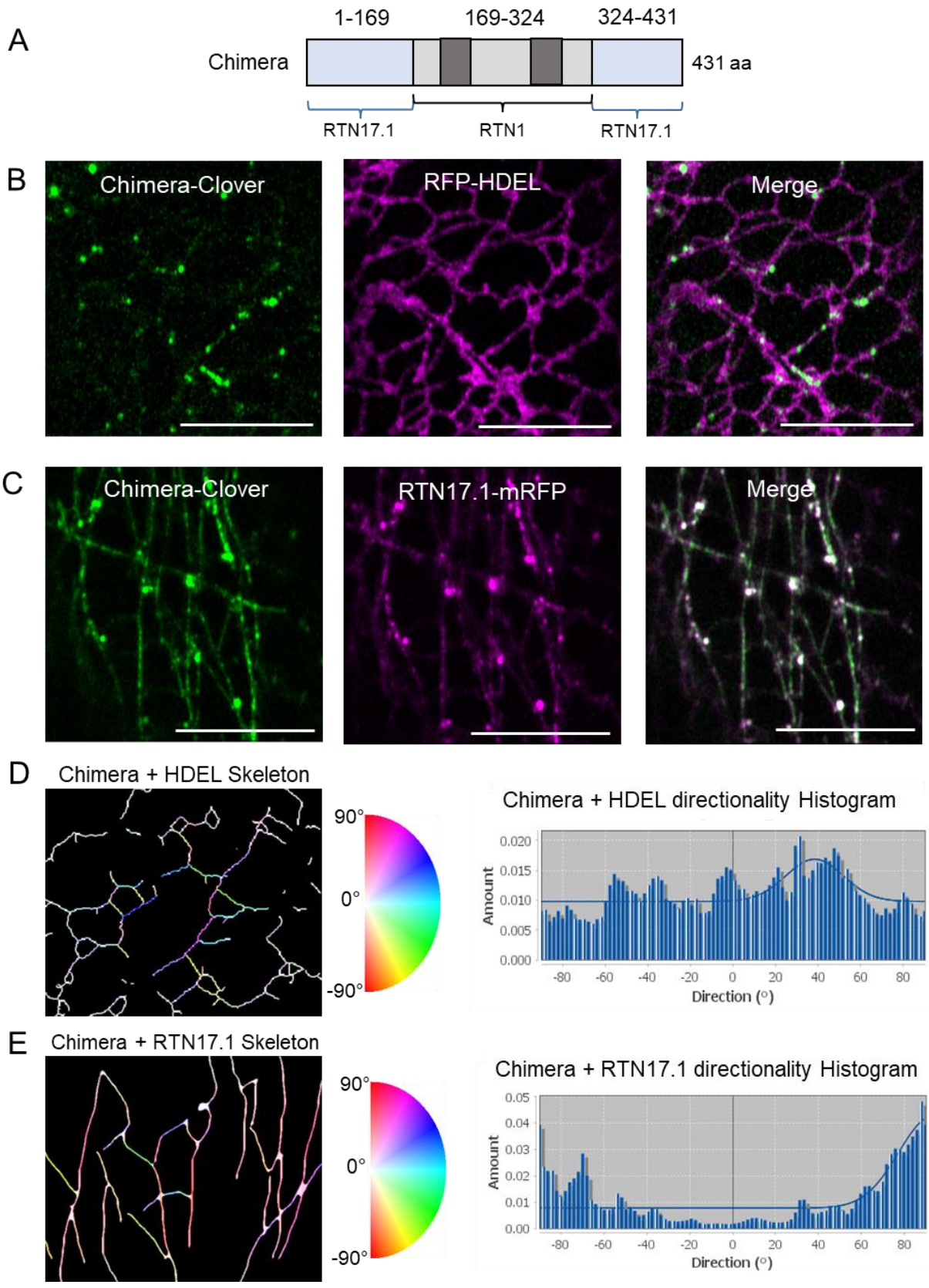
A
1-169
169-324
324-431
Chimera
431 aa
RTN17.1
RTN1
RTN17.1
B
Chimera-Clover
RFP-HDEL
Merge
C
Chimera-Clover
RTN17.1-mRFP
Merge
D
Chimera + HDEL Skeleton
90°
0°
-90°
Chimera + HDEL directionality Histogram
Amount
0.020
0.015
0.010
0.005
0.000
-80
-60
-40
-20
0
20
40
60
80
Direction (°)
E
Chimera + RTN17.1 Skeleton
90°
0°
-90°
Chimera + RTN17.1 directionality Histogram
Amount
0.05
0.04
0.03
0.02
0.01
0.00
-80
-60
-40
-20
0
20
40
60
80
Direction (°)

Figure 5.4 – Chimeric protein localises to puncta and acts synergistically with RTN17.1

A. Graphical representation of Chimera with regions to scale. Light grey = RHD, light blue = terminal extensions. **B.** Representative image of Chimera-Clover co-expressed with RFP-HDEL. **C**. Chimera-Clover co-expressed with RTN17.1-mRFP. Scale bars = 10 μm **D**. Skeletonised networks of examples from **B**, with directionality of tubule angle coloured. Colour wheel for angle representation. Histogram of angles from the skeleton. **E.** Skeletonised networks of examples from **C,** with directionality of tubule angle coloured. Colour wheel for angle representation. Histogram of angles from the skeleton.

5.3 – Discussion

Previously it has been demonstrated that the clade 6 RTNs have distinct properties to that of other clades of Arabidopsis RTNs. Specifically, it has been shown that RTN17.1, RTN21.2 and RTN18 localise throughout the ER (Chapter 3) as puncta with a preference for 3-way junctions (Fig 3.4). RTN17.1 furthermore has a confirmed interaction with the ER morphogen, RHD3, suggesting further importance in the formation of 3-way junctions (Fig 4.2). The clade 6 RTNs all share a generic structure consisting of an RHD with both N- and C-terminal extensions (Fig 2.1). Within the structure there is no homology for particular domains aside from the highly conserved RHD, however both the N- and C- terminus are highly disordered (Fig 2.3). Due to IDRs implications with protein-protein and protein-lipid interactions (Xie et al., 2007), it was imperative to determine if and which of the terminal extensions were acting as functional domains, dictating the unique properties and characteristics observed for RTN17.1, and if the other functional domain of the RHD is distinct to that of clade 1-4 RTN RHDs.

5.3.i - RTN17 Splice variants localise as punctate structures consistent with RTN17.1

Previously experimentation has focussed on the full-length product of the *RTN17* gene, RTN17.1. As details about RTN17.1 have been uncovered, including its unique localisation and interaction with RHD3, the next step was to examine the naturally occurring RTN17 splice variants in terms of their localisation within the ER and any different characteristics compared to the full-length protein. Firstly, RTN17.2 is a natural truncation of the C-terminal extension (Fig 5.1B), which previously has been shown to contain both a putative extra TMD as well as a high degree of intrinsic disorder (Fig 2.3). Surprisingly removal of the RTN17 C-terminus had little effect on the distribution or localisation of the protein, with the puncta still being present and of similar size

(Fig 5.1C; Supplementary Figure 1; Supplementary movie 4). The impact of RTN17.2-Clover expression appears to be more inconsistent than for RTN17.1 for example, which expresses very consistently despite the fluorescent tag used. Across different biological repeats, RTN17.2 produced equal proportions of what appears to be differing degrees of constriction (Fig 5.1D; Supplementary movie 4). When the puncta are more regular in appearance, there is no constriction phenotype that can be observed, with the width of tubules maintaining a regular appearance throughout the length, similar to the effects of RTN17.1 expression. In other cases, there are clear inconsistencies in the signal and widths of ER tubules, usually in association with an RTN17.2 puncta which may indicate some impact on the tubule morphology at these localised points (Fig 5.1D). The final group of RTN17.2 images see clear constriction effects, with HDEL being absent from the length of tubules and condensed into pockets. The RTN17.2 puncta are also less consistent shaped puncta and some slight elongated labelling throughout the tubule (Fig 5.1D). As these examples could all be seen within an individual biological repeat and are all a result of the same OD of infiltration media, it is unclear whether this is a dose dependent effect of RTN17.2 expression, or potentially artefacts produced from ER stress with this construct.

It is interesting to theorise that by deletion of the C-terminal domain and it's putative TMD, the hydrophobic domains of RTN17s RHD may assume the typical "W" shape, or still be capable of inducing hydrophobic wedging, allowing the induction of membrane curvature. TOPCONS consensus predicts that RTN17.2 retains a 2-1 TMD layout in the RHD (Supplementary figure 3) and as such fully elucidating the topology of RTN17.1 would aid in understanding the exact impact of C-terminal deletion and whether this alters the hydrophobic domains within the RHD. Despite this potential constriction effect, with the N-terminal still present, the puncta formation is maintained, and RTN17.2 is unable to diffusely label the tubules and edges of sheets as seen with clade 1-4 RTNs (Tolley et al., 2008; Sparkes et al., 2010). The cell coverage of successful infiltration attempts was much lower than with RTN17.1, and as such a more reliable and consistent construct would allow a broader population of images to be acquired and quantification of the impact of RTN17.2 expression could be achieved.

RTN17.3 was synthesised for generating constructs and use in live cell imaging as it could not be extracted from cDNA. RTN17.3 is comprised of the full sequence of RTN17.1 minus a 13 amino acid deletion in the N-terminal IDR (Fig 5.1D). Upon transient expression of RTN17.3, as with RTN17.1 and RTN17.2, the punctate distribution is retained (Fig 5.1E). Aside from a sparser distribution of puncta, qualitative assessment does not indicate any significant changes in characteristics compared to the full-length protein. However, as with RTN17.2-clover, RTN17.3 was equally unreliable, with transient expression not being successful in a given experiment or having a low % of cell coverage when it is successful. As such full quantification or co-localisation experiments were unable to be completed for the splice variants.

5.3.ii - RTN17.1 N-terminal IDR mediates RHD3 interaction

As RTN17.2 encodes a natural truncation of the C-terminus, a synthetic construct had to be generated to investigate the impact of the N-terminal region of RTN17. RTN17Δ1-168 was produced by removing the first 168 amino acids of the full-length protein, up to the beginning of the RHD. This resulting protein tagged with a C-terminal fluorophore first appears indistinguishable from that of RTN17.1, with a similar distribution of puncta across the ER network. However, when co-expressing RTN17TΔ1-168 with RHD3 the typically strong co-localisation and change in RHD3 distribution when co-expressed with full-length RTN17.1 (Fig 4.2) is abolished by removal of the N-terminal extension. This allows RHD3 to label the ER much more ubiquitously, with only slight enrichment and puncta visible at 3-way junctions as shown in chapter 4 and previous publications (Cao et al., 2008). As RTN17.3 contains a deleted section of the N-terminal IDR, we attempted to investigate whether RTN17.3 and could still co-localise, however the co-expression was never successful.

In general, disordered regions reach a greater degree of surface interface with fewer residues than ordered globular protein interactions, however disordered regions typically span from 30-

200 amino acids long and work as continuous entities rather than segmented sections coming together (Mészáros et al., 2007; Oates et al., 2013). Smaller residues between 10-70 amino acids long that are integral to context-dependent binding within IDRs are known as molecular recognition features (MoRFs; Mohan et al., 2006). These regions undergo disorder-to order transitions as the initial stage of disorder mediated protein-protein interaction (Kotta-Loizou et al., 2013). Assessing the distribution of MoRFs within the RTN17.1 structure does not identify the missing 12 amino acids from RTN17.3 within a predicted MoRF (Malhis et al., 2016)(Supplementary figure 4), and so whilst these missing residues may be present within the binding area involved in RTN17 and RHD3s interaction, it is unlikely to a specific recognition site that is integral to the induction of the protein-protein interaction. A larger proportion of the N-terminal IDR, if not all of it as indicated by the context-binding disorder profile (Fig 2.3; Mészáros et al., 2018), is more likely to be relevant for interaction between RTN17.1 and RHD3

Within the diverse functionality of IDP/IDRs, two specific functions are likely to be relevant to the N-terminal extension of RTN17.1. One mechanism may be that RTN17.1s N-terminus acts as a 'disordered assembler'. This is where a region within a protein in a physiological environment remain disordered, and upon contact with a binding partner, transitions into an ordered protein-complex incorporating multiple proteins (Van der Lee et al., 2014). Examples of this phenomena are those involved in the assembly of the ribosome whereby disordered ribosomal proteins undergo conformational change upon binding rRNA (Scripture & Huber, 2011) and form a rigid multi-component complex, as well as the Axin scaffold protein complex that utilises long disordered termini to accumulate other proteins into a larger multi-protein hub (Xue et al., 2013). This function is why IDP/IDRs are commonplace within hub proteins and scaffolding regions (Haynes et al., 2006; Cortese et al., 2008), which could be the function of RTN17.1 and explain the punctate localisation which consists of RHD3 as well as other proteins involved in the mediation of 3-way junction formation. A similar role of IDR's that may be relevant for RTN17.1 is that of 'disordered effectors. These are when the binding of disordered regions and subsequent disorder-order transition can affect the capabilities of the target protein if such protein contains

a catalytic domain, with the most well studied example being the regulation of Cyclin-dependent kinases via P21 and P27, which are two disordered effectors (Galea et al., 2008). As RHD3 contains a GTPase domain required for the homotypic fusion capabilities of the protein (Lai et al., 2014) it is possible to conceive that the N-terminal extension of RTN17.1 alters the functional capacity of RHD3 by inducing a disorder-order transition in either one of proteins during complex formation.

5.3.iii - RTN17 RHD is potentially involved with association to the actin cytoskeleton

As the functionality of most Arabidopsis RTNs are determined by the properties and topology of the RHD as well as the presence of the APH (Sparkes et al., 2010; Tolley et al., 2010; Breeze et al., 2016), we also truncated both terminal extensions simultaneously to determine how analogous the resulting RHD would be to a clade 1-4 RTN (Fig 5.3A). The resulting 156 amino acid, RTN17ΔTermini protein exhibits some intriguing properties. Firstly, RTN17ΔTermini-Clover expression shows a degree of ubiquitous labelling throughout the ER, not seen in the full-length protein or other isoforms and truncations (Fig 5.3). However, there are still a portion of puncta visible during this, which suggests that the oligomerisation capabilities of RTN17 are intrinsic to the RHD, rather than an interaction as a result of the terminal extensions (Fig 5.3B). When co-expressed with an actin marker, Lifeact-RFP, the majority of puncta correspond with areas in which the ER network overlaps with that of cytoskeleton (Fig 5.3C) and are extremely stable over the observed time scales compared to puncta not co-localising with an actin filament (Fig 5.3E). This is consistent with the properties observed by the full-length RTN17.1 when co-expressed with Lifeact (Fig 5.3D). It is therefore possible that within the RTN17.1 RHD alone, there is the capability to interface with the actin-cytoskeleton, either directly or indirectly through undiscovered interactors. There may also be more general mechanisms impacting punctate

formation, such as stability at these points, as EPCS proteins for example are typically less dynamic and form larger puncta associated with the cytoskeletal networks (Wang et al., 2017).

It is unlikely to be mediated by the RHD3 interaction, as this requires the presence of the N-terminal IDR (Fig 5.2C) and RHD3 has been shown to be more involved with the ER-microtubule interface via ARK1 (Sun et al., 2021). An RHD3 mutation appears to have an impact on actin organisation though, potentially due to overall ER morphology disruption (Hu et al., 2003). A direct interaction with both actin and microtubules has been confirmed to be mediated by the mammalian RTN4B isoform (Rodríguez-Feo et al., 2016), which is comprised of an RHD and a short N-terminal extension and is implicated in tubule formation similarly to the canonical, RTN function (Rämö et al., 2016). However, specifically which aspect of the RTN structure is responsible for this interaction was not confirmed. For plant RTNs the association between RTNs and the cytoskeleton appears to be indirect via proteins such as NET3c and VAP27 and their implications in ER morphology maintenance and EPCS formation (Zhang et al., 2021). Identification of more confirmed interactors of RTN17.1, and greater analysis of the puncta association with the actin cytoskeleton may lead to a more concrete mechanism behind RTN17s RHD and how it may mediate this connection.

As the puncta were also present with the terminal extensions truncated, a chimeric protein containing the 156 amino acids of RTN1s RHD instead of RTN17.1s RHD was designed. This chimera maintained both RTN17.1 terminal extensions, which are highly disordered and implicated in the interaction between RTN17.1 and RHD3 (Fig 5.2). This exchange of RHDs maintains the overall length of the protein at 431 amino acids, but the 2 RHDs share only 31% amino acid identity and differ in lengths of the hydrophobic domains. The resulting protein localises exclusively to puncta across the network, similar to the original full-length protein. This, along with the observation of diffuse labelling present upon deletion of the terminal extensions (Fig 5.3) suggests that to achieve an exclusively punctate labelling requires the terminal IDRs. However, as mentioned previously another mechanism may cause the RHD alone to be capable

of forming punctate structures observed at ER-actin interfaces (Fig 5.3). The punctate localisation is therefore primarily a product of the IDRs, perhaps caused by a combination of factors such as the interaction with RHD3 (Chapter 4), as well as the presence of the C-terminal TMD outside of the RHD which also appears to allow punctate localisation (Fig 5.1B).

Upon co-expression of the chimera with the original RTN17.1, there is a strong colocalization, and cytoskeletal like patterning as seen in some cases of RTN17.1 overexpression (Fig 4.3) as well as co-expression with RHD3 (Fig 4.2). This distribution is distinct from that of a typical ER network, which have a greater variety of different tubule angles as would be expected of a polygonal network. Conversely, this co-expression labels structures with a strongly polarised orientation, with the majority of angles falling within a narrow range of angles (Fig 5.4D,E). Based on this co-localisation it seems the chimeric protein is capable of still interacting with the clade 6, despite not sharing the original RHD. Therefore, the homo-oligomerisation properties of Clade 6 RTNs does not appear to be intrinsic to the RHD. As this distribution and patterning is seen in several cases of RTN17.1 over-expression and combinations (Fig 4.3) it may be that the co-expression of the chimera works synergistically with the full-length protein, resulting in extreme activity levels of RTN17.1. This subsequently pushes the ER into a closer association with the cytoskeleton, which usually acts as an anchor point for remodelling and subsequently where 3-way junctions arise from, hence the change in distribution. Deciphering whether like mammalian RTNs (Rodríguez-Feo et al., 2016), Arabidopsis RTNs of all clades can directly interact with cytoskeletal components, and furthermore which specific part of the protein would greater help the understanding of functions for RTN17.1 and RHD3.

5.3.iv - Summary and conclusion

Overall, the truncations as well as the splice variants offer valuable insight into the domains relevant for RTN17.1s function. By understanding the nature of disordered regions in other proteins it is possible to hypothesise that the N-terminal extension of RTN17.1 either acts as an assembler or effector of RHD3 to facilitate the formation of 3-way junctions. Although an exclusively punctate localisation occurs with either both or either of the N- and C- terminal IDRs (Fig 5.5), there is the ability for limited puncta to form even when the termini have been deleted, which are primarily localised at points in which the ER interfaces with the actin cytoskeleton, and here they are stable throughout the observation duration.

These factors, including the association between RTN17.1 and cytoskeletal components (Fig 4.3) suggest that there may be a currently undiscovered interactor of RTN17.1 that is responsible for this association with the cytoskeleton and mediated via the RHD (Fig 5.5). As mammalian RTNs are capable of direct interaction with cytoskeletal components (Rodríguez-Feo et al., 2016), it is also possible that the cytosolic facing loop of the RTN17.1 RHD may directly interact with a cytoskeletal component as this is the longest cytosolic residing section of the RTN17ΔTermini construct and therefore be physically capable of contacting the cytoskeleton. Furthermore, in mammalian proteins the cytosolic facing loop of RTN4 is integral to the interactions with NogoR, and subsequently of key importance to the overall function of the protein in the physiological context of neurite outgrowth (Fournier et al., 2001; Li et al., 2005), suggesting that the sequence of this length and general structure is capable of mediating protein-protein interactions.

This cytoskeletal interaction may be utilised as an anchor point for 3-way junction formation, as these cytoskeletal-ER interfaces often localise at EPCSs and are mediated by other proteins such as NET3C and VAP27 (Wang et al., 2014; Wang et al., 2016). Unfortunately, co-expression with these proteins with either the full-length RTN17.1 or splice variants and truncations was unsuccessful, but these proteins are prime candidates for potential interactors that mediate this

association between RNT17.1 and the actin cytoskeleton. Subsequently by RTN17.1 recruiting RHD3 at these points in the network via the N-terminal IDR, or by inducing the correct folding of RHD3, homo-typic tubular fusion to occur and maintain the correct morphological organisation of the ER.

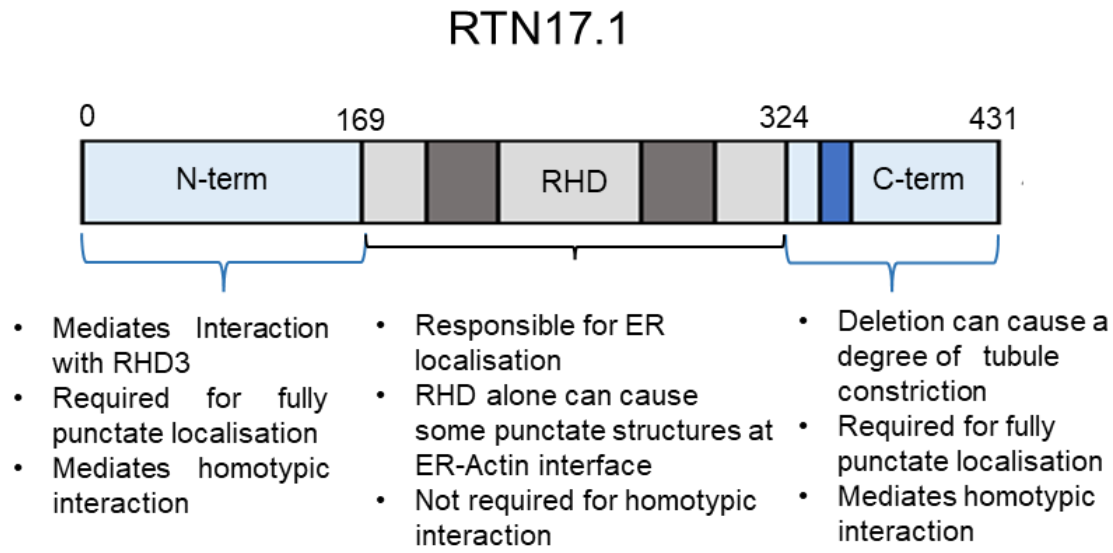

Figure 5.5 – Graphical summary of domains and respective functions

Summary of RTN domains and their relevant impacts on RTN17.1 function. Grey = RHD, dark grey = hydrophobic domains, light blue = terminal IDRs, and dark blue = putative TMD in C-terminal extension.

Chapter 6 – Impact of Clade 6 Reticulon Expression

6.1 – Introduction

Currently, it has been shown that clade 6 RTNs contain unique properties when compared to other clades of Arabidopsis RTNs. In particular, the distribution, interactions and function of the proteins is distinct from the classical tubule forming role of RTNs (Voeltz et al., 2006; Hu et al., 2008; Tolley et al., 2010). Typical RTNs have a morphogenic role, in which the properties of the RHD induce and maintain curvature in tubules and the edges of sheets. As such, the generic structure of 4 TMDs within the RHD and typical RTN function is highly conserved across all eukaryotic RTNs (Tolley et al., 2010). Although clade 6 RTNs contain this conserved RHD, they do not localise or function via the same mechanism as classical RTNs and contain terminal extensions which may impact the "W" shaped topology of the protein. However, despite the distinct properties of Arabidopsis clade 6 RTNs, a morphogenic impact on the ER structure when expressing these proteins transiently in tobacco epidermal leaf cells has still been observed. Qualitatively a lack of cisternae can be detected, and a more minimal network with fewer, longer tubules. These morphological changes do not appear to be a result of induced hyper-constriction, as previously shown (Fig 3.5) and so to understand how the clade 6 still is capable of shifting the balance of the network from cisternal to tubular, the effects on the ER network structure upon expression RTN17.1 and RTN21.2 will be assessed quantitatively.

The distribution of the ER differs across Eukarya, with mammalian cells having ER throughout the cytoplasm occupying a larger cellular volume, whereas in plants the ER is effectively a single layer called the cortical ER due to the presence of the vacuole. Beyond this, the general morphological features that make up the ER are consistent. The peripheral ER in all Eukarya

consists of the cisternae, tubules and interconnecting 3-way junctions to form a polygonal network (Terasaki & Jaffe, 1991; Voeltz et al., 2002; Sparkes et al., 2009a). This organisation is extremely dynamic between cell type, through development (Ridge et al., 1999) and over short time scales (Quader et al., 1989). The majority of the dynamics are mediated by the actin cytoskeleton (Ueda et al., 2010) mediated by myosin XI's (Sparkes et al., 2009a), with some specific aspects such as anchor points and tubule elongation occurring via microtubule interactions (Hamada et al., 2014). However, establishing the general structure ER requires the balance and activity of three classes of protein, namely the RTNs, RHD3/ATL/Yop1p and LNP proteins.

6.1.i - RTNs generate ER tubules

The first experiment to show RTNs having a direct impact on ER morphology rather than their function in neurite outgrowth was when RTN4 was shown to produce a tubular network from suspended Xenopus membrane fractions (Voeltz et al., 2006). Furthermore, the localisation being exclusive to areas of high membrane curvature, and an abolishment of peripheral ER sheets upon over-expression of RTN4a further confirmed this role in forming the tubular aspects of the ER network (Voeltz et al., 2006). In yeasts, deletion of Rtn1p resulted in a predominantly cisternal cortical ER with a lack of tubular structures (De Craene et al., 2006). Subsequently Arabidopsis RTNs from clade 1-4 were shown to be responsible for forming and stabilising tubules within the network and producing a hyperconstriction phenotype upon overexpression (Sparkes et al., 2010). This is based on the properties of the RHD which is conserved across Eukarya and contains two hydrophobic domains (Nziengui et al., 2007). Each hydrophobic domain contains two transmembrane domains that act as a hydrophobic wedge, and subsequent oligomerisation stabilises this curvature induction (Tolley et al., 2010), consistent with the capabilities and properties of other Eukaryotic RTNs (Shibata et al., 2008). These morphological changes in mammalian, yeast and plant cells observed upon manipulating RTN activity via deletion, mutation

or over-expression produce extremely dramatic phenotypes, and have largely only been qualitatively assessed.

6.1.ii - RHD3/ATL and Sey1p

The GTPases, ATL, yeast Sey1p and Arabidopsis RHD3 are responsible for the homotypic fusion of tubules and subsequent formation of 3-way junctions (Hu et al., 2009; Anwar et al., 2012), via the dimerization (Moss et al., 2011) and hydrolysis of GTP (Orso et al., 2009). The 2 transmembrane domains as well as C-terminus of ATL has been shown to be required for efficient fusion to occur and may be due to the presence of an APH in the c-terminus that may induce some membrane curvature, to subsequently act as the point in which membranes can fuse, where the TMD's are required for the membrane anchoring and oligomerisation capabilities (Liu et al., 2012). ATL is both essential and sufficient in producing a polygonal network as exampled by a reconstituted membrane system forming a network in a GTP-dependent manner, whereas Sey1p requires the presence of other curvature stabilising proteins such as Yop1p (Powers et al., 2017). This may be due to a lack of the APH in Sey1p, whereas ATL is capable of inducing membrane curvature, although this is not confirmed. Although the 3 proteins share the same general structure despite sequence disparity, RHD3 has only been shown to require the C-terminus due to phosphorylation of certain residues, but the other aspects of the C-terminal structure have not been tested or shown to be consistent with ATL (Ueda et al., 2016).

Stable RHD3 overexpression in Arabidopsis was shown to rescue the root defected and general dwarfism of the *rhd3-1* Arabidopsis mutant, and live cell imaging revealed that YFP-RHD3 localises throughout the ER as well as occasionally concentrated in sparse puncta along tubules and at 3-way junctions (Chen et al., 2011). Although no qualitative assessment of the ER morphology was acknowledged in the initial study of RHD3 live cell imaging, the polygonal

network appears similar to that of HDEL labelled ER, with a perhaps smaller proportion of cisternae present, similar to what our own images suggest. Expression of a non-functional mutant, RHD3(S51N) that perturbs the GTPase domain, does have a drastic effect on ER morphology, producing condensed and unbranched tubules (Chen et al., 2011). This morphology is also exhibited when observing the ER of *rhd3-8* mutants (Zhang et al., 2013, as well as in the gom8 mutant allele which has a mutation in the membrane anchor region, but despite the effected morphology fusion was still observed (Stefano et al., 2012). These studies all suggest that RHD3, with all the correct unmutated structural aspects is extremely important in the generation of the fine polygonal network of the ER and is functionally similar and complementary to ATL and Sey1p (Zhang et al., 2013), although repeat complementation studies did not find RHD3 capable of complementing Sey1p mutation (Chen et al., 2011).

6.1.iii – Impact of Lunapark proteins on ER morphology

Arabidopsis AtLNP1 and AtLNP2 proteins upon over-expression cause an increase in the proportion of ER cisternae in a dose dependent manner, with AtLNP1 labelling cisternae moreexclusively, and AtLNP2 the whole network (Kriechbaumer et al., 2018a). LNP proteins are evolutionarily conserved across Eukarya (Spitz et al., 2003), although their implications on ER morphology appears to differ slightly from Arabidopsis LNP. Deletion of yeast Lnp1 results in a densely reticulated ER network with an increased number of small polygons (Chen et al., 2012), whereas *lnp1* and *lnp1/lnp2* amiRNA Arabidopsis mutants have a decrease in the proportion of cisternae, and larger polygonal regions (Kriechbaumer et al., 2018a). Furthermore, mLnp1 deletion increased the presence of cisternae within COS-7 cells, as well as a decrease in 3-way junctions (Chen et al., 2015), and inactivation of Lnp in Xenopus eggs during interphase causes a transition from ER tubules to cisternae (Wang et al., 2013). This is similar to the changes observed during mitotic events, whereby the ER changes from primarily distal tubules aside from the NE, to condensed and stacked cisternae (Lu et al., 2009), suggesting Lnp activity may be implicated

in such events. This discrepancy may be due to the localisation of mLnp1 and Lnp1p compared to AtLNP1/AtLNP2, where rather than localising or labelling cisternae, the homologues instead localise and are thought to stabilise 3-way junctions (Chen et al., 2012; Chen et al., 2014). It is suggested that mLnp1 and Lnp1p have antagonistic relationships with ATL (Wang et al., 2016; Zhou et al., 2019) and Yop1p respectively (Chen et al., 2012), the GTPases that mediate the initial formation of 3-way junctions.

This interplay between proteins may be based on interaction and ubiquitination properties of the LNP proteins, as both mLnp1 (Zhao et al., 2016) and AtLNP1/AtLNP2 (Sun et al., 2020) have been shown to act as ubiquitin ligases, with AtLNP directly ubiquitinating RHD3. Although LNP proteins across Eukarya share lots of similar properties, the end results of their over-expression or deletion appear to have differing effects, and the complexity of their interaction with the GTPases and role in forming 3-way junctions, or cisternae requires further study into the biogenesis of both morphologies. It is also worth noting that in mammalian cells, deletion of a protein Climp63 reduces the presence of peripheral ER sheets, and over-expression increases the cisternal proportion of the network, similar to AtLNP although the proteins share no sequence or structural identity (Shibata et al., 2010). As there is no Arabidopsis homologue identified for Climp63, it is possible that regulation of cisternae formation within the ER is controlled via different mechanism between plants and the rest of Eukaryotic kingdoms of organisms.

6.1.iv - Aims and objectives

To fully interpret how the morphology of such complicated, dynamic and diverse organelle is truly achieved, a greater emphasis on quantitative analysis is required. To achieve this, Pain et al developed the software AnalyzER to produce detailed information from a multitude of parameters in a semi-high through put workflow (Pain et al., 2019). In this chapter this powerful tool will be used to quantify and confirm the previous qualitative assessments of RTN17.1 and RTN21.2 and pinpoint the specific effects of overexpressing these proteins on ER morphology to

better understand their role within the ER and functional relation to other Arabidopsis RTNs. Furthermore, whilst it was not possible to interrogate the morphological effects of decreased clade 6 RTNs expression, with the use of mutant lines for RTN17, RTN18 and RTN21, they were successfully utilised for quantitative lipidomic analysis, to further identify potential phenotypes related to modulating expression of clade 6 RTNs.

6.2 – Results

6.2.i - Utilising AnalyzER for quantitative analysis of the ER morphology

In this chapter, the AnalyzER software package (Pain et al., 2019) was utilised to extensively quantify the morphological changes in the ER produced by RTN17.1 or RTN21.2, respectively. Here images of the HDEL labelled ER network co-expressed with RTN1.1 or RTN21.2, are compared against a HDEL label alone. Firstly, the initial image (Fig 6.1A) is imported as a time series. Following this, a network template and phase-congruency based enhanced image is produced (Fig 6.1B). This step allows accurate identification of tubules in an intensity independent manner as segmentation based on intensity can often lead to errors and discontinuous tubule labelling. From this enhanced image, a single pixel wide skeleton can be isolated, and cisternal boundaries can be labelled (Fig 6.1C). Cisternal areas are regions greater than 0.3 μm^2 based on prior literature characterising non-cisternal junctions and static points, which are subsequently incorporated as tubular nodes (Sparkes et al., 2009a). Regions within the ER network that are bordered by fully enclosed tubules or cisternal perimeters are then isolated as polygonal regions from which morphological parameters can be quantified (Fig 6.1D). Once the parameters have been established and set within the software, a vast array of parameters measuring morphological dynamics or structural aspects can be interrogated further in detail. One example is the production of graph representation for several tubular parameters such as length (Fig 6.1E), width, speed and persistency. These graphs assess the properties of each tubule within an image and assigns the specific value as a colour grade. From each image the software produces an extensive datasheet detailing all the parameters (100+) with every value for every individual feature segmented. This data can then be compiled, processed, and analysed for statistical significance in the AnalyzER stats package.

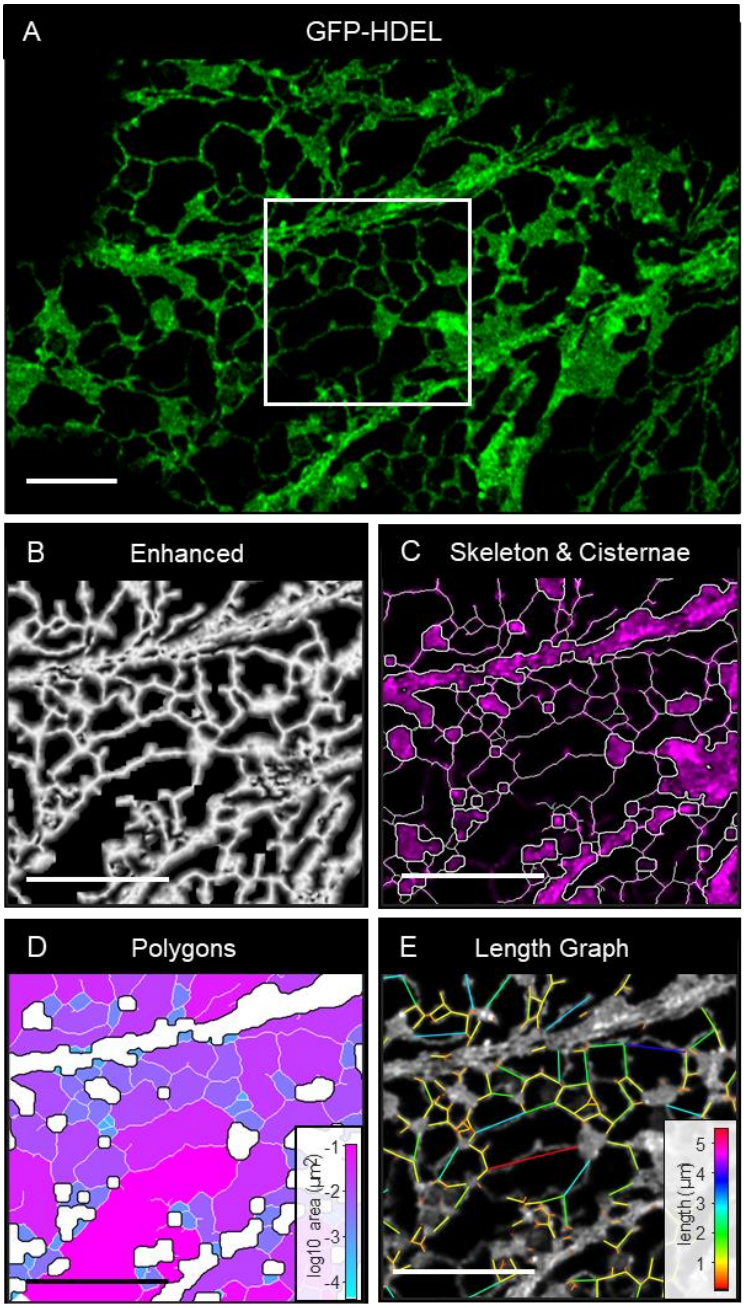

Figure 6.1 – Producing quantitative data from confocal images of ER networks.

A. Initial image of GFP-HDEL labelled ER, from transient expression in tobacco leaf epidermal cells. White box represents zoomed portion for more detail in the processed images. **B**. Enhanced network mask from phase-congruency analysis to allow intensity independent measures. **C**. Tubules represented by a pixel-wide skeleton (green), and cisternae perimeter (white). **D**. Polygonal regions colour coded by the area, with cisternal boundaries (black). **E**. Template network with tubule length graph superimposed, with colour coded lengths. All scale bars represent 5 µm.

6.2.ii - RTN17.1 and RTN21.2 over-expression produce a distinct ER morphology

As mentioned, a control data set consisting of just GFP-HDEL labelled networks (Fig 6.2A)(n=23 across 3 biological experimental repeats, where n is the number of independent 20 frame time series images) is to be compared with networks from mCherry-RTN17.1 co-expressed with GFP-HDEL images (Fig 6.2B)(n=28), as well as GFP-RTN21.2 co-expressed with RFP-HDEL (Fig 6.2C)(n=27). No RFP based RTN21.2 construct was consistent enough in its expression to be utilised for this analysis, however RFP-HDEL was shown to have identical labelling properties of the ER network so was deemed suitable for use in this comparison (Pain et al., 2019). From these datasets, a multi-variate analysis of variance (MANOVA) was carried out to determine whether across 23 selected parameters there is a statistically significant distinction between the ER morphologies of HDEL labelled networks when co-expressed with RTN17.1 or RTN21.2. Here it is confirmed that each treatment is significantly altered by co-expression, under all hypothesis tests (Pillai's trace $p = 8.0477e^{-24}$, Roy's largest root $p = 6.9987e^{-16}$, Wilks' Lambda $p= 7.1241e^{-24}$, Hotelling's T^2 $p=6.0255e^{-24}$). The visual representation also shows the treatments cluster effectively for all observed parameters (Fig 6.2D). From the MANOVA, subsequent ANOVA analysis can be utilised to reveal which individual metrics included in the analysis are significantly different between the treatments. These are detailed in Table 1, and later in this chapter each category will be discussed separately to fully analyse the statistics and differences induced by expression of RTN17.1 and RTN21.2. From this analysis the mean values for each treatment within a parameter are also given, and so % differences compared to the control can be determined for both RTN17.1 and RTN21.2 expression (Table 1).

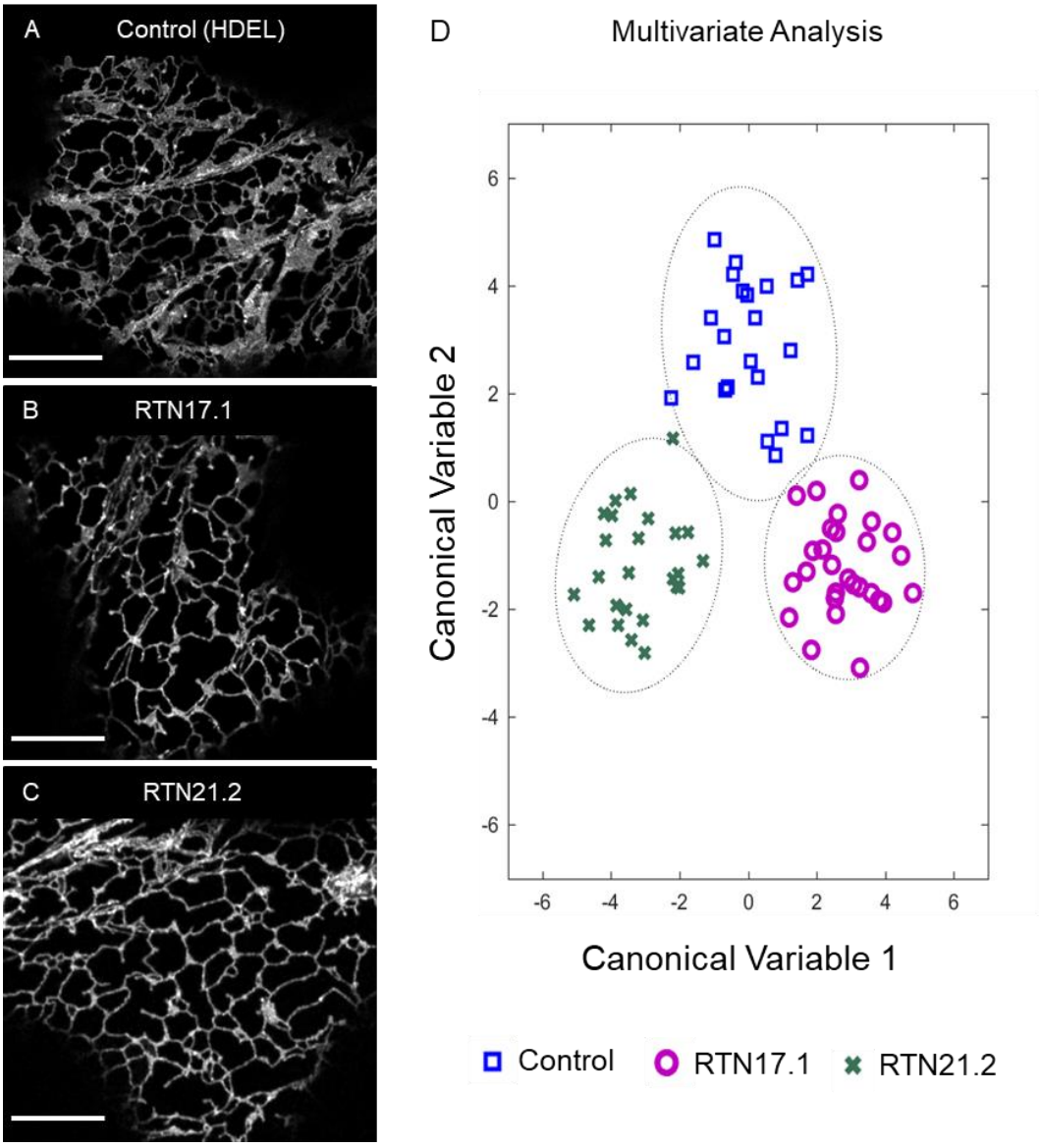

Figure 6.2 – Multivariate analysis of RTN17.1 and RTN21.2 over-expression compared to a HDEL-labelled control network.

Representative network image for **A.** GFP-HDEL labelled ER (n=23 across 3 biological experimental repeats, where n is the number of independent 20 frame time series), **B**. mCherry-RTN17.1 co-expressed with GFP-HDEL (n=28), and **C**. GFP-RTN21.2 co-expressed with RFP-HDEL (n=27). Each image contains 20 frames for dynamic analysis. Scale bar represents 10μm. **D**. Scatter plot of canonical variable separation based on over-expression. Dotted line represents $p<0.05$.

Table 6.1 – ANOVA results from multivariate analysis and parameter changes from mean.

ANOVA results of variables included in MANOVA. Confidence intervals (CI) * = p<0.05, ** = p<0.01, *** - p<0.001. Difference from control mean represented as % increase (blue bar) or decrease (orange bar).

Category	Parameter	ANOVA P Value	CI	Treatment	Difference from mean (%)
Tubule	Length	0.000345807	***	RTN17.1	15.17
				RTN21.2	17.81
	Speed Local	3.46812E-07	***	RTN17.1	-44.98
				RTN21.2	-45.46
	Speed Max	5.75398E-07	***	RTN17.1	-42.53
				RTN21.2	-42.31
	Flow Coherence	0.066625503		RTN17.1	-1.77
				RTN21.2	-2.64
	Persistency	0.003956214	**	RTN17.1	10.65
				RTN21.2	15.21
Cisternae	Contrast	0.018021762	*	RTN17.1	20.39
				RTN21.2	1.53
	Correlation	1.15749E-11	***	RTN17.1	-0.97
				RTN21.2	3.37
	Energy	0.117715369		RTN17.1	-6.94
				RTN21.2	-18.34
	Homegeneity	0.017054747	*	RTN17.1	-4.18
				RTN21.2	-1.49
	Speed Local	7.14181E-07	***	RTN17.1	-44.70
				RTN21.2	-45.91
	Speed Max	8.20412E-09	***	RTN17.1	-45.28
				RTN21.2	-44.80
	Flow Coherence	0.139692296		RTN17.1	2.84
				RTN21.2	0.70
	Persistency	0.005827446	**	RTN17.1	0.99
				RTN21.2	11.69
	Circularity	0.069838128		RTN17.1	2.62
				RTN21.2	1.52
	Elongation	0.878643262		RTN17.1	0.39
				RTN21.2	1.49
	Roughness	0.210945307		RTN17.1	-4.33
				RTN21.2	-4.61
	Area	0.014598698	*	RTN17.1	-18.07
				RTN21.2	-13.72
Polygons	Area	0.00603774	***	RTN17.1	31.35
				RTN21.2	31.84
	Circularity	0.041633677	*	RTN17.1	-1.25
				RTN21.2	-1.86
	Roughness	0.096937348		RTN17.1	2.19
				RTN21.2	0.76
	Elongation	0.028909899	*	RTN17.1	2.75
				RTN21.2	-1.11

6.2.iii - Tubule length is increased, and polygonal region area decreased by RTN17.1 and RTN21.2 expression.

Of the static parameters pertain to tubule morphologies, tubule length is of most interest. This can be visually assessed by overlaying the tubule graph image on the template networks for Control (Fig 6.3A), RTN17.1 (Fig 6.3B) and RTN21.2 (Fig 6.3C). Specifically looking at static polygonal parameters, the area is the most important measure of morphological changes, and other features such as elongation of polygonal regions may reveal how in which the areas are changing due to co-expression (Fig 6.3D, E, F). For tubule length we see a 15.17% and a 17.81% increase in RTN17.1 ($p = 0.009$) and RTN21.2 ($p = 0.0003$) overexpression respectively (Fig 6.3G). The polygonal region area is increased in both co-expressions, with 31.35% increase in RTN17.1 and 31.84% for RTN21.2 however despite the similar percentage increases, only RTN21.2 is significant compared to control ($p = 0.004$) (Fig 6.3H). This increase in polygon area is not associated with a change in directionality of the polygons, with only minor (<3%) increases or decreases in regard to circularity, roughness and elongation (Fig 6.3I). Elongation is a measure of the ratio between major and minor axis through the polygon. This suggests shape and perimeter features of the polygonal areas in the control and co-expressions are the same, but simply occupy a greater area in the RTN17.1 and RTN21.2 over-expression networks.

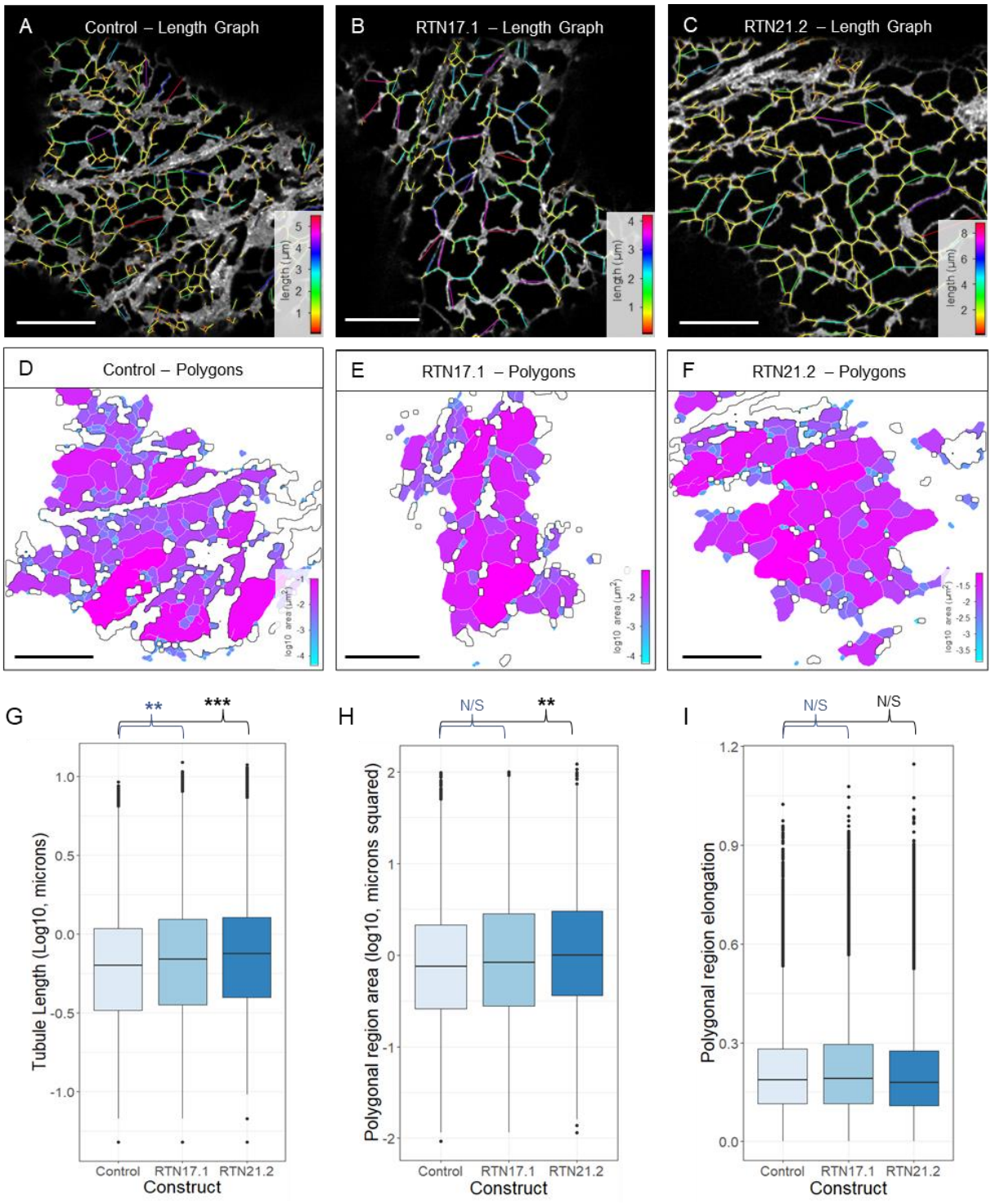
A
Control – Length Graph
B
RTN17.1 – Length Graph
C
RTN21.2 – Length Graph
length (µm)
D
Control – Polygons
E
RTN17.1 – Polygons
F
RTN21.2 – Polygons
log10 area (µm²)
G
**
***
Tubule Length (Log10, microns)
H
N/S
**
Polygonal region area (log10, microns squared)
I
N/S
N/S
Polygonal region elongation
Control
RTN17.1
RTN21.2
Construct

Figure 6.3 – Static tubule and polygon parameter assessment

Representative network template with overlayed length graph from **A**. Control (GFP-HDEL) labelled ER **B**. mCherry-RTN17.1 co-expressed with GFP-HDEL and **C**. GFP-RTN21.2 co-expressed with RFP-HDEL. Same dataset but with Polygonal regions labelled from **D**. Control, **E**. RTN17.1, and **F**. RTN21.2. Scale bars represent 10µm. **G**. Bar graph of tubule lengths comparing between Control, RTN17.1 and RTN21.2 datasets. Control vs RTN17.1 p value = 0.009. Control vs RTN21.2 p Value = 0.0003. H. Bar graph of polygonal region areas. Control vs RTN21.2 p Value = 0.004. I. Bar graph of polygonal region elongation. Dots represent outliers.

6.2.iv - Cisternal area is decreased by RTN17.1 over-expression

Cisternal parameters are largely split between static morphological features, textural parameters and dynamic parameters, of which the former two will be featured in this section. During the analysis the cisternae are segmented from the ER network and can be measured individually. From this the areas, perimeter and other shape measures can be taken (Fig 6.4A- C). Furthermore, as fluorophore signals even within a cisterna are not uniform, as well as the presence of fenestrations, and a generally uneven signal intensity across a typical cisternae (Ridge et al., 1999; Nixon-Abel et al., 2016) it is necessary to assess this signal discrepancy across these subdomains, which is referred to as texture. The cisternal area is significantly decreased in RTN17.1 expression, by 18.07% ($p = 0.11$), and decreased by 13.72% with RTN21.2 co-expression but not to a statistically significant degree (Fig 6.4D). Similarly, to the polygonal regions, the circularity, roughness, and elongation (Fig 6.4E) are only minorly (<5%) affected by co-expression with RTN17.1 or RTN21.2, with none of these parameters being significantly different compared to control. Again, this suggests the shape of the cisternae are unaffected by over-expression, however the overall area does increase, possibly proportional to the increase in tubule length and polygonal region area. Cisternae contrast, which is a texture measure comparing intensity differences between neighbouring pixels is significantly increased in RTN17.1 by 20.39% ($p = 0.031$), and only minorly affected (1.53%) by RTN21.2 expression (Fig 6.4F). Cisternae homogeneity compares distribution of elements in the grey level co-occurrence matrix (GLCM). Cisternae homogeneity is significantly decreased in RTN17.1 by 4.18% ($p = 0.02$), and decreased by 1.49% in RTN21.2 co-expression, but not to a significant degree. An idealised cisterna would have a cisternal contrast measure of 0, and a cisternal homogeneity measure of 1 of which all datasets are close to, however along with the cisternal decrease that is strongest in RTN17.1 co-expression, there also appears to be textural differences in the RTN17.1 group, though not in the RTN21.2 suggesting they are closer aligned with a normal cisterna in terms of texture measures.

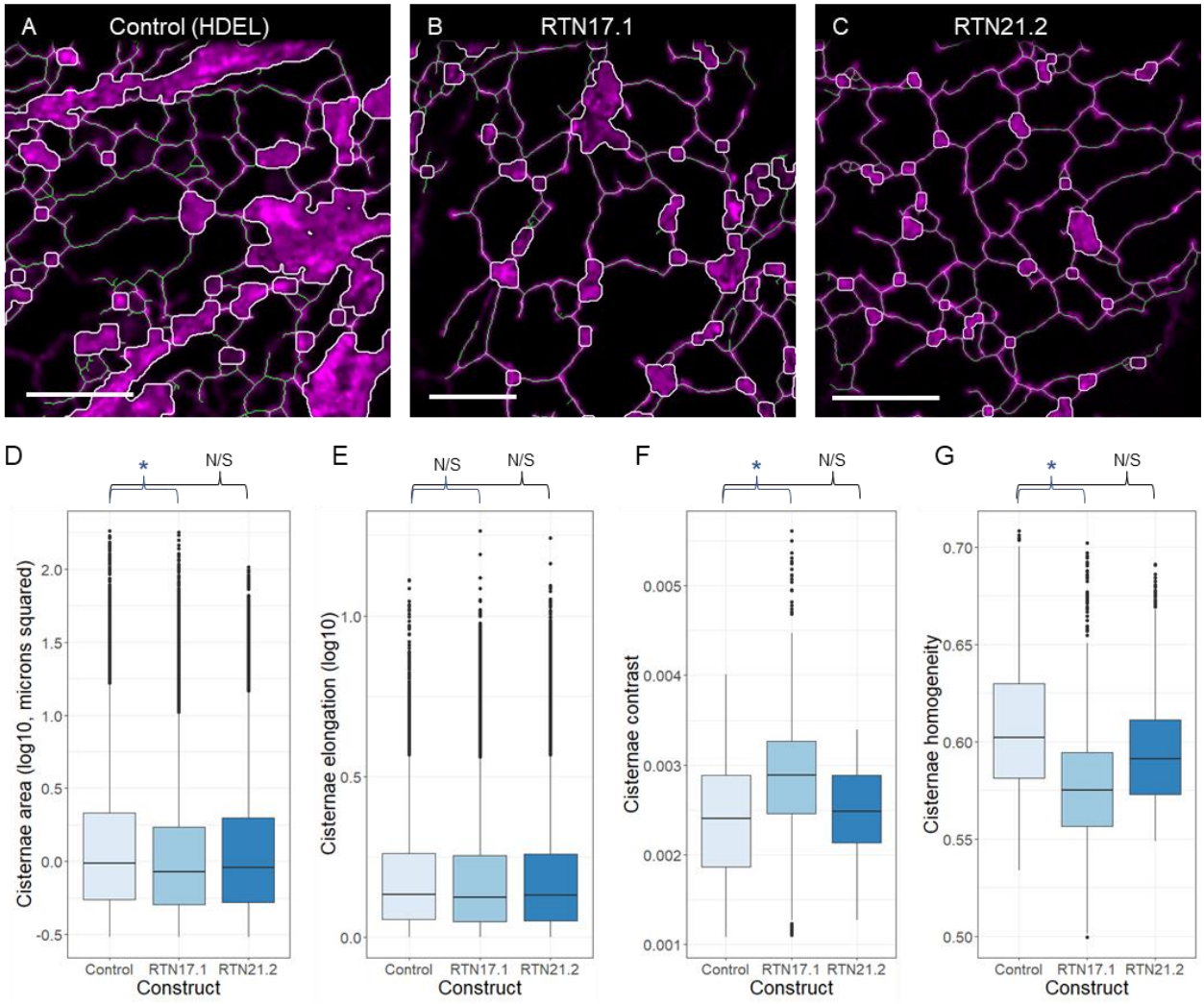

Figure 6.4 – Static cisternal morphological parameter assessment

Representative network template with overlayed tubule skeleton (green) and cisternae perimeter (white) graph from **A**. Control (GFP-HDEL) labelled ER, **B**. mCherry-RTN17.1 co-expressed with GFP-HDEL and **C**. GFP-RTN21.2 co-expressed with RFP-HDEL. Scale bars represent 10µm. **D**. Bar graph of cisternal areas comparing between Control, RTN17.1 and RTN21.2 datasets. Control vs RTN17.1 p value = 0.01. **E**. Bar graph of cisternal elongation. **F**. Bar graph of cisternal contrast. RTN17.1 p value = 0.03. **G**. Bar graph of cisternal homogeneity. RTN17.1 p value = 0.01756. Dots represent outliers.

6.2.v – RTN17.1 and RTN21.2 over-expression creates more persistent and slower moving ER sub-compartment

By utilising time series images in the AnalyzER software package, network dynamics can also be assessed. Each image contains 20 frames with a 1.04 second frame interval, in which optical flow measures can be taken via a Farnebäck algorithm which calculates velocity of pixel groups, and the segmented cisternae and tubules can be assessed independently. From this the local (average) speed, maximum speed and other measures pertaining to optical flow can be deducted. For persistency analysis, frames with a lag of 12 seconds are compared to determine which pixels were stationary throughout the given time frame indicating stable points within the network (Fig 6.5A, B, C). Both tubule local (Fig 6.5D) and tubule max speed (Fig 6.5E) are vastly decreased in RTN17.1 co-expression group, with 44.98% ($p = 3.90E^{-06}$) and 42.53% reductions ($p = 5.37E^{-06}$) respectively, and similar decreases for RTN21.2 with 45.46% ($p = 2.97E^{-06}$) for local speed and 42.31% ($4.38E^{-06}$) for maximum speed. This is accompanied by a significant increase of 10.65% in tubule persistency for RTN17.1 ($p = 0.01$), and an even further increase in the RTN21.2 group, with an increase in tubule persistency of 15.21% ($p = 0.001$) (Fig 6.5F). A similar trend is observed with cisternal local (Fig 6.5G) and cisternal max speed (Fig 6.5H) both being decreased in RTN17.1 co-expression group, with 44.70% ($p = 7.53E^{-06}$) and 45.28% reductions ($p = 1.00^{-07}$) respectively. Cisternal local and max speeds are both decreased also for RTN21.2 with 45.91% ($p = 4.57E^{-06}$) for local speed and 44.80% ($p = 1.52E^{-07}$) for maximum speed. Similarly, to that of the tubule persistency, this decrease in speed is associated with in an increase in cisternal persistence for RTN21.2 co-expression, with an 11.69% ($p = 0.01$). As was the case with tubular persistency, RTN21.2 co-expression has a greater impact on persistency, as RTN17.1 co-expression only increased cisternae persistency by 0.99% which was not statistically significant.

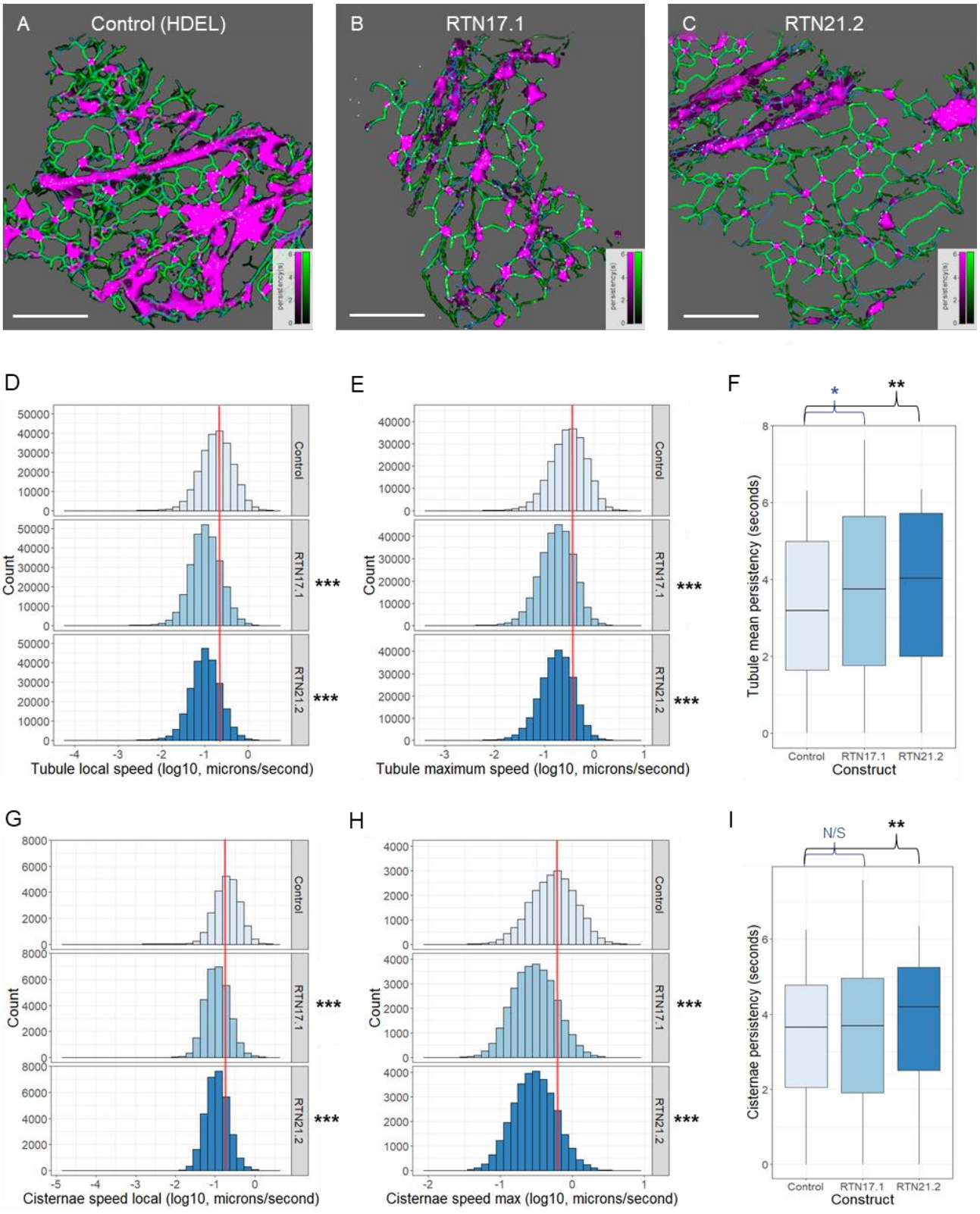
A
Control (HDEL)
B
RTN17.1
C
RTN21.2
D
Count
Control
RTN17.1
RTN21.2
***
***
Tubule local speed (log10, microns/second)
E
Count
Control
RTN17.1
RTN21.2
***
***
Tubule maximum speed (log10, microns/second)
F
*
**
Tubule mean persistency (seconds)
Control
RTN17.1
RTN21.2
Construct
G
Count
Control
RTN17.1
RTN21.2
***
***
Cisternae speed local (log10, microns/second)
H
Count
Control
RTN17.1
RTN21.2
***
***
Cisternae speed max (log10, microns/second)
I
N/S
**
Cisternae persistency (seconds)
Control
RTN17.1
RTN21.2
Construct

Figure 6.5 – ER dynamic parameter assessment

Representative network showing tubule persistency (green shades) and cisternae persistency (magenta shades) from **A**. Control (GFP-HDEL) labelled ER, **B**. mCherry-RTN17.1 co-expressed with GFP-HDEL and **C**. GFP-RTN21.2 co-expressed with RFP-HDEL. Scale bars represent 10μm. **D**. Histogram of tubule local speed comparing between Control, RTN17.1 and RTN21.2 datasets. Control vs RTN17.1 p value = $3.90E^{-06}$. Control vs RTN21.2 p value = $2.97E^{-06}$. **E**. Histogram of tubule maximum speed. Control vs RTN17.1 p value = $5.37E^{-06}$. Control vs RTN21.2 P value = $4.38E^{-06}$. **F**. Bar graph of tubule persistency. Control vs RTN17.1 p value = 0.01. Control vs RTN21.2 P value = 0.01. **G**. Histogram of cisternae local speed. Control vs RTN17.1 p value = $7.53E^{-06}$. Control vs RTN21.2 P value = $4.57E^{-06}$. **H**. Histogram of cisternae maximum speed. Control vs RTN17.1 p value = $1.00E^{-07}$. Control vs RTN21.2 p value = $1.52E^{-07}$. **I**. Bar graph of cisternae persistency. Control vs RTN21.2 p value = 0.01. Red lines represent mean of control speeds.

6.2.vi - Mutation of Clade 6 RTNs affects lipid composition

Despite the identification and confirmation of knock out mutant lines for clade 6 *RTN* genes, *RTN17*, *18* and *21,* attempts to produce stably transformed lines with an ER marker to allow quantification of the ER were unsuccessful. However, the lines were successfully assessed for their lipid phenotypes via lipidomic analysis (Fouillen et al., 2018). This experiment explored the quantitative changes in total lipid production of the mutant root and leave sections compared to a wild type control. In 15 day old Arabidopsis leaves, deletion of *RTN17* results in a 14% increase in phosphatidylcholine (PC) content (Fig 6.6A), 9% increase for phosphatidylethanolamine (PE) (Fig 6.6B), 24% for phosphatidylserine (PS) (Fig 6.6C), 23% for phosphatidylinositol (PI) (Fig 6.6D), and 14% for sterol content. (Fig 6.6E). Conversely, in 15 day old Arabidopsis roots, deletion of *RTN17* results in decreases of 13%, 17%, 28%, 32% and 14% for PC, PE, PS, PI and sterols respectively (Fig 6.6). Of these changes in lipid content, for *RTN17* they were all statistically significant, except for the increase in leaf sterol content (Fig 6.6).

For deletion of *RTN18*, there was only an increase of 1% in leaf PC (Fig 6.6A) content, and 6% in PS (Fig 6.6C). Otherwise, there were primarily decreases in lipid content, ranging from 13%-41% across the sampled lipid types in roots (Fig 6.6), and reductions of 10% in leaf PE (Fig 6.6B), 14% in leaf PI (Fig 6.6D), and 1% in leaf sterol content (Fig 6.6E). Of the leaf changes, only the PE was statistically significant, whilst in roots only the changes in PC were insignificant.

Deletion of *RTN21* resulted in a similar lipid profile to *rtn17,* with increases of 6%, 14%, 14%, and 2% for PC, PS, PI and sterols respectively, and no change in leave PE content (Fig 6.6), however none of these increases were statistically significant. In roots, deletion of *RTN21* causes decreases of 9%, 14%, 21%, 28% and 13% in PC, PE, PS, PI and sterols respectively (Fig 6.6), of which all these reductions where statistically significant except for PE. In general, deletion of *RTN17* and *RTN21* result in increases of all lipid content in leaves, and decreases in roots of Arabidopsis seedlings, especially in PS and PI content, whilst *RTN18* deletion primarily results in decreases of lipid content, except for PS and PC content in leaves where it causes an increase in content.

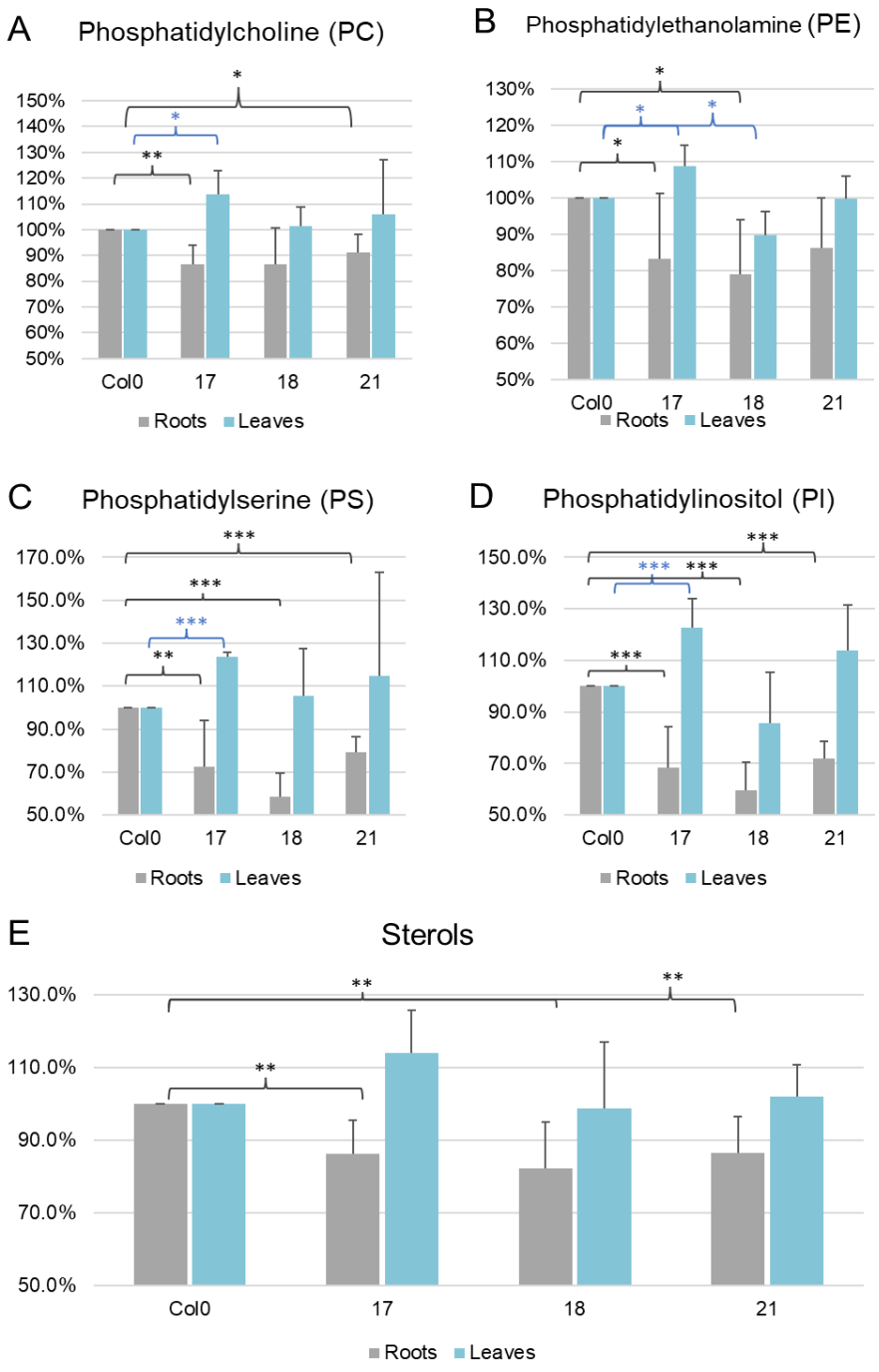

Figure 6.6 – Clade 6 RTN mutants have a lipid phenotype

A. Change in phosphatidylcholine (PC) composition as a percentage, compared to WT Col0, in roots and leaves of 15 day old seedlings. **B.** Change in phosphatidylethanolamine (PE) composition. **C**. Change in phosphatidylserine (PS) composition. **D**. Change in phosphatidylinositol (PI) composition. **E**. Change in sterols composition. n =3 biological repeats, 20 seedlings per set. * = 0.05<p<0.1. ** = p<0.05. *** = p<0.01.

6.3 – Discussion

6.3.i - Quantitative analysis of RTN17.1 and RTN21.2 over-expression

Initial experiments expressing RTN17.1 transiently in tobacco leaf cells suggested a decreased proportion of cisternal content in the network. However, under native conditions the ER network is highly dynamic, depending on cell type or stage of development (Shibata et al., 2006; Ridge et al., 1999). This pleomorphism therefore means that the network morphology within an individual cell at a given moment during an experiment may not be a representative or repeatable phenotype. When investigating the effects of different variables of interest, in our case the expression of other proteins such as RTN17.1 and RTN21.2, it is imperative to sample a larger cohort across multiple experiments and quantify the resulting networks to remove bias. This is a more a robust method to assessing morphological changes and is achieved by utilising tools such as the AnalyzER software package (Pain et al., 2019). This software allows us to sample a larger proportion of networks and assess the morphology across 4 dimensions to extensively quantify the changes induced by expression of the protein of interest. From this we have confirmed the previously observed changes in ER morphology, with statistically significant decreases in cisternal area (Fig 6.4D), increases in tubule length (Fig 6.3G) and polygon (Fig 6.3H) region area for RTN17.1 over-expression. Similarly, RTN21.2 shows increases in tubule length (Fig 6.3G), and polygonal area (Fig 6.3H), however the decrease in cisternal area of 13% was a trend but not statistically significant (Fig 6.4D). The other major difference resulting from RTN17.1 or RTN21.2 expression was that the networks are slower in average and maximum speeds, and subsequently more stable over time (Fig 6.5). These changes are responsible for generating a distinct ER morphogen based on the expression of RTN17.1 and RTN21.2 (Fig 6.2D).

Perhaps the most interesting outcome of this analysis is the confirmation that RTN17.1 significantly decreases cisternal content of the ER, in a distinct manner to that seen in other clades of Arabidopsis RTNs (Sparkes et al., 2010) and other eukaryotic RTNs (Voeltz et al., 2006). Typically, RTNs utilise the properties of the RHD as well as their oligomerisation capabilities, to embed in the membrane and induce a curvature (Tolley et al., 2010; Shibata et al., 2008). Over-expression of these proteins results in a drastic decrease in cisternae content in the network, as well as a hyperconstriction of the tubules, with the proteins exclusively labelling areas of high membrane curvature (Tolley et al., 2008; Sparkes et al., 2010). In contrast to this, RTN17.1, with its motile punctate distribution throughout the ER and preferential localisation to 3-way junctions, is still capable of reducing the cisternal content of the ER, as well as increasing tubule length without hyperconstricting them. This knowledge of the specific morphological impacts of RTN17.1 expression can be combined with the previous experiments, which have assessed the structural components of the protein and the interaction with RHD3. This will help formulate the mechanism in which RTN17.1, and other clade 6 RTNs may enact their function. The effect on cisternal content also suggests that RTN17.1, like RHD3 (Wang et al., 2016; Zhou et al., 2019), may act antagonistically against LNP, adding further complication between the balance of these proteins and their regulation of 3-way junctions and cisternae.

Expression of RTN17.1 or RTN21.2 leads to a slower moving and more static ER network (Fig 6.5). Interestingly, this is consistent with the effects of LatB treatment, which inhibits the repolymerisation of the actin cytoskeleton, and as such perturbs the ER dynamics which are mediated by an intact actin cytoskeleton (Sparkes et al., 2009a). LatB and heat shock treatment were both found to increase the persistency of the network, as well as decrease speed of both cisternal and tubular compartments in the ER (Pain et al., 2019). However, unlike RTN17.1 and RTN21.2, these changes affecting the ER-actin interface are often associated with an increase in cisternal area across the network (Sparkes et al., 2009a; Pain et al., 2019). Static points within the network are often EPCS, where proteins such as NET3c are localised and link EPCS to the actin cytoskeleton providing their stability (Wang et al., 2014). NET3c interacts with another EPCS

localised protein VAP27, and within these ER subdomains there is close association to both the actin and microtubular cytoskeleton, with EPCS perhaps utilising the filamentous network to further stabilise and anchor the ER (Wang et al., 2016). Based on potential cytoskeletal interaction between RTN17.1, as well as EPCS occupying most of the 3-way junctions in the network, it is possible this increase in stability is based on the ER-actin interface. RHD3 has also been shown to interact with Armadillo-repeat kinesin 1 (ARK1), which associates with microtubule plus ends, impacting tubule growth (Sun et al., 2020). These aspects and the interconnection between 3-way junctions, EPCSs and the RTN17.1 may explain the increased persistency, however for optical flow the mechanism behind this decrease is less clear and may requires more assessment of other ER morphogens and their impact on optical flow.

6.3.ii - Clade 6 *rtn* mutants have a lipid phenotype

So far in this chapter we have focussed on the quantification of the phenotype when overexpressing RTN17 and RTN21 transiently in Tobacco. Whilst identification and isolation of confirmed knock out lines for each of the clade 6 *RTN* genes was achieved, attempts to stably transform each mutant with an ER marker were unsuccessful. This would have allowed imaging and potential quantification of the impacts of reduced expression of each respective protein. These mutant lines did not appear to show any growth phenotypes or other noticeable characteristics compared to wild type.

However, these lines were still viable for other quantitative assessment, such as full lipidomic analysis being achieved utilising these mutants, in which it was revealed that deletion of clade 6 *RTNs* causes distinct lipid phenotypes (Fig 6.6). Not only is the ER a primary site of lipid biogenesis within eukaryotic cells (Fagone & Jackowski, 2009), but also the composition of the ER phospholipid bilayer can also influence morphological contents of the ER, with excessive levels of PE and diacyl glycerol (DAG) resulting in increased tubular content (Ulloa et al., 2019).

Previous studies have shown that in Arabidopsis *rhd3* mutants also showed an increase in phospholipid levels, potentially through the deregulation of phosphatidylinositol synthase 1 (PIS1), an enzyme required for PI synthesis, as well as promotes PE and DAG (Maneta-Peyret et al., 2014).

This increase in lipid content is consistent with that of the effect of *rtn17* deletion in leaves, however, is opposite within seedling root tissue. Lipid regulation via RHD3 and RTN17, as well as their general mechanism of action may therefore have tissue specificity, possibly based on the endogenous expression of either protein as well as the lipid differences between cell types or developmental stage. Interestingly clade 5 *RTN* deletions also produced a decrease in sterol content specifically in the roots (Kriechbaumer et al., 2018b), consistent with the effect of clade 6 *RTN* deletions. Further lipidomic analysis of other ER morphogens and a greater insight of how morphology is induced by changes in lipid composition and vice versa will further the understanding of how lipid biosynthetic pathways can be influenced by the expression levels of certain proteins such as RHD3, the RTNs and other ER morphogens. Furthermore, complementation studies of this phenotype would further support the current lipidomic assessment, however floral dips of functional constructs back into the mutant lines was unsuccessful when attempted.

6.3.iii – Conclusions and future work

Within this chapter an important step has been taken from qualitative assessment to robust quantitative analysis of the impact of clade 6 RTNs, specifically RTN17.1 and RTN21.2, on the ER network morphology. This allows us to confirm the visually apparent distinctions between a 'normal' ER network labelled singularly with GFP-HDEL, and the networks upon expression of the clade 6 RTNs.

Going forward, this dataset can become part of an increasing cohort of quantitative analysis of ER morphogens. Utilising AnalyzER, as other ER morphogens are studied in more detail, their potential physiological impacts of mutation, deletion, or over-expression, we can begin to better assign certain outcomes with specific changes in ER morphology. This can be particularly effective for subtle morphological distinctions that may be missed with qualitative assessments of a network. Ideally a quantitative analysis of RHD3 over-expression and potentially deletion or mutations (Chen et al., 2011) would be useful to compare to the effects of RTN17.1 expression, considering their strong interaction and involvement in 3-way junction formation. Quantitative analysis of morphological changes described in regard to Rtn4a (Voeltz et al., 2006) and Rtn1p (De Craene et al., 2006) would be advantageous to identify similarities and differences between RTNs across all eukaryotic domains, and whether the reduction in cisternae caused by overexpression of these mammalian and yeast proteins is to a similar degree as Arabidopsis RTNs. A larger dataset for the Clade 6 RTNs and including RTN18 would be ideal to enhance this dataset out further. However, when acquiring the data aiming for a comparative sample set as for RTN17 and 21, multiple images had to be removed due to issues in generating the network mask as the software demands a high-fidelity image for effective analysis. It was deemed analysis with fewer samples would be more valuable than including images with non-optimal masking as this would affect the quantification and is line with the experimental procedures utilised in the original publication (Pain et al., 2019).

Chapter 7 – General Discussion

7.1 - RTN17.1 works synergistically with RHD3

7.1.i – A RTN17.1/RHD3 complex mediates fusion of parallel tubules to increase polygon size

Of the three splice variants, RTN17.1 is both the full-length protein as well as the main transcript isolated from cDNA and thus highest transcribed in the sampled tissue (Fig 2.2). RTN17.2 was isolated from cDNA but insertion in the expression vector was unsuccessful, and so, along with RTN17.3, was later generated via PCR-based truncations or gene synthesis, respectively. RTN17.1 constructs were generally easier to express and had a greater success especially in co-expressions with other proteins, and so is considered the main variant of interest. With no obvious protein domain identified from bioinformatic databases within the extended termini of RTN17.1, it was subsequently revealed that the intrinsically disordered termini are the main distinguishing aspect of RTN17.1s structure (Fig 2.3). This feature is commonly implicated in the facilitation of protein-protein and protein-lipid interactions across a large proportion of the proteome (Mészáros et al., 2009). Within these IDR's, multiple Low-complexity regions (LCR's) were identified which are sequences of low amino acid composition variety. Notably, the proportion of both LCRs and IDRs is increased in hub proteins (Ekman et al., 2006), and LCRs in terminal sequences are more prevalent in proteins implicated in stress-response and translation modification, whereas transcriptional factors tend to have more centrally located LCR's (Coletta et al., 2010). These factors support the idea that based on the localisation and interaction with RHD3, RTN17.1 acts as an ER localised hub protein, mediating an interaction with RHD3 through the N-terminal IDR. We hypothesise that this complex is implicated in the generation of 3-way junctions, and generation of the polygonal network.

From our quantitative assessment of ER morphology changes induced by expression of RTN17.1 the key findings are a more static network consisting of larger polygonal regions, longer tubules and decreased cisternal area (Fig 6.3, Fig 6.4, Fig 6.5). Furthermore, we have established the strong interaction with RHD3 (Fig 4.2C), as well as an association with the cytoskeletal network, with puncta aligning with both actin and microtubule filaments. Co-expression of both RTN17.1 and RHD3, as well as some cases of high RTN17.1 expression alone induce a more cytoskeletal pattern of labelling (Fig 5.2E). Understanding these elements as well as the functionality of RHD3 as the Arabidopsis homologue to the GTPases that mediate 3-way junction formation across Eukarya (Chen et al., 2011), we can begin to generate a theoretical mechanism in which RTN17.1 over-expression induces these morphological changes.

In previous literature, when discussing the activity of ATL/Sey1p/RHD3 and the formation of 3-way junctions, fusion events are often described in terms of elongating tubules crossing a polygonal region to fuse with an opposing tubule running perpendicular to the tip of the outgrowing tubule (Fig 7.2.1A) (Moss et al., 2011; Blackstone, 2012; Westrate et al., 2015). With the potential role of RTN17.1 in 3-way junction formation, the presence of RTN17.1 puncta both at the end of some elongating tubules was observed, as well as at the site in which elongating tubules fuse and form a new junction, which corresponds to the previously described model of perpendicular fusion (Fig 3.2). However, these events are infrequent relative to the number of RTN17.1 or RHD3 puncta (when co-expressed) present throughout the network at a given time. What was noticed occurring at a much more frequent rate was the collapsing of elongating tubules into a parallel tubule, or the converging of parallel tubules within smaller polygons (Supplementary movie 6). Predominantly, these fusion events occur with an RTN17.1 puncta localised at the epicentre (Fig 7.1B; Supplementary movie 6). The collapsing of parallel tubules is encompassed within the documented ER dynamic of 'ring closure' and is a key aspect of generating the polygonal network, mediated by the microtubule cytoskeleton in mammalian cells (Lee & Chen, 1988), and actin cytoskeleton in plants (Sparkes et al., 2009a). However, what has not been noted is that these events involve a form of homotypic fusion of the converging tubules,

as they go from 2 distinct entities to a singular tubule. Therefore, it is important to consider that if ATL/Sey1p/RHD3 are responsible for mediating homotypic fusion, are they relevant for these parallel fusion events also, especially considering this offers a larger surface area for protein activity and dimerization to occur across rather than the area of a singular tip of an elongating tubule.

Based on RTN17.1s function as a hub protein, we suggest that this RTN17.1/RHD3 complex is implicated in both the perpendicular fusion events, but more frequently the parallel fusion events, with the complex acting as a zipper between two tubules, and by fusing at this interface it closes the polygonal region (Fig 7.1B; Supplementary movie 6). This complex is likely to include other proteins such as ARK1, which was identified and confirmed to interact with RHD3, and is responsible for association of RHD3 with the microtubular cytoskeleton in plant cells (Sun et al., 2020). As RTN17.1 has also shown an association with the actin cytoskeleton, as well as ring closure events and general ER remodelling being linked to actin/myosin complexes (Sparkes et al., 2009a), either RTN17.1 is directly mediating an interaction via the RHD as shown by the truncation experiments or is interacting with an unidentified actin binding protein as part of this complex also. This complex can therefore utilise the underlying cytoskeletal networks as a scaffolding, and axis in which to travel along, and the RHD3 can generate the necessary force required to fuse the parallel tubules via dimerization and GTP hydrolysis in the GTPase domains, as is the canonically described mechanism for ATL/Sey1p/ RHD3 (Genny et al., 2009; Hu et al., 2009; Sun et al., 2018; Wang & Rapoport, 2019). It is important to note that the C-terminal portion that does not consist of the GTPase domain in ATL/Sey1p/RHD3 is also implicated in the correct functioning and formation of the polygonal network (Liu et al., 2012). Furthermore, some complementation studies indicate Sey1p and RHD3 may not be completely functional analogues (Zhang et al., 2013), and so whether this mechanism and complex formation is involved in all types of cells and for other fusogens cannot be confirmed.

Observing these parallel fusion events in greater detail, utilising the temporo-spatial resolution offered with AiryscanFast detection (Wu & Hammer, 2021) we can begin to decipher how this putative mechanism and organisation of proteins translates into the observed morphological changes. Within the duration of 8 seconds, RTN17.1 moves from the base of a polygon along a certain axis. Parallel to this axis on either side, tubules begin to converge and meet at the point in which the RTN17.1 puncta resides at. As the puncta continues its trajectory along its axis of travel, the tubules fuse until they are both incorporated, and the RTN17.1 puncta now resides at the resulting three-way junction (Fig 7.1C). From this closure and counting the present polygonal regions at the beginning of the time series, and after, the total number of polygons has been reduced from 7 to 5. As the same field of view is being maintained, this in turn means the polygonal region area has effectively increased, as two polygons of a smaller total area have been replaced by a singular polygon of a larger area (Fig 7.1D). This is reflected in the polygonal area increases seen from the AnalyzER analysis, whereby RTN17.1 overexpression results in a 31.35% increase in polygonal area (Fig 6.3). Furthermore, as more polygonal regions mean more 3-way junctions, each tubule has a shortened length prior to the parallel fusion event, as the length is calculated from node to node. As the ring closure events happen, the 2 lengths across 2 polygons are now a singular longer length, again which is reflected in the overall 15.17% increase (Fig 6.3) determined from the quantitative analysis (Fig 7.1D).

This facet of homotypic tubular fusion is an interesting avenue to explore and consider in future analysis of membrane fusion as previously there has been a large focus on the perpendicular fusion events in relation to ATL and Sey1p (Lin, et al., 2012; Zhao et al., 2016), and even the investigation of vesicular fusion via Sey1p (Kim et al., 2017). However, these putative parallel fusion events offer a greater surface area of membrane interaction and therefore could be of even greater importance in terms of fusion and modulation of the polygonal network. Key to concretely confirming this model would include determining how RTN17.1 interacts with the actin cytoskeleton and potentially identifying the actin binding protein, as well as in vitro visualisation of the RTN17.1, RHD3, the ER network and cytoskeletal network at the same time. Unfortunately,

attempts of triple localisations, as well as the generation of fluorescent fusion proteins of RTN17.1 and RHD3 have been unsuccessful. Based on the association between RTN17.1 and the cytoskeletal networks, as well as their implications in general ER morphology and 3-way junction formation, it is possible to suggest that the axis of puncta travel observed may align with either the actin or microtubule cytoskeleton (Fig 7.1D).

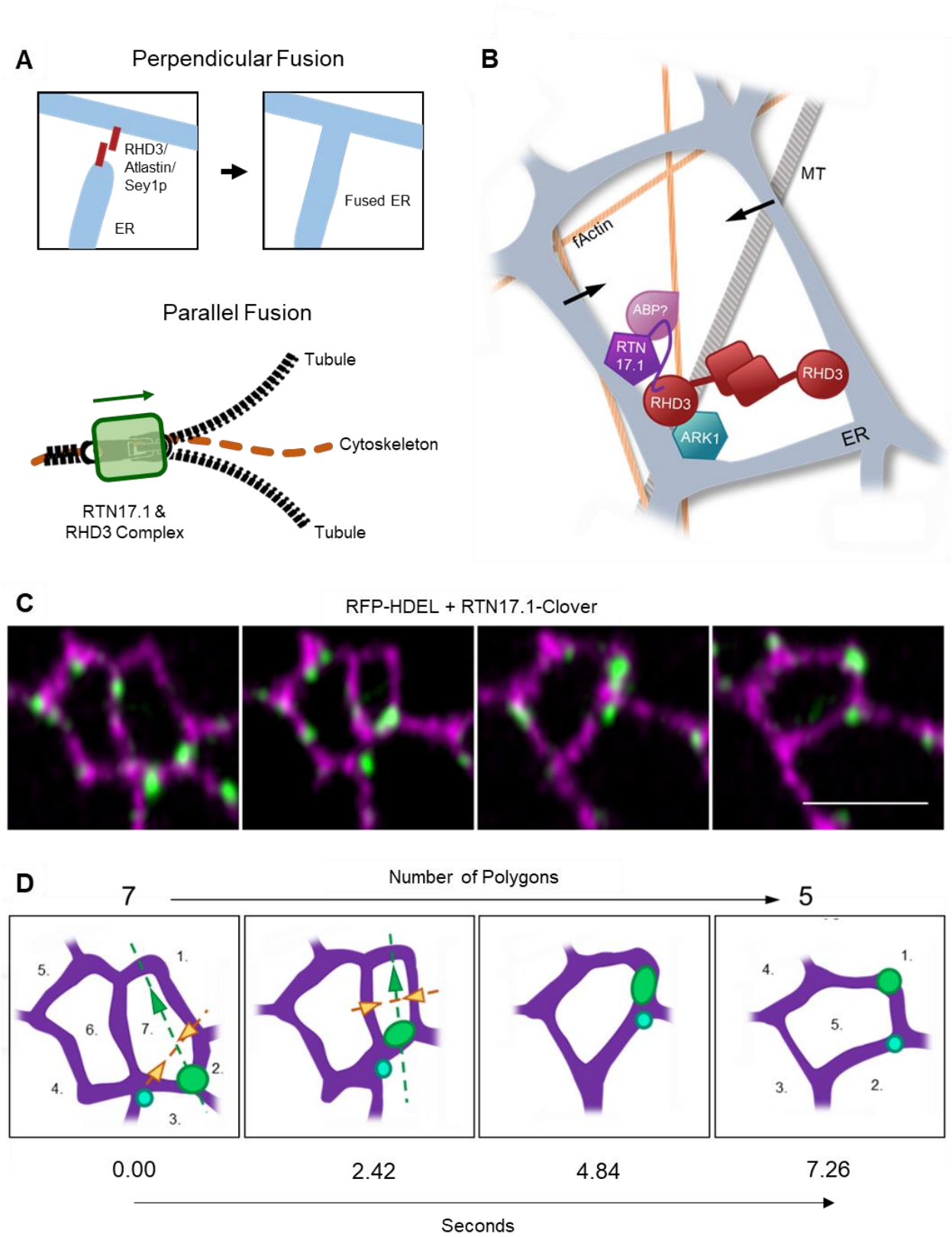
A
Perpendicular Fusion
RHD3/
Atlastin/
Sey1p
ER
Fused ER
Parallel Fusion
Tubule
Cytoskeleton
RTN17.1 &
RHD3 Complex
Tubule
B
MT
fActin
ABP?
RTN
17.1
RHD3
RHD3
ARK1
ER
C
RFP-HDEL + RTN17.1-Clover
D
Number of Polygons
7
5
1.
2.
3.
4.
5.
6.
7.
0.00
2.42
4.84
7.26
Seconds

Figure 7.1 – RTN17.1 mediates parallel tubule fusion

A. Generic model of homotypic tubule fusion and formation of 3-way junctions. Adapted from Rogers et al., 2014. **B** Proposed RTN17.1/RHD3 complex, with ARK1 and putative actin binding protein (ABP). Arrows show direction of tubule collapse during ring closure. **C** Live cell image of RTN17.1 puncta mediating parallel tubular fusion. HDEL in Magenta, RTN17.1 in green. Scale bar = 2 μm. **D**. Schematic representation of dynamics in C. Polygons labelled by number, and puncta of interest in green with additional associated puncta in teal. Green arrows axis of main puncta travel, yellow arrows direction of tubule travel. Each frame represents 2.4 seconds in time series.

7.1.ii - RTN17.1/RHD3 labelled 3-way junctions mitigate cisternae formation

Another key finding from both qualitative assessment and the quantitative analysis of RTN17.1 was the decreased cisternal area. With the previously described mechanism being responsible for the elongated tubules and increased polygonal area, it is more difficult to postulate the exact mechanism behind the decreased cisternal content. Key things to consider are that so far there have been 3 ways to observe a shift from cisternal to more tubule dominant contents in the plant ER: overexpression of clade 1-4 RTNs (Sparkes et al., 2010), overexpression of clade 6 RTNs, and reduction of functional LNP (Kriechbaumer et al., 2018a) (Fig 7.2). Recent studies have shown LNP to ubiquitinate RHD3 resulting in local levels of RHD3 and suggested that this required for the stabilisation of 3-way junctions (Sun et al., 2020). This is consistent with the proposed idea that yeast Sey1p works antagonistically against LNP at 3-way junctions, and the balance of these two proteins is required for co-ordinated generation of the network (Chen et al., 2012), and similar phenomena is observed between mammalian ATL and LNP (Zhou et al., 2019). Therefore, whilst a balance of LNP activity may be required for stabilisation of 3-way junction formation, it appears through over-expression studies and general ER dynamics that 3-way junctions are the site in which cisternae biogenesis originates from. Consequently, increased LNP activity promotes the shift from 3-way junctions into full cisternae via a so far unknown mechanism (Kriechbaumer et al., 2018a)(Fig 7.2). Conversely, when the levels of RHD3 and LNP are closer to equilibrium and the degradation of RHD3 is not so excessive, a normal population of 3-way junctions can be observed, and the degree of cisternae biogenesis is reduced, as suggested by RHD3 and LNP's antagonistic relationship (Chen et al., 2012; Zhao et al., 2016). As RTN17.1 is closely associated with RHD3, and potentially responsible for its localisation, or even involved in the correct folding of the protein based on capabilities of the IDR in the N-terminal extension (Wright & Dyson, 2015), over-expression of RTN17.1 therefore may promote general RHD3 activity and minimise the effect of LNPs degradation.

However, to fully understand this relationship between RTN17.1, RHD3 and LNP requires further understanding of cisternae biogenesis in general. AtLNP1 and AtLNP2 localise differentially within the ER, with AtLNP1 having a specific labelling of cisternae and some puncta, whereas AtLNP2 is capable of labelling the entirety of the ER (Kriechbaumer et al., 2018a). When co-expressing RTN17.1 with AtLNP1, the signals are mutually exclusive and RTN17.1 puncta can be seen adjacent to AtLNP1 labelled cisternae, or within perforations in the cisternae (Fig 7.2). In contrast, RTN17.1 puncta when co-expressed with LNP2 are capable of residing within the cisternae (Fig 7.2). Some studies have also hypothesised cisternae to consist of dense tubular matrices (Nixon-Abell et al., 2016), or contain an abundance of nano-holes only distinguishable via sub diffraction limited means of microscopy (Schroeder et al., 2019). This high-resolution assessment of mammalian ER also identified differing types of cisternae within areas of the network, with variations of perforated tubular matrices and uniform sheets, and is also dependent on the presence or absence of RTNs (Schroeder et al., 2019). Considering these factors and the differential localisation of Arabidopsis LNPs and of RTN17.1 puncta when co-expressed, it is possible that either AtLNP1 or AtLNP2 activity could be responsible for differing populations of ER cisternae. Overall, despite this complex interplay of activity between RTN17.1, RHD3 and LNP, it is likely that RTN17.1 is implicated in this antagonistic relationship between RHD3 and LNP, and over-expression appears to help prevent the degradation of RHD3 and subsequent promotion of cisternal content within the ER.

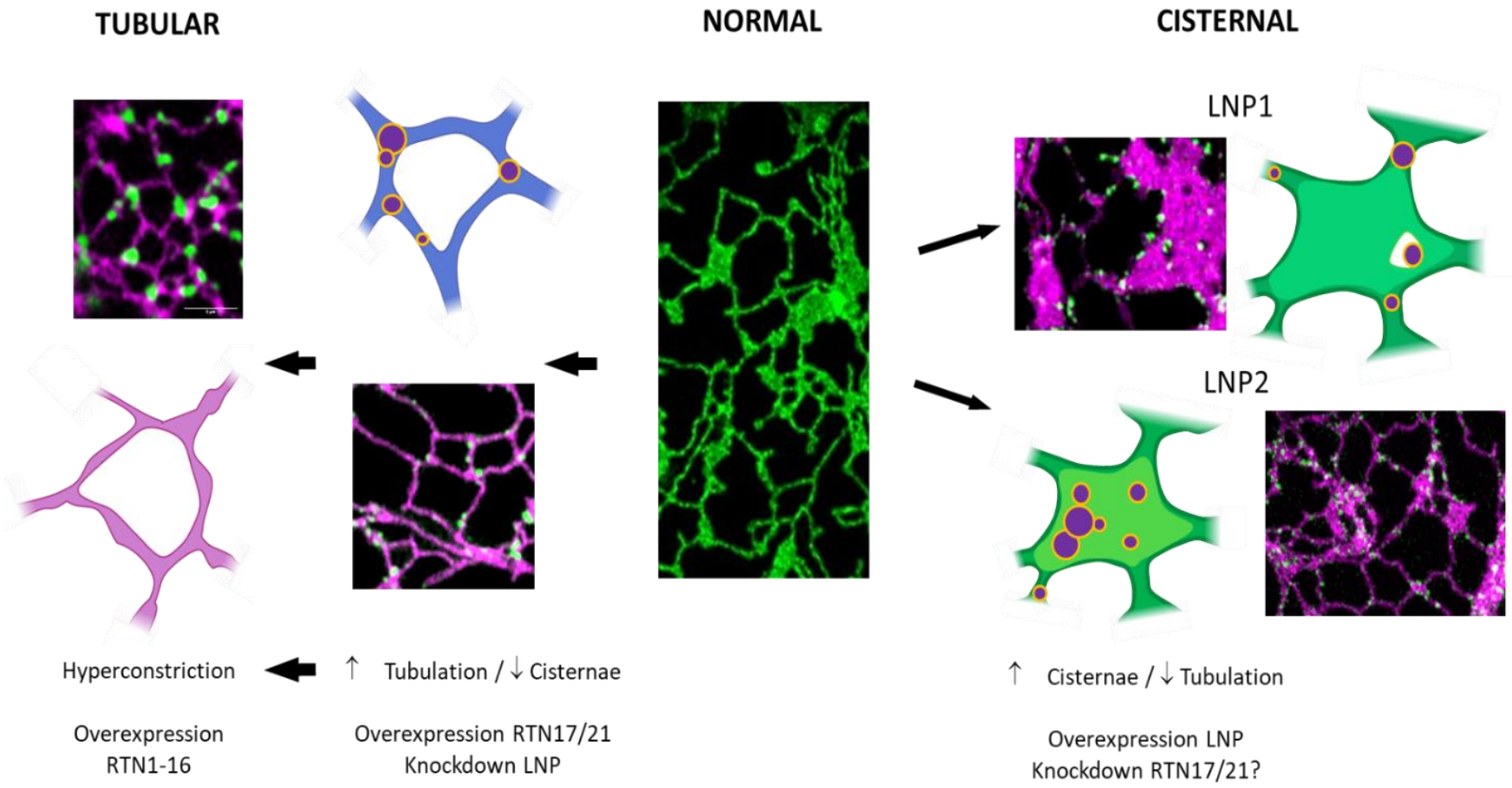
TUBULAR
NORMAL
CISTERNAL
LNP1
LNP2
Hyperconstriction
↑ Tubulation / ↓ Cisternae
↑ Cisternae / ↓ Tubulation
Overexpression
RTN1-16
Overexpression RTN17/21
Knockdown LNP
Overexpression LNP
Knockdown RTN17/21?

Figure 7.2 – RTN17.1/RTN21.2 promote a tubular ER network

Schematic and summary of how LNP1 and RTN17/21 work antagonistically to either increase cisternal, or tubular content of the network respectively. Centre image represents a typical ER network, as identified with GFP-HDEL (green). Near Left represents overexpression of RTN17 (green) resulting in a network consisting of larger polygonal regions and a lack of cisternae (magenta = HDEL). This phenotype is also exhibited by knock down of LNP1 and LNP2, suggesting there is an antagonistic relation between the two families of proteins. Far left represents a clade 1-4 RTN overexpression where the HDEL (green) is hyperconstricted by RTN1 (magenta). Right panels show an increase in cisternal content seen overexpressing LNP1 or LNP2 (magenta) is observed. Co-expressing LNP proteins with RTN17 (green) shows how different cisternae are exclusive or inclusive to RTN17.

7.2 - Clade 6 RTNs are ER intrinsic hub proteins

7.2.i - RTN21.2 may act as a hub protein

When transiently expressed in tobacco epidermal leaf cells, RTN21.2 resides in puncta reminiscent of RTN17 puncta in size, however the distribution is much sparser, and more stable over time (Fig 3.2). The puncta exclusively localise to persistent points within the network, around which tubule rearrangement occurs. These are typically associated with points in which the ER is anchored to the plasma membrane, hence the increased stability, and are known as ER-plasma membrane contact sites (EPCS). Bayer et al (2017) postulated that undescribed RTNs may act as putative EPCS marker, and regulate EPCS formation (Fig 7.4). This makes it tempting to speculate that based on RTN21.2s structural similarity and over-expression effects to RTN17.1, RTN21.2 may act as a hub protein with a preference for 3-way junctions that are also EPCS, based on the different dynamic properties compared to RTN17.

There are multiple proteins associated with EPCS, namely, VAP27, NET3c, (Wang et al., 2014), SYT1 (Sia et al., 2016) and other broader components to consider such as the phospholipid bilayers of the two membranes in question, as well as actin and microtubule cytoskeletal elements. In general, RTN21.2 was much a much more difficult protein to assess due to inconsistent constructs. Unfortunately, attempts to co-express RTN21.2 with VAP27, NET3c and RHD3 were unsuccessful. RHD3 and VAP27 have also been shown to interact with RTN3 and RTN6 via FRET-FLIM studies (Kriechbaumer et al., 2015), and as such clade 6 RTNs in general may have some degree of association with EPCS proteins as well as indirectly with other RTNs in complex multi-protein hubs. REEP proteins are mammalian ER shaping proteins, which utilise a disordered C-terminus (REEP 1-4) to link the ER to microtubules (Park et al., 2010). As there is no plant homologue identified for this ER morphogen, RTN21.2 could be a functional homologue

with the disordered termini utilise this method to interact with cytoskeletal components, stabilising the ER at an EPSC where microtubules are present and assist with their formation. Overall, RTN21.2 specific interactions have yet to be elucidated but based on the extensive presence of IDRs and the dynamic characteristics of the puncta, it is possible it has a similar role to RTN17.1 as a hub protein localised and mediating 3-way junction formation, however specific to junctions that correspond with EPCSs. As EPCS are dynamic hubs with a large cohort of proteins and functionality included relevance to Ca^{2+} signalling (Wang et al., 2016), future analysis of RTN21 as well as the other clade 6 RTNs may reveal strong implications in other physiological aspects within the plant cell, beyond the role of regulating ER morphology.

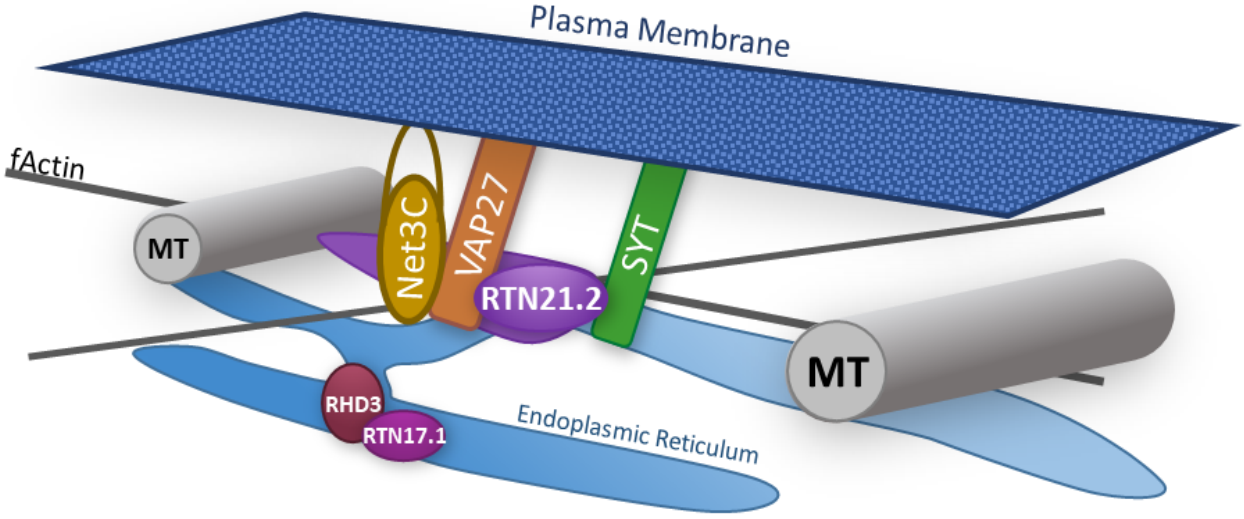

Figure 7.3 – RTN21.2 may be involved in EPCS 3-way junctions

Prospective role for RTN21.2 in mediating EPCS formation, amongst the key players such as NET3c, VAP27 Synaptotagmin (SYT), and the surrounding actin and microtubular cytoskeleton. Adapted from (Bayer, et al. 2017).

7.3 - Summary and future work

7.3.i - Summary

Through this thesis the aim of describing the previously uncharacterised clade 6 Arabidopsis RTNs was achieved. This includes isolating the genes from cDNA and cloning into several fluorescent protein fusion constructs, including truncations and splice variants. This resulted in the first visualisation of RTN17.1 *in planta*, revealing a mobile punctate distribution with a preference for 3-way junctions, seen in both stable and transient expression systems (Chapter 3). From here co-expression with other proteins of interest, mostly other ER morphogens has allowed us to identify the key relation between RTN17.1 and RHD3 (Chapter 4). These proteins were shown to interact *in planta*, via the intrinsic disordered N-terminus of RTN17.1, a hall mark feature found in the clade 6 RTNs (Fig 5.2). Quantitative assessment of transient expression of both RTN17.1 and RTN21.2 revealed significant modifications to the ER networks compared to wild-type networks.

These changes include a decrease in cisternal area, accompanied by longer tubules and larger polygonal regions. Assessing the movement and association of RTN17.1 and RHD3 with 3-way junctions closely, puncta moving along tubules accompanying the fusion of parallel tubules can be seen (Fig 7.1). This avenue of fusion appears to be the mechanism behind increasing polygonal areas and lengthening tubules, whilst the resulting 3-way junctions with over-expressed RTN17.1/RHD3 complexes may work antagonistically against cisternae formation from proteins such as AtLNP1 and AtLNP2 (Fig 7.4). Furthermore, RTN21.2 has similar impacts on ER morphology when overexpressed. RTN21.2 puncta dynamics suggest a preference for 3-way junctions that correspond to EPCS regions within the network, and thus may have implications on the functionality of EPCSs in general. These experiments have identified another novel

functionality within the family of Arabidopsis RTNs and unlike the addition of enzymatic domains such as with RTN19 and RTN20, the presence of intrinsic disorder within the protein sequence is sufficient in endowing a host of different characteristics.

7.3.ii - Future Work

There are several future experiments that would aid in understanding the exact mechanics of the clade 6 RTNs function. Firstly, although RTN18 was cloned and imaged, it was never successful co-expressed with other proteins such as RHD3. Successful attempts would confirm whether, as it's structural and sequence similarity would suggest, it is functionally analogous to RTN17.1, or whether RTN18 is functionally distinct from RTN17.1 despite similar localisation and distribution characteristics.

An attempted triple co-expression for RTN17.1, RHD3 and either an actin marker or microtubule marker were unsuccessful. Following this the generation of a RTN17.1-RHD3 construct linked via a self-cleaving peptide to potentially simplify the infiltration and fluorophore complexities was also ineffective. Being able to visualise the presence of RTN17.1 with RHD3 and the cytoskeleton at the same time, or with an ER label would help to elucidate the direct interface of the puncta with the cytoskeletal network, and whether the morphological changes and ring closure events are occurring in close association with either actin or microtubule filaments.

RTN21 was difficult to co-express with other proteins and resulted mainly in one or the other protein expressed per cell but not in combination. A key starting point would be to identify potential interactions with EPCS localised proteins and determine whether the localisation is specifically at EPCS, or other static 3-way junctions as shown by the different dynamics compared to RTN17.1. Furthermore, the same approach to truncations as RTN17.1 will be key to identify

whether the terminal extensions are functionally similar in mediating protein interactions as a hub protein.

Although mutant lines were identified and successfully utilised for assessing their lipid profiles, attempts to investigate the effects on ER morphology from deletion of these proteins were unsuccessful. Both Rhodamine B staining of mutant Arabidopsis plants nor dipping with GFP-HDEL as an ER marker produced images of sufficient quality or signal for effective analysis. Generating effective lines with ER labels, as well as multi-knock out lines to avoid complementation of other clade 6 RTNs may be advantageous in understanding the significance of their role in regulating ER morphology. Furthermore, these knockout lines could also be used to assess the functionality of the fusion proteins, comparing the rescue phenotype of an untagged construct with that of one of the fluorescent fusion proteins.

Utilising native promoter constructs for RTN17.1 and RTN21.2 produced Col-0 Arabidopsis seedlings that suggested positive transformation of the based-on media selection, however fluorescence was never observed. This may be due to low levels of gene expression, and imaging with systems optimised for low level detection may produce information about the properties of clade 6 RTNs under native expression levels, and whether this aligns with the over-expression studies.

Overall, the key aims of the thesis have been achieved, and with more details from future work with RTN18 and RTN21, a comprehensive assessment of the clade 6 RTNs and their unique functionality within the plant ER will be fully elucidated. This is further contribution to the general understanding of how the morphology of the ER is regulated and may support future work in understanding the link between structure and function.

Chapter 8 – Methods

8.1 – Bioinformatics

8.1.i – Sequence analysis

Genes for the RTNs of interest were identified in the The Arabidopsis Information Resource (TAIR, Berardini et al., 2015; https://www.arabidopsis.org) database. Accession numbers are: At2g20590 (RTN17), At4g28430 (RTN18), At2g26260 (RTN19), At2G43420 (RTN20), At5g58000 (RTN21). Here also predicted splice variants were identified. Sequences of the full-length proteins were interrogated via Protein BLAST in TAIR (Berardini et al., 2015; https://www.arabidopsis.org/Blast/index.jsp) and UniProt (UniProt Consortium, 2021; https://www.uniprot.org/blast/) databases, as well as individual elongated termini to determine any homology between these regions and other proteins across organisms. Multiple sequence alignment and percentage identity matrix of clade 6 RTNs were produced via Clustal Omega (Madeira et al., 2019; https://www.ebi.ac.uk/Tools/msa/clustalo/). A phylogenetic tree was produced via phylogeny.fr one-click analysis (Anisimova & Gascuel, 2006; https://www.phylogeny.fr/). Transcript data was gathered from EFP browser (Winter et al., 2007; http://bar.utoronto.ca/efp2/Arabidopsis/Arabidopsis_eFPBrowser2.html).

8.1.ii – Topology and domain analysis

Sequences of all genes and their splice variants were analysed for topology and TMD presence via TOPCONS consensus database (Tsirigos et al., 2015; https://topcons.net/) and TMHMM (Möller et al., 2001; https://services.healthtech.dtu.dk/service.php?TMHMM-2.0). Intrinsic disorder profiles and context-dependent binding profiles were assessed via both DISOPRED3 (Jones &

Cozzetto, 2015; http://bioinf.cs.ucl.ac.uk/psipred) and IUPREDlong2 with Anchor2 (Mészáros et al., 2018; https://iupred2a.elte.hu). Single Modular Architecture Research Tool (SMART) database (Letunic et al., 2020; http://smart.embl-heidelberg.de), PSIPRED4.0 (Buchan & Jones, 2019; http://bioinf.cs.ucl.ac.uk/psipred) and DomPred (Bryson et al., 2007; http://bioinf.cs.ucl.ac.uk/psipred) were also utilised to identify any other structural features in the proteins.

8.2 - Molecular Biology

8.2.i - Mutant line assessment

Available T-DNA insertion mutant lines of the genes of interest were ordered from NASC and grown in the greenhouse. The lines ordered were as follows SALK_203638c, SALK_207412c (RTN17), SAIL_178_G04 (RTN18), and SALK_132081 (RTN21) (Alonso et al., 2003). Initially seeds were sowed onto solid media plates of 0.8% phytoagar with 2.4gl^{-1} Murashige and Skoog in deionised water and placed for 2 days in 4°c and darkness for vernalization. Then plates were moved to a 22°c incubator for 1 week before soil with 16h/8h light-dark cycle. 14-day old plant material was homogenized using a sterile mortar in a genomic DNA extraction buffer (200 mM Tris-HCl, pH 7.5; 250 mM NaCl; 25 mM EDTA; 0.5% SDS) followed by centrifugation and precipitation with isopropanol, and final ethanol washes. Genomic DNA was used as template for PCR. Protocol is according to the instructions for NEB Onetaq PCR kit, with primers and design based on SALK-T-DNA primer design (Alonso et al., 2003) to allow identification of T-DNA insertion and confirmation of gene knockout (Table 8.1).

8.2.ii - Reverse transcriptase – PCR

Monarch® Total RNA Miniprep Kit (New England Biolabs) protocol and contents were utilised to extract RNA from 35-day old bud, flower, leaf, and silique tissue, as well as 1 week old seedling root and shoot material, or whole seedlings for genotyping. ProtoScript® II First Strand cDNA synthesis (New England Biolabs) with M-MuLV reverse transcriptase was employed to synthesise cDNA from RNA samples according to manufacturer's instructions. The full-length genes of interest were then probed via primers (Table 8.1) using Q5® High-Fidelity DNA Polymerase (New England Biolabs). Each RT-PCR product was then identified and ran with an actin control via gel electrophoresis on 1% agar, 1x TAE gels with DNA labelling from 2µl:100ml SYBR safe stain (Invitrogen). Subsequent to appropriate gel separation, after 30 minutes at 90 volts, gels were imaged and relative signal ratios to the Actin control were used as a semi-quantitative measure of cDNA expression.

8.2.iii - Cloning of expression plasmids

For RTN17.1, RTN17.2, RTN21.1 and RTN21.2 constructs, bands from RT-PCR gel electrophoresis were cut, and then DNA isolated with Monarch® DNA Gel Extraction Kit (New England Biolabs). Gateway technology DNA isolate was then cloned into the pB7RWG2 for N-terminal RFP, and pB7WGR2 for C-terminal RFP constructs. Subsequent truncations were produced via the use of designed primers (Table 8.1), with T1 forward primers corresponding with deletion of the N-terminal extension up to the RHD, and T2 corresponding with the C-terminal deletion. A combination of both were utilised for generation of the RTN17ΔTermini construct. For RTN17.3, RTN18 and RTN17.1/RTN1-Chimeric construct, these were synthesised into Gateway compatible entry vectors via Twist Bioscience.

All fluorescence constructs were generated via a Gateway cloning protocol. First, the isolated genes of interest were cloned into pDONR-221 Gateway entry vectors via a BP Clonase II enzyme

reaction in accordance with manufacturer protocol (ThermoFisher). Subsequently the reaction product is transformed into competent *E. coli* (NEB 5-alpha) and suspended in 200µl SOC media prior to plating on agar plates with relevant antibiotics for selection. In the case of pDONR-221 vectors, 50µg/ml of Kanamycin. After 1 day of incubation at 37°c, colonies were selected and tested for successful transformations via a colony PCR, and positive colonies grown in liquid culture for a further day at 37°c with agitation. After liquid suspension has grown, the pure plasmid DNA for transient expression was extracted via Monarch® Plasmid Miniprep Kit (New England Biolabs) following the manufacturer's instructions. Plasmid sequences at this point were sequenced to confirm correct cloning via Eurofins genomics. Successfully transformed plasmids were then cloned into fluorescence conjugate vectors via an LR reaction mediated by LR Clonase II enzyme, in accordance with manufacturer's instructions (ThermoFisher). Similar to the BP reaction, *E. coli* were transformed and grown on antibiotics with colony PCR checks to confirm successful transformation, and minipreps produce the final LR construct available for later agrobacterium transformation. All clade 6 RTN constructs contain Cauliflower Mosaic Virus (CaMV) 35s promoters, aside from mRFP-RTN17.1 featured in Fig 3.1 which utilised a Ubiquitin 10 promoter.

Table 8.1 - Primer sequences

Table denoting primers utilised for **A**. genotyping of mutant lines from TAIR and **B**. cloning, including truncations. T1 denotes primer used for N-terminal deletion, and T2 denotes primer used for C-terminal deletion. Combinations of these then subsequently used for RTN17ΔTermini and Chimera constructs.

A

Genotyping Primers

Gene	ID		Direction	Primer Sequence
RTN17	**SALK_207412C**	N697393	LP	AACTTCCTCGGGAGTTAGCTG
			RP	TCTCTGGTTTGGTTTTGGATG
RTN18	**SAIL_178_G04**	N860507	LP	GAATGCAGTAACTGCAGAGCC
			RP	GCTCATTCGATTTCACTTTCG
RTN21	**SALK_132081**	N632081	LP	GTTTTCTGCCACAAAAAGCTG
			RP	CTTCCAAGTCCGTCTCTTTCC

B

Cloning Primers

Primer	Acession Number	Direction	Primer Sequence
RTN17.1 Gate		Forward	gggg aca agt ttg tac aaa aaa gca ggc tct ATGGAGTCTA CGCCT
RTN17.1 Gate		Reverse	gggg acc act ttg tac aag aaa gct ggg tc AGTTTCTGCAACCACC
RTN17.2 Gate		Reverse	gggg acc act ttg tac aag aaa gct ggg tc TTCTTCACCTTTTTGGCTA
RTN17T1 Gate	**At2g20590**	Forward	gggg aca agt ttg tac aaa aaa gca ggc tct ATGGTGATTTGGTAATGTG
RTN17T1 Gate		Reverse	gggg acc act ttg tac aag aaa gct ggg tc AGTTTCTGCAACCAC
RTN17T2 Gate		Forward	gggg aca agt ttg tac aaa aaa gca ggc tct ATGGAGTCTA CGCCT
RTN17T2 Gate		Reverse	gggg acc act ttg tac aag aaa gct ggg tc GCTCGTCAAGTTCCAAAAC
RTN18 Gate	**At4g28430**	Forward	gggg aca agt ttg tac aaa aaa gca ggc tct ATGGACTCTA CTACCAC
RTN18 Gate		Reverse	gggg acc act ttg tac aag aaa gct ggg tc ATAAAGCTTCTTTGGTGC
RTN21.1 Gate		Forward	gggg aca agt ttg tac aaa aaa gca ggc tct ATGACGCCGA GG
RTN21.1 Gate	**At5g58000**	Reverse	gggg acc act ttg tac aag aaa gct ggg tc AGAAATTTTCTTGAGTTTATTAGG
RTN21.2 Gate		Forward	gggg aca agt ttg tac aaa aaa gca ggc tct ATGGACCCAAGTAGTAT

8.3 – Plant Expression

8.3.i - Stable transformation in Arabidopsis

Stable transformation lines of RTN17.1-Clover were achieved via floral dipping in accordance with Clough & Benet, 1998. Agrobacterium cultures are pelleted prior to resuspension in 500 µl/litre and 5% sucrose solution. Mature *Arabidopsis thaliana* Columbia-0 (Col-0) plants that have just begun to flower are then dipped into this solution with gentle agitation for 30 seconds, before being placed in cling filmed trays to retain humidity and promote transformation efficiency. One week after the previous steps are repeated with the same construct suspension. Following the growth of siliques and subsequent drying, the seeds are threshed and selected utilising 5µg/ml of BASTA on 1/4MS soaked silica dioxide plates (Davis et al., 2009). Non-transformant seedlings do not grow effectively under BASTA treatment, allowing easy selection of successful transformants, which are then selected and grown in soil. The T2 generation of seeds from these plants can then be imaged and checked for fluorescence.

8.3.ii - Transient expression in tobacco

Transient expression of fluorescent constructs was mediated by infiltration of Agrobacteria, in accordance with Sparkes et al, 2006. In brief, 6 week old tobacco plants (*Nicotiana tabacum* SR1 cv Petit Havana) from the greenhouse were selected. Competent Agrobacterium GV3101 were transformed via heat-shock, and then plated on agar containing antibiotic (50 µg/ml spectinomycin with 25 µg/ml rifampicin for RTN constructs, 50 µg/ml kanamycin and 25 µg/ml rifampicin for HDEL) and grown for 48 hours at 28°C. Individual colonies were selected for growth overnight in liquid media with respective antibiotic, at 28°C with shaking at 180 rpm. The culture was then pelleted by centrifugation at 4,000 RPM for 5 minutes at room temperature, and

re-suspended with infiltration buffer (50 mM MES, 2 mM $Na_3PO_4 \cdot 12H_2O$, 0.1 mM acetosyringone and 5mg/ml glucose), followed by another round of pelleting and resuspension. This suspension was diluted to a final OD_{600} of 0.1, before being injected into the lower epidermal surface of the leaf with a 1ml syringe sans needle. Infiltrated plants were then incubated in a growth cabinet at 22°C for 48hours before leaf sections were taken for imaging.

8.4 – Confocal imaging and image analysis

8.4.i - General Imaging

All imaging was done on laser scanning confocal microscopes. Either Zeiss LSM800 and Zeiss LSM880 with Airyscan detector with either 63x/1.46 NA 100x/1.46 NA oil immersion objectives, or a 10x air objective for Fig 3.1C. GFP based fluorophores such as GFP, eGFP and Clover were imaged utilising a 488nm excitation wavelength, and emission spectra of 493-598. RFP based fluorophores such as mRFP and mCherry were imaged using excitation wavelengths of 561nm and emission spectra of 595-652. Images and time series acquired with multi-track and line switching and GFP based fluorophores represented in green and RFP represented in magenta throughout the body of work. High speed acquisition utilising Airyscan fast mode was done for assessment of homotypic fusion model in Fig 7.2.

8.4.ii - Puncta Analysis

For puncta distribution, representative images from RTn17.1 over-expression were manually assessed for puncta subdomain localisation. N=4, 365 puncta assessed. For puncta size measurement, first, single frame from images were manually thresholded to generate a binary image of the puncta. This binary image was then watershed to separate 2 close puncta with some

overlapping signal. Then puncta were measured via Image J Analyze particle function, with a threshold size of 0.01-2μm μm^2 areas and edges excluded. Resulting average areas per frame were then converted into a diameter. RTN17.1 puncta analysis is based on 4 biological replicas and 22 experimental repeats with 2877 puncta analysed. RTN17.2, RTN17.3, RTN18 and RTN21.2 had a 1 biological repeat with 3 experimental repeats, with 188, 293, 305 and 202 puncta measured, respectively. For puncta speed, threshold time series from the same images were analysed for speed via Image J track mate plugin. Blob diameters were set from 0.1-2μm.

8.4.iii - Acceptor photobleaching – Förster resonance energy transfer

Acceptor photobleaching – Förster resonance energy transfer (AP-FRET) was done in accordance with Graumann et al. (2014). In short, regions of interest (ROIs) were imaged for 5 frames prior to bleaching with 100% 561nm laser power via 20 iterations. The following 15 frames were then recorded. The first 5 frames had the GFP signal averaged to generate a pre-bleach value and compared to the first post-bleach value of the GFP fluorophore to generate the FRET efficiency as a percentage. RTN1-GFP and RTN1-mRFP were used as a positive control due to previous confirmation via FRET-FLIM (Sparkes et al, 2010; Kriechbaumer et al., 2015), and RTN17.1-mRFP and GFP-HDEL were used as a negative control. A minimum n=3 biological repeats and 25 experimental repeats were utilised. Students t-test comparing each dataset was utilised to determine statistical significance. Confidence intervals * = <0.05, ** = <0.01, *** = < 0.001.

8.4.iv - Hyperconstriction analysis

High resolution networks (1024x1024 pixels, 4x averaging) of GFP-HDEL labelled ER co-expressed with RTN1-mRFP, CXN-RFP or RTN17.1-mRFP were imported as single frames into AnalyzER. Analysis parameters were set in accordance with the tutorial (Pain et al., 2019). Representative tubule traces were produced via selecting two nodes 3-4 μm apart to produce the images and plots for Figure 3.5. Full tubule morphological data for each image was then utilised to produce bar graphs of mean trough width, trough width and mean peak widths. N=3 per co-expression.

8.4.v - AnalyzER

HDEL labelled networks from either HDEL alone, or with RTN17.1-mCherry and RTN21.2-GFP were utilised for AnalyzER analysis. Twenty frame time series images of 512x512 and 1.04 or1.27 second frame intervals were uploaded, and parameters for each window were set in accordance with the tutorial provided as part of the software package, as determined by the images (Pain et al., 2019). This produced full network analysis of all measured parameters, of which 21 relevant were chosen and assessed further, the full list of which can be found in table 6.1. MANOVA statistical analysis was subsequently tested with Pillai's trace, Roy's largest root, Wilks' Lambda, Hotelling's T^2 tests to determine statistical significance. N=3 biological repeats and minimum of 23 experimental repeats for each treatment. Data output was utilised to generate boxplots in R, and representative images and scale bars from each data display acquired from the software for the required figures.

8.5 – Lipidomics

Lipidomic analysis was carried out by Lilly Maneta-Peyret and Patrick Moreau according to Kriechbaumer et al (2018b) and Fouillen et al (2018). For lipidomic analyses, 20 T2 seedlings of SALK_207412c (RTN17), SAIL_178_G04 (RTN18), and SALK_132081 (RTN21) as well as control WT-Col0 Arabidopsis were grown to 15 day olds prior to separation between the hypocotyls and roots. After transfer into 6 ml glass tubes, lipids were extracted overnight on an orbital rotator (40 rpm) at room temperature via homogenisation with 2ml chloroform/methanol/hydrochloric acid (100:50:1; v/v/v). Subsequently, each tube was centrifuged at 1000xg for 10 min. The organic phases were collected in new tubes and the samples were re-extracted with 2 ml chloroform/methanol (2:1, v/v) for 2h. After another step of centrifugation, the organic phases of each sample were combined, mixed with 1.5 ml 0.9% NaCl and centrifuged at 1000g for 10 min. The organic phases were evaporated to dryness under N2 gas exposure, re-suspended in 100 µl chloroform/methanol (1:1, v/v) and stored at -20 °C. Phospholipid and Sterol contents were then assessed via high performance thin layer chromatography (HPTLC). Aliquots (20 µl) of lipid extracts were loaded onto 10x10cm silica gel 60F254 HPTLC plates (Merck) and developed either in a solvent mixture of methyl acetate/n-propanol/chloroform/methanol/0.25% KCL (25/25/25/10/9, v/v) for phospholipid separation or hexane/ethylether/acetic acid (90:15:2 v/v) for sterol analysis. Following co-migration with known standards, lipids were identified and quantified by densitometry with a TLC scanner (CAMAG, Switzerland) as described in Laloi et al (2007). Lipid analyses were carried out on 3 independent sets of seedlings. Statistical significance of lipid profiles was tested via Welch T-test, confidence intervals represented as * = $0.05<p<0.1$, ** = $p<0.05$ and ***= $p<0.01$.

Appendix

I - Supplementary Figures

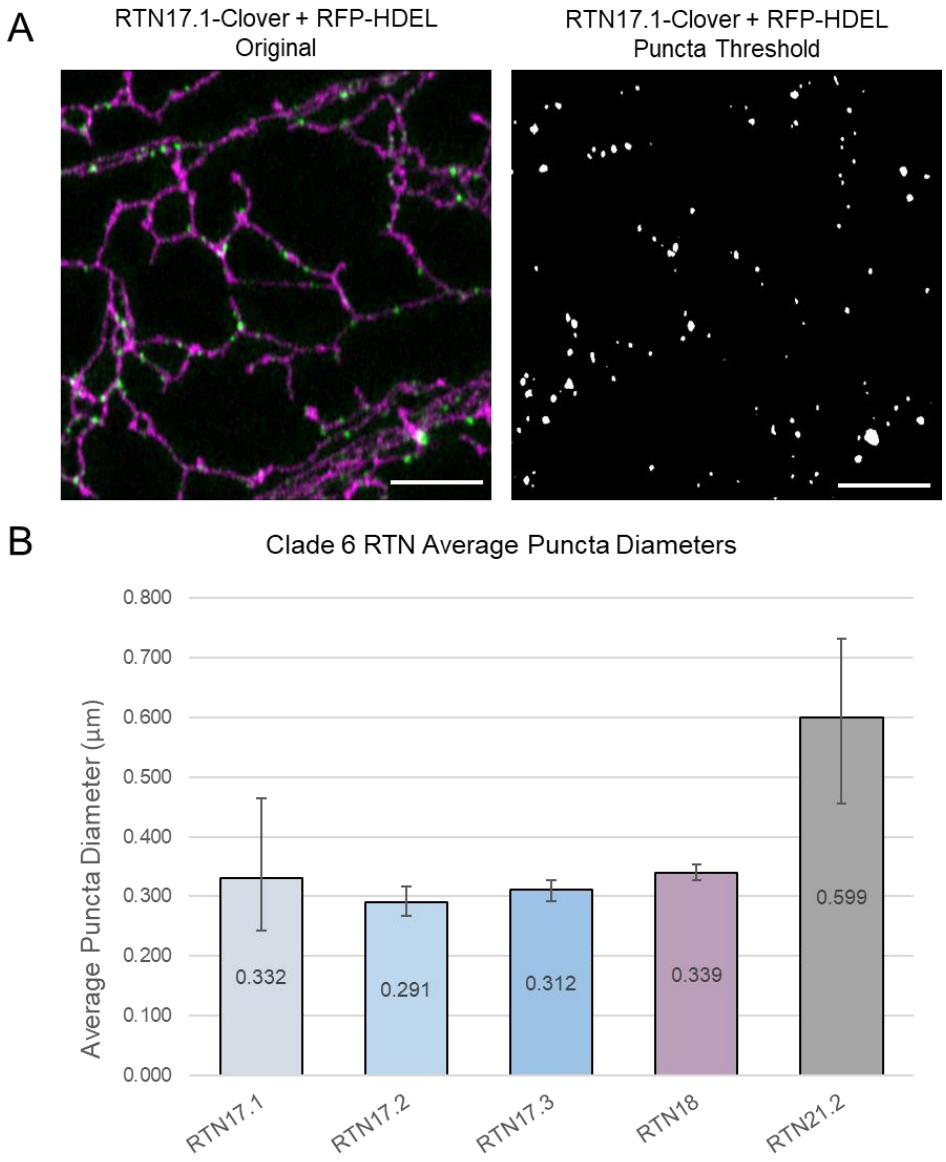

Supplementary Figure 1 – Clade 6 RTN puncta diameter analysis

A. Representative image of RTN17.1-Clover co-expressed with RFP-HDEL, and resulting image post thresholding of puncta to allow quantification. Scale bars = 5 µm **B**. Average puncta diameter of clade 6 RTNs. Error bars represent range. N= minimum of 3 biological repeats, between 188 and 2877 puncta.

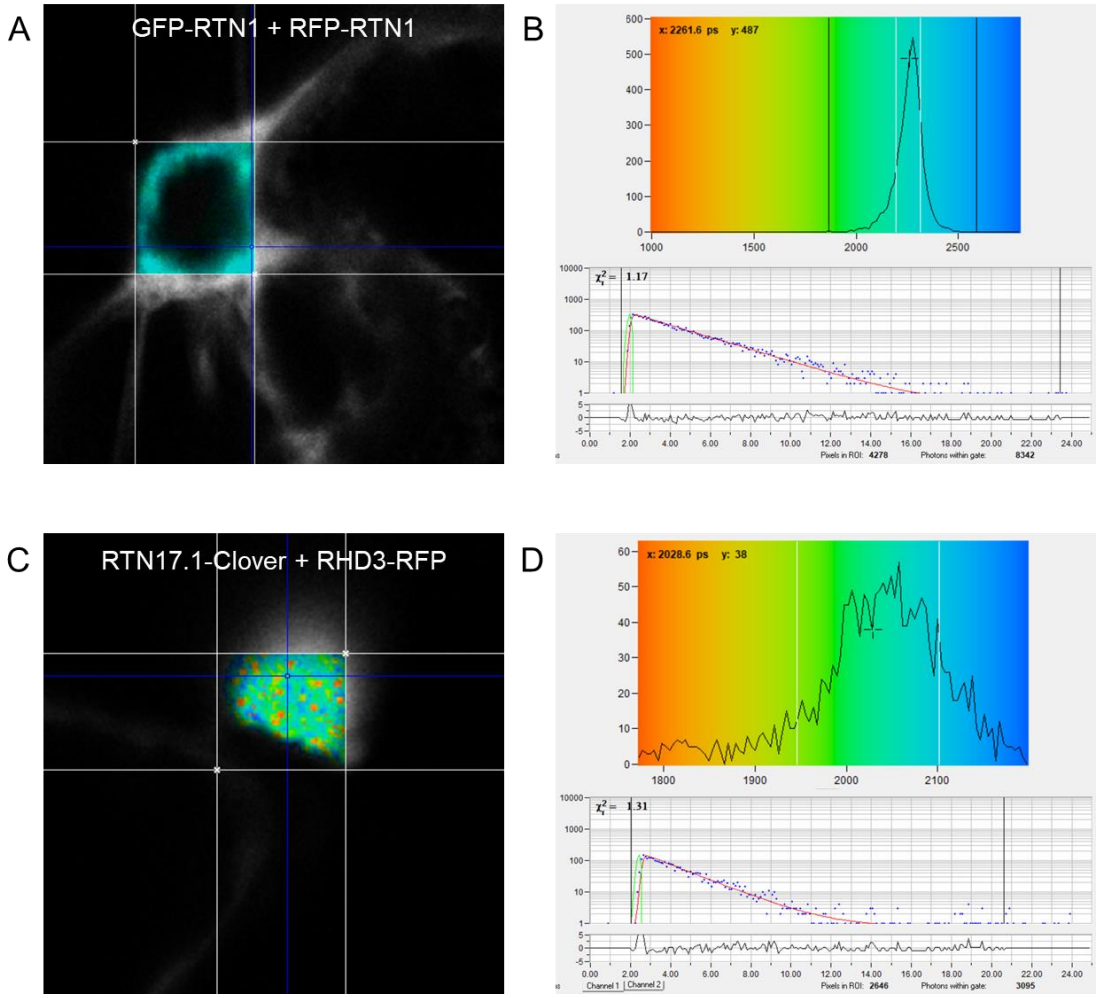

Supplementary Figure 2 – FRET-FLIM attempts with RTN17.1

A. Example FRET-FLIM acquisition of GFP-RTN1 co-expressed with RFP-RTN1. **B**. Lifetime data assessment and Chi² profile of A. **C**. Example FRET-FLIM acquisition of RTN17.1-Clover co-expressed with RHD3-RFP **D**. Lifetime data assessment and Chi² profile of C. Note elevated Chi² and heterogeneous lifetime signal/peak.

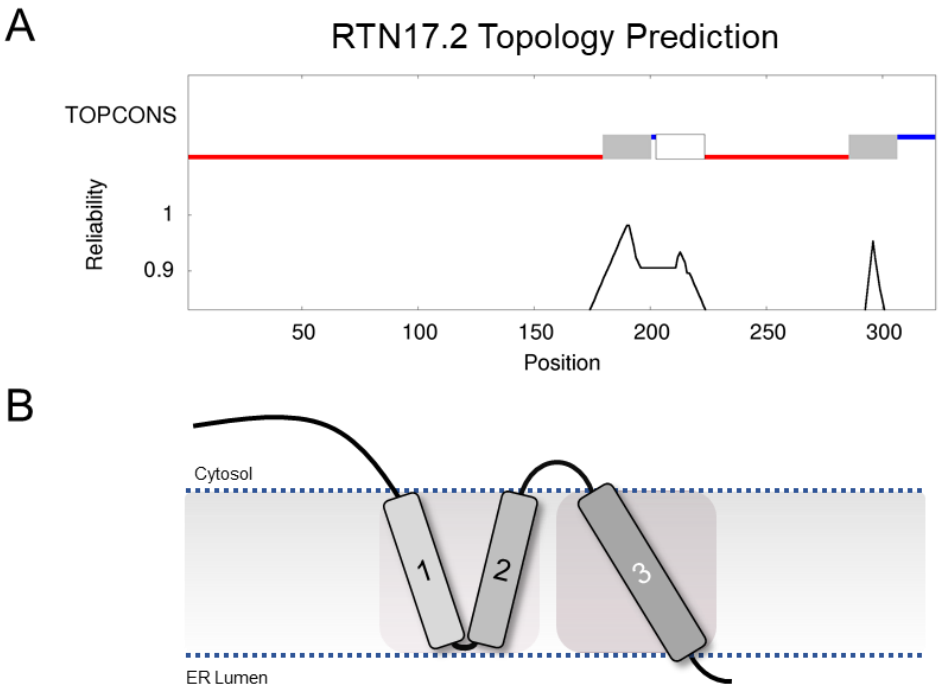

Supplementary Figure 3 – RTN17.2 topology prediction

A. TOPCONS consensus prediction of RTN17.2 topology. **B**. Schematic representation of RTN17.2 topology based on consensus prediction.

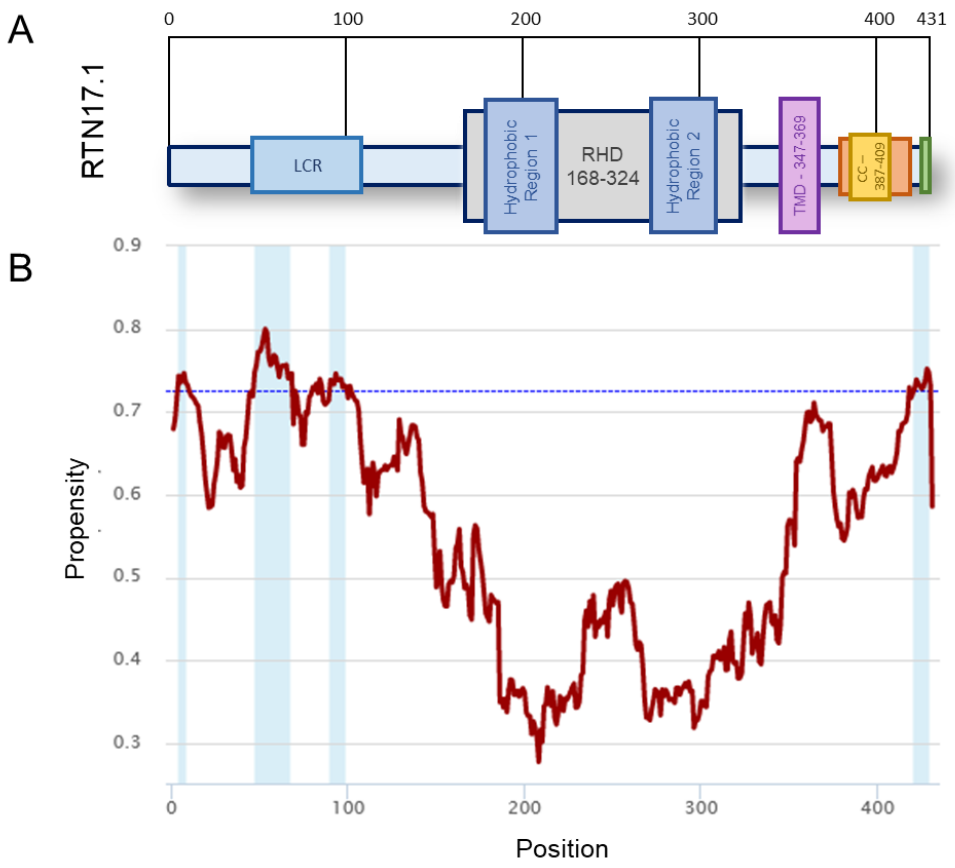

Supplementary Figure 4 – RTN17.1 MORFChibi prediction

A. RTN17.1 Schematic of structure, aligned with **B**. MORFChibi MCW (Mahlis et al., 2016) output. Residues above the 0.725 threshold (blue dotted line) for MORF prediction highlighted in light blue.

II – Supplementary Movies

1. **RTN17.1 overexpression**
2. **RTN18 transient expression in tobacco**
3. **RTN21.2 transient expression in tobacco**
4. **RTN17.2 transient expression in tobacco**
5. **RTN17.3 transient expression in tobacco**
6. **RTN17.1 fusion events compilation**

For movies, please see file: Stefan Wojcik - Thesis Supplementary Movies.ppt

Or find at:

https://drive.google.com/drive/folders/1VqcXg67bxDCvIiGh6Uv-kWxNapO-FzAX?usp=sharing

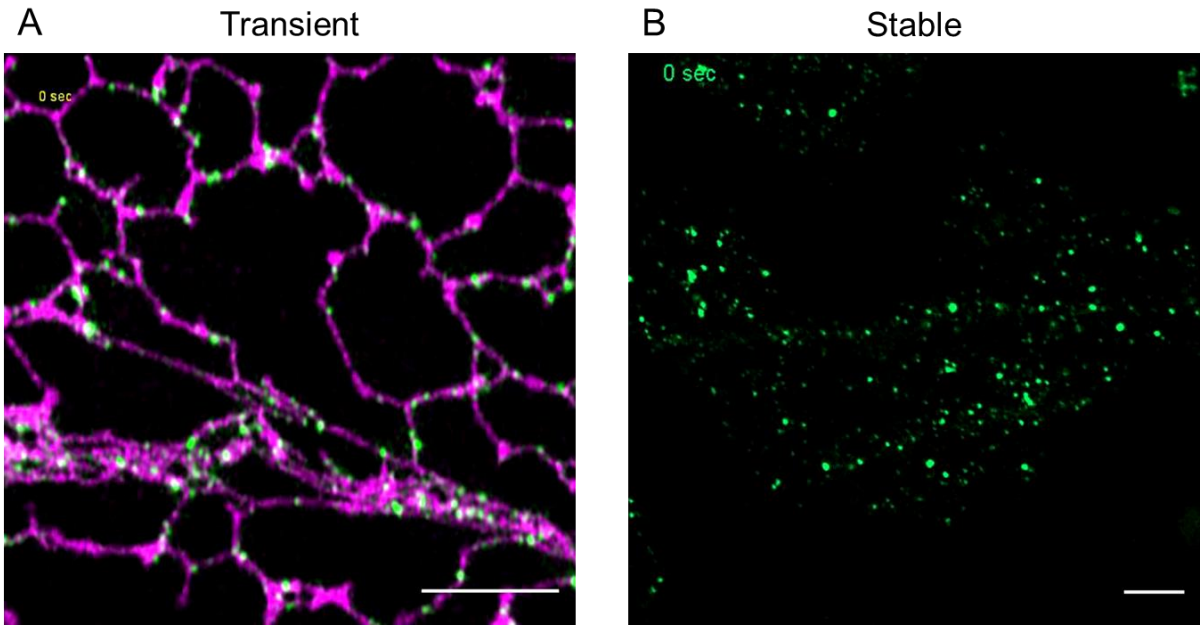

Supplementary Movie 1 – RTN17.1 over-expression

Representative time series of **A**. RTN17.1-Clover co-expressed with RFP-HDEL, transient in tobacco. 0.27s

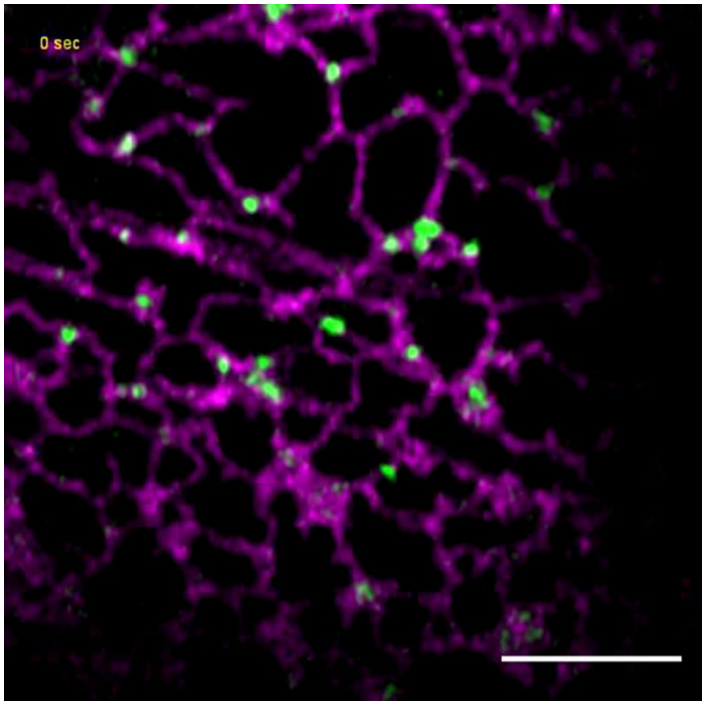

Supplementary Movie 2 – RTN18 transient expression in tobacco

Representative time series of RTN18-Clover co-expressed with RFP-HDEL, transient in tobacco. 0.27s

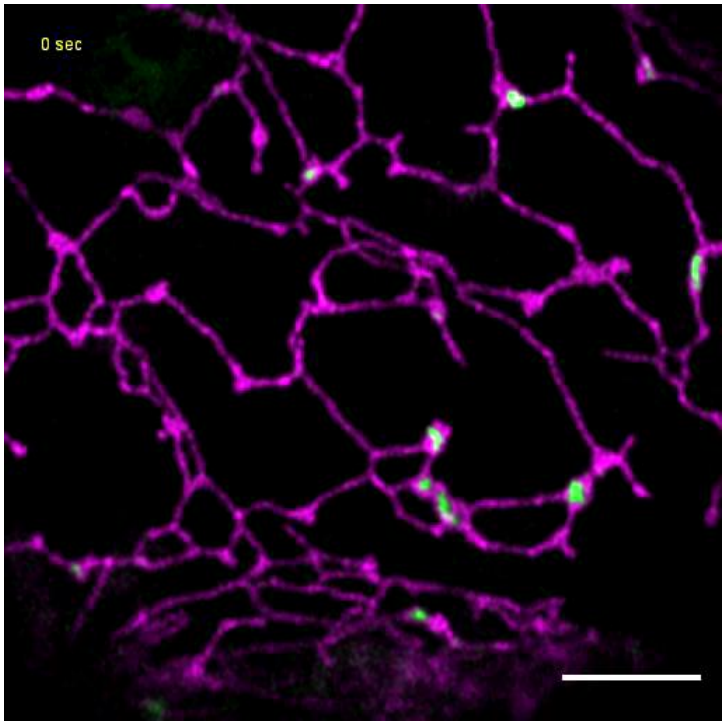

Supplementary Movie 3 – RTN21.2 transient expression in tobacco

Representative time series of GFP-RTN21.2 co-expressed with RFP-HDEL, transient in tobacco. 1.27s frame interval. Scale bar = 5µm

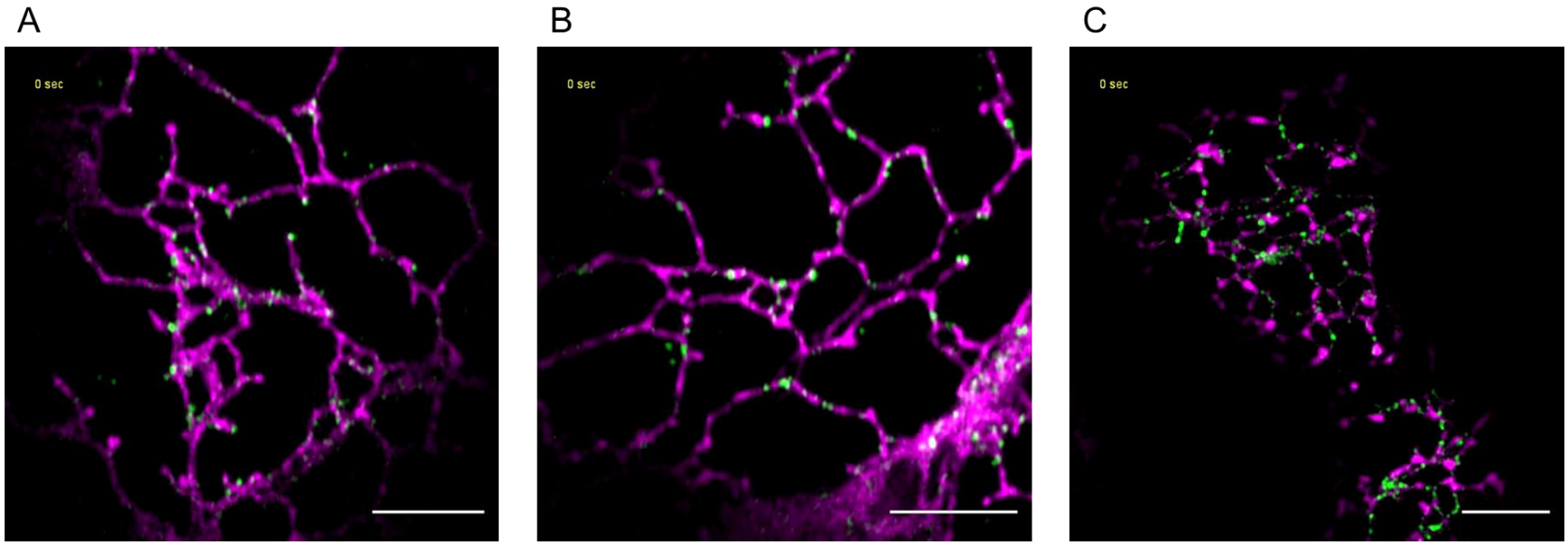

Supplementary Movie 4 – RTN17.2 transient expression in tobacco

Representative time series of RTN17.2-Clover co-expressed with RFP-HDEL, with varying effects on ER morphology, and increasing degrees of constriction from **A**. to **B**. and **C**. with the highest degree. Scale bar = 5µm

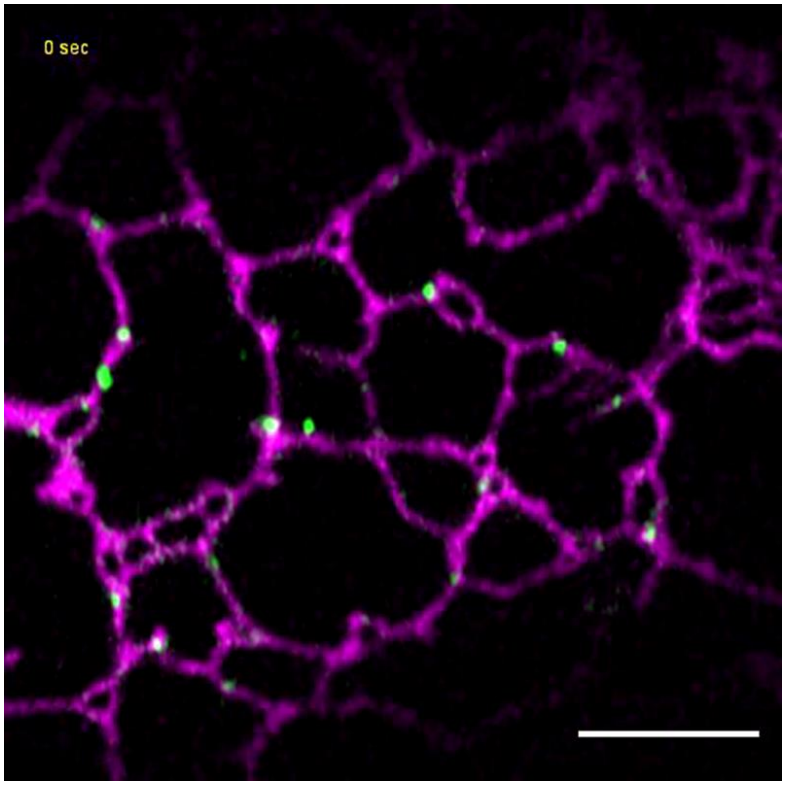

Supplementary Movie 5 – RTN17.3 transient expression in tobacco

Representative time series of RTN17.3-Clover co-expressed with RFP-HDEL, transient in tobacco. 0.52s frame interval. Scale bar = 5µm

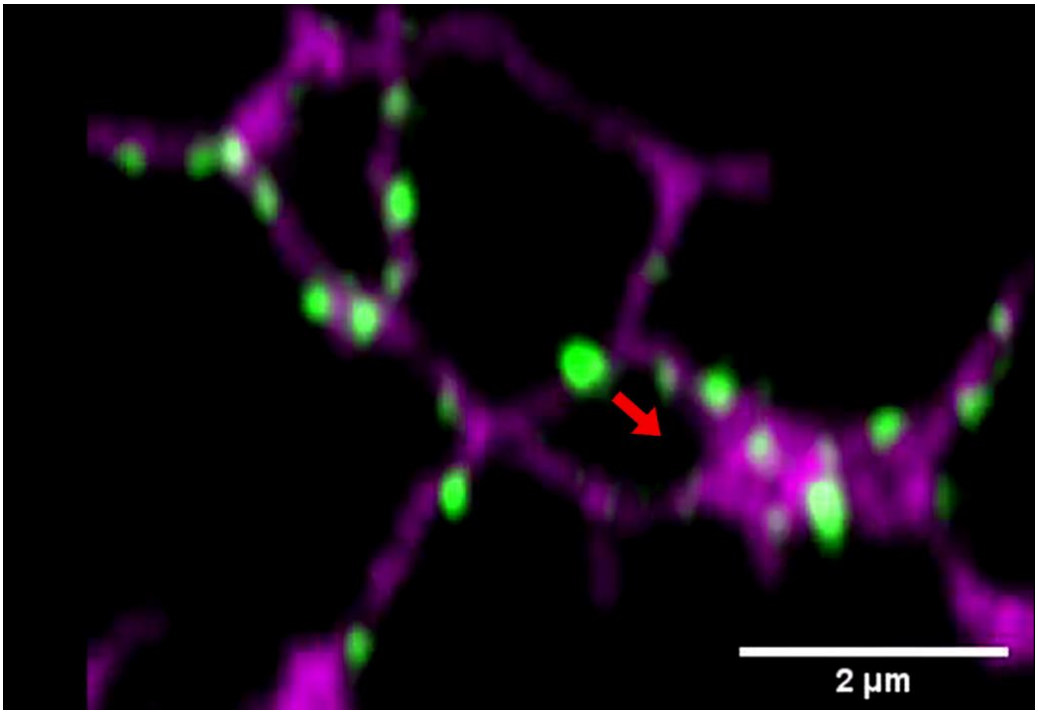

Supplementary Movie 6 – RTN17.1 fusion events compilation

Close up and high speed acquisition (0.25-0.5s frame intervals) of RTN17.1-Clover and RFP-HDEL showing puncta activity and their role in mediating different fusion events such as ring closure (parallel) and tubule elongation (perpendicular).

III – Publication contributions and presentations from the course of this programme

- Pain C, Tolmie F, Wang P, **Wojcik S**, Kriechbaumer V. intER-ACTINg: investigating the inter-relationship between the structure and dynamics of the actin cytoskeleton and the endoplasmic reticulum. Plant Physiol. – In Revision.

- **Wojcik S**, Kriechbaumer V. Go your own way: membrane-targeting sequences. Plant Physiol. 2021;185(3):608-618

- Vieira V, Pain C, **Wojcik S**, Spatola Rossi T, Denecke J, Osterrieder A, Hawes C, Kriechbaumer V. Living on the edge: the role of Atgolgin-84A at the plant ER-Golgi interface. *J Microsc*. 2020;280(2):158-173.

- Oxford Brookes BMS – 2021; Symposium Talk

- Oxford Brookes BMS – 2020; Symposium Poster

- IWPMB – 2019; Poster & Elevator Talk

- RMS Botanical Microscopy – 2019; Talk

- LSF User Meeting – 2019; Poster

Latest Talk Abstract (Oxford Brookes BMS Symposium, 2021):

The plant endoplasmic reticulum (ER) has two main morphological forms, cisternae (sheets) and tubules, proportions of either each can fluctuate within individual cells and between cell types. ER structure and function is important for cellular health as well as biotechnological applications due to its influences on protein productivity. Reticulons (RTN) are responsible for stabilising regions of high membrane curvature such as those found in tubules, edges of sheets, and PD. This work aims to characterise previously a previously undescribed subgroup of the 21 Arabidopsis RTNs. RTN17, 18 and 21 contain unique structural differences, and while still localising to the plant ER they do not exhibit the typical properties of regular RTNs. Instead, localising to three-way junctions, these demonstrate that Arabidopsis RTNs are more functionally dynamic and a have greater impact on the ER function, beyond that of just curvature stabilisation.

Latest Poster Presentation:

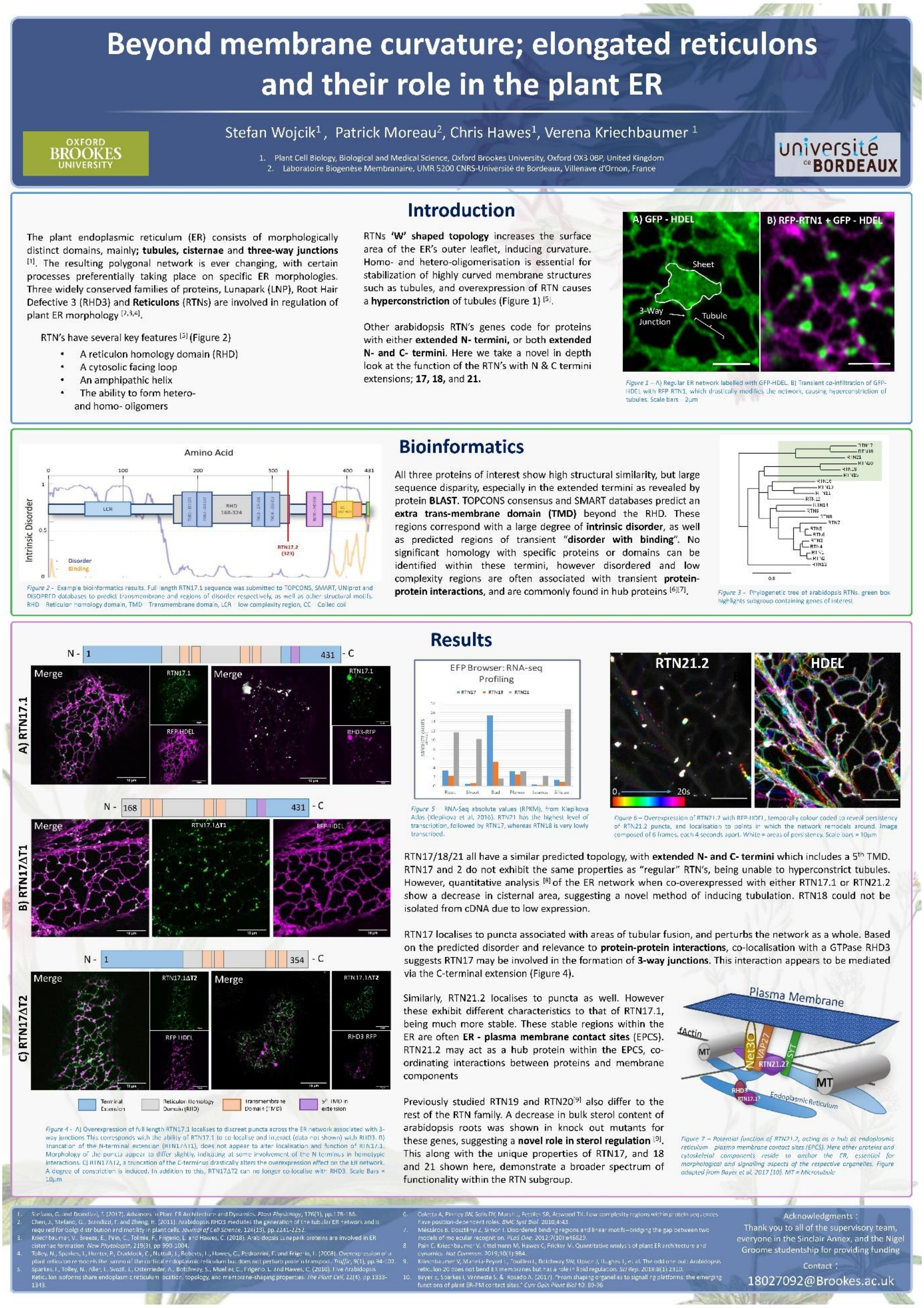

Pages 180-190 have been removed.

They contained the article 'Go your own way: membrane-targeting sequences ' by Stefan Wojcik and Verena Kriechbaumer from the journal *Plant Physiology* (https://doi.org/10.1093/plphys/kiaa058)

IV – References

Akopian D, Shen K, Zhang X, Shan SO. Signal recognition particle: an essential protein-targeting machine. Annu Rev Biochem. 2013;82:693-721.

Alberts B, Johnson A, Lewis J, Morgan DO, Raff M, Roberts K, & Walter P. Molecular Biology of the Cell. 6th. New York: Garland Science. 2014.

Alonso J, Stepanova A, Leisse A, Kim C, Chen H, & Shinn P. Genome-Wide insertional mutagenesis of Arabidopsis thaliana. Science. 2003;301(5633):653-657.

Anisimova M, Gascuel O. Approximate likelihood-ratio test for branches: A fast, accurate, and powerful alternative. Syst Biol. 2006;55(4):539-552.

Anwar K, Klemm RW, Condon A, et al. The dynamin-like GTPase Sey1p mediates homotypic ER fusion in S. cerevisiae. J Cell Biol. 2012;197(2):209-217.

Baumann O, Walz B. Endoplasmic reticulum of animal cells and its organization into structural and functional domains. Int Rev Cytol. 2001;205:149-214.

Bayer E, Sparkes I, Vanneste S, Rosado A. From shaping organelles to signalling platforms: the emerging functions of plant ER-PM contact sites. Curr Opin Plant Biol. 2017;40:89-96.

Bell RM, Ballas LM, Coleman RA. Lipid topogenesis. J Lipid Res. 1981;22(3):391-403.

Berardini TZ, Reiser L, Li D, Mezheritsky Y, Muller R, Strait E, Huala E. The Arabidopsis information resource: Making and mining the "gold standard" annotated reference plant genome. Genesis. 2015;53(8):474-85.

Bertolotti A, Zhang Y, Hendershot LM, Harding HP, Ron D. Dynamic interaction of BiP and ER stress transducers in the unfolded-protein response. Nat Cell Biol. 2000;2(6):326-332.

Blackstone C. Cellular pathways of hereditary spastic paraplegia. Annu Rev Neurosci. 2012;35:25-47.

Boevink P, Santa Cruz S, Hawes C, Harris N and Oparka, K. (1996), Virus-mediated delivery of the green fluorescent protein to the endoplasmic reticulum of plant cells. The Plant Journal, 10: 935-941

Bolte S, Cordelière F. A guided tour into subcellular colocalization analysis in light microscopy. Journal of Microscopy. 2006;224(3): 213-22

Brady JP, Claridge JK, Smith PG, Schnell JR. A conserved amphipathic helix is required for membrane tubule formation by Yop1p. Proc Natl Acad Sci U S A. 2015;112(7):E639-E648.

Breeze E, Dzimitrowicz N, Kriechbaumer V, et al. A C-terminal amphipathic helix is necessary for the in vivo tubule-shaping function of a plant reticulon. Proc Natl Acad Sci U S A. 2016;113(39):10902-10907.

Brooks RL, Mistry CS, Dixon AM. Curvature sensing amphipathic helix in the C-terminus of RTNLB13 is conserved in all endoplasmic reticulum shaping reticulons in Arabidopsis thaliana. Sci Rep. 2021;11(1):6326.

Bryson K, Cozzetto D, Jones DT. Computer-assisted protein domain boundary prediction using the DomPred server. Curr Protein Pept Sci. 2007;8(2):181-8.

Buchan DWA, Jones DT. The PSIPRED Protein Analysis Workbench: 20 years on. Nucleic Acids Res. 2019;47(W1):W402-W407.

Burgoyne RD. Neuronal calcium sensor proteins: generating diversity in neuronal Ca2+ signalling. Nat Rev Neurosci. 2007;8(3):182-193.

Buschmann H, Zachgo S. The Evolution of Cell Division: From Streptophyte Algae to Land Plants. Trends Plant Sci. 2016;21(10):872-883.

Calero M, Whittaker GR, Collins RN. Yop1p, the yeast homolog of the polyposis locus protein 1, interacts with Yip1p and negatively regulates cell growth. J Biol Chem. 2001;276(15):12100-12.

Cao P, Renna L, Stefano G, Brandizzi F. SYP73 anchors the ER to the actin cytoskeleton for maintenance of ER integrity and streaming in Arabidopsis. Curr Biol. 2016;26 (23): 3245-54.

Casey AK, Chen S, Novick P, Ferro-Novick S, Wente SR. Nuclear pore complex integrity requires Lnp1, a regulator of cortical endoplasmic reticulum. Mol Biol Cell. 2015;26(15):2833-2844.

Chen JW, Romero P, Uversky VN, Dunker AK. Conservation of intrinsic disorder in protein domains and families: I. A database of conserved predicted disordered regions. J Proteome Res. 2006;5(4):879-887.

Chen J, Stefano G, Brandizzi F, Zheng H. Arabidopsis RHD3 mediates the generation of the tubular ER network and is required for Golgi distribution and motility in plant cells. J Cell Sci. 2011;124(Pt 13):2241-52

Chen S, Novick P, Ferro-Novick S. ER network formation requires a balance of the dynamin-like GTPase Sey1p and the Lunapark family member Lnp1p. Nat Cell Biol. 2012;14(7):707-716.

Chou T, Kim KS, Oster G. Statistical thermodynamics of membrane bending-mediated protein-protein attractions. Biophys J. 2001;80(3):1075-87.

Clapham DE. Calcium signaling. Cell. 2007;131(6):1047-1058.

Clough SJ, Bent AF. Floral dip: a simplified method for Agrobacterium-mediated transformation of Arabidopsis thaliana. Plant J. 1998;16(6):735-743.

Coletta A, Pinney JW, Solís DY, Marsh J, Pettifer SR, Attwood TK. "Low-complexity regions within protein sequences have position-dependent roles." BMC Syst Biol. 2010;4:43.

Connell JW, Lindon C, Luzio JP, Reid E. Spastin couples microtubule severing to membrane traffic in completion of cytokinesis and secretion. Traffic. 2009;10(1):42-56.

Cortese MS, Uversky VN, Dunker AK. Intrinsic disorder in scaffold proteins: getting more from less. Prog Biophys Mol Biol. 2008;98(1):85-106.

Cosson P, Perrin J, Bonifacino JS. Anchors aweigh: protein localization and transport mediated by transmembrane domains. Trends Cell Biol. 2013;23(10):511-7.

Davis AM, Hall A, Millar AJ, Darrah C, Davis SJ. Protocol: Streamlined sub-protocols for floral-dip transformation and selection of transformants in Arabidopsis thaliana. Plant Methods. 2009;5:3

Day RN, Periasamy A, Schaufele F. Fluorescence resonance energy transfer microscopy of localized protein interactions in the living cell nucleus. Methods. 2001;25(1):4-18

De Craene JO, Coleman J, Estrada de Martin P, Pypaert M, Anderson S, Yates JR 3rd, Ferro-Novick S, Novick P. Rtn1p is involved in structuring the cortical endoplasmic reticulum. Mol Biol Cell. 2006;17(7):3009-20.

D' Eletto M, Risuglia A, Oliverio S, Mehdawy B, Nardacci R, Bordi M, Di Sano F. Modulation of autophagy by RTN-1C: role in autophagosome biogenesis. Cell Death Dis. 2019 Nov 18;10(12):868.

Deng Y, Srivastava R, Howell SR. Endoplasmic reticulum (ER) stress response and its physiological roles in plants. Int J Mol Sci. 2013;14(4):8188-212.

De Pinto VD, Palmieri F. Transmembrane arrangement of mitochondrial porin or voltage-dependent anion channel (VDAC). J Bioenerg Biomembr. 1992;24(1):21-26.

Di Sano F, Fazi B, Tufi R, Nardacci R, Piacentini M. Reticulon-1C acts as a molecular switch between endoplasmic reticulum stress and genotoxic cell death pathway in human neuroblastoma cells. Journal of Neurochemistry. 2007;102(2);345-353.

Dunker AK, Cortese MS, Romero P, Iakoucheva LM, Uversky VN. Flexible nets. The FEBS Journal. 2005;272: 5129-5148.

Dyson HJ, Wright PE. Intrinsically unstructured proteins and their functions. Nat Rev Mol Cell Biol. 2005;6(3):197-208

Ekman D, Light S, Björklund Ak, & Elofsson A. What properties characterize the hub proteins of the protein-protein interaction network of *Saccharomyces cerevisiae*?. Genome Biol. 2006;7(6):R45.

Erdős G, Dosztányi Z. Analyzing protein disorder with IUPred2A. Current Protocols in Bioinformatics. 2020;70, e99

Evans EA, Gilmore R, Blobel G. Purification of microsomal signal peptidase as a complex. Proc Natl Acad Sci U S A. 1986;83(3):581-585.

Fagone P, Jackowski S. Membrane phospholipid synthesis and endoplasmic reticulum function. J Lipid Res. 2009;50:S311-S316.

Fazi B, Melino S, Di Sano F, Cicero DO, Piacentini M, Paci M. Cloning, expression, and preliminary structural characterization of RTN-1C. Biochem Biophys Res Commun. 2006;342(3):881-886.

Fouillen L, Maneta-Peyret L, Moreau P. ER Membrane Lipid Composition and Metabolism: Lipidomic Analysis. In: Hawes C., Kriechbaumer V. The Plant Endoplasmic Reticulum. Methods in Molecular Biology. Humana Press, New York, NY. 2018;1691:125-137.

Fournier AE, GrandPre T, Strittmatter SM. Identification of a receptor mediating Nogo-66 inhibition of axonal regeneration. Nature. 2001;409(6818):341-6.

Galea CA, Wang Y, Sivakolundu SG, Kriwacki RW. Regulation of cell division by intrinsically unstructured proteins: intrinsic flexibility, modularity, and signaling conduits. Biochemistry. 2008;47(29):7598-609.

Gilmore R, Blobel G, Walter P. Protein translocation across the endoplasmic reticulum. I. Detection in the microsomal membrane of a receptor for the signal recognition particle. J Cell Biol. 1982;95(2 Pt 1):463-469.

Gong L, Tang Y, An R, Lin M, Chen L, Du J. RTN1-C mediates cerebral ischemia/reperfusion injury via ER stress and mitochondria-associated apoptosis pathways. Cell Death Dis. 2017;8(10):e3080.

Goyal U, Blackstone C. Untangling the web: mechanisms underlying ER network formation. Biochim Biophys Acta. 2013;1833(11):2492-8.

Graumann K, Vanrobays E, Tutois S, Probst A, Evans DE, Tatout C. Characterization of two distinct subfamilies of SUN-domain proteins in Arabidopsis and their interactions with the novel KASH-domain protein AtTIK. J Exp Bot. 2014;65(22):6499-512.

Griffing LR, Gao HT, Sparkes I. ER network dynamics are differentially controlled by myosins XI-K, XI-C, XI-E, XI-I, XI-1, and XI-2. Front Plant Sci. 2014;5:218.

Grigoriev A. On the number of protein-protein interactions in the yeast proteome. Nucleic Acids Res. 2003;31(14):4157-4161.

Guenoune-Gelbart D, Elbaum M, Sagi G, Levy A, Epel BL. Tobacco mosaic virus (TMV) replicase and movement protein function synergistically in facilitating TMV spread by lateral diffusion in the plasmodesmal desmotubule of Nicotiana benthamiana. Mol Plant Microbe Interact. 2008;21(3):335-345.

Hamada T, Ueda H, Kawase T, Hara-Nishimura I. Microtubules contribute to tubule elongation and anchoring of endoplasmic reticulum, resulting in high network complexity in Arabidopsis. Plant Physiol. 2014;166(4):1869-1876.

Hawes C, Kiviniemi P, Kriechbaumer V. The endoplasmic reticulum: A dynamic and well-connected organelle. Journal of Integrative Plant Biology. 2015;57(1):50-62.

Hawkins TJ, Deeks MJ, Wang P, Hussey PJ. The evolution of the actin binding NET superfamily. Front Plant Sci 2014;5:254.

Haynes C, Oldfield CJ, Ji F, Klitgord N, Cusick ME, Radivojac P, Uversky VN, Vidal M, Iakoucheva LM. Intrinsic disorder is a common feature of hub proteins from four eukaryotic interactomes. PLoS Comput Biol. 2006;2(8):e100.

He W, Shi Q, Hu X, Yan R. The membrane topology of RTN3 and its effect on binding of RTN3 to BACE1. J Biol Chem. 2007;282(40):29144-51

Henneberry AL, Wright MM, McMaster CR. The major sites of cellular phospholipid synthesis and molecular determinants of Fatty Acid and lipid head group specificity. Mol Biol Cell. 2002;13(9):3148-3161.

Hepler PK, Palevitz BA, Lancelle SA, Mccauley MM, Lichtschidl L. Cortical endoplasmic reticulum in plants. J Cell Sci. 1990; 96 (3): 355–373.

Hogan P, Lewis RS, Rao A. 2010. Molecular basis of calcium signaling in lymphocytes: STIM and ORAI. Annu Rev Immunol. 2010;28:491-533.

Hu J, Shibata Y, Voss C, Shemesh T, Li Z, Coughlin M, Kozlov MM, Rapoport TA, Prinz WA. Membrane proteins of the endoplasmic reticulum induce high-curvature tubules. Science. 2008;319(5867):1247-50.

Hu J, Shibata Y, Zhu PP, Voss C, Rismanchi N, Prinz WA, Rapoport TA, Blackstone C. A class of dynamin-like GTPases involved in the generation of the tubular ER network. Cell. 2009;138(3):549-61.

Hu Y, Zhong R, Morrison WH 3rd, Ye ZH. The Arabidopsis RHD3 gene is required for cell wall biosynthesis and actin organization. Planta. 2003;217(6):912-921.

Iwahashi J, Hamada N. Human reticulon 1-A and 1-B interact with a medium chain of the AP-2 adaptor complex. Cell Mol Biol (Noisy-le-grand). 2003;49 Online Pub:OL467-71

Iwahashi J, Hamada N, Watanabe H. Two hydrophobic segments of the RTN1 family determine the ER localization and retention. Biochem Biophys Res Commun. 2007;355(2):508-12.

Jan CH, Williams CC, Weissman JS. Principles of ER cotranslational translocation revealed by proximity-specific ribosome profiling. Science. 2014;346(6210):1257521.

Jékely G. Origin of eukaryotic endomembranes: a critical evaluation of different model scenarios. Adv Exp Med Biol. 2007;607:38-51.

Jones DT, Cozzetto D. DISOPRED3: precise disordered region predictions with annotated protein-binding activity. Bioinformatics. 2015;31(6):857-63

Kaya L, Meissner B, Riedl MC, et al. Direct association of the reticulon protein RTN1A with the ryanodine receptor 2 in neurons. Biochim Biophys Acta. 2013;1833(6):1421-1433.

Kenworthy AK. Imaging protein-protein interactions using fluorescence resonance energy transfer microscopy. Methods. 2001;24(3):289-96.

Kim H, Kwon H, Kim S, Kim MK, Botella MA, Yun HS, Kwon C. Synaptotagmin 1 negatively controls the two distinct immune secretory pathways to powdery mildew fungi in Arabidopsis. Plant and Cell Physiology. 2016;57(6):1133-1141.

Kim KT, Moon Y, Jang Y, et al. Molecular mechanisms of atlastin-mediated ER membrane fusion revealed by a FRET-based single-vesicle fusion assay. Sci Rep. 2017;7(1):8700.

Klepikova A, Kasianov A, Gerasimov E, Logacheva M, Penin A. A high resolution map of the *Arabidopsis thaliana* developmental transcriptome based on RNA-seq profiling. Plant J. 2016;88(6):1058-1070.

Knox K, Wang P, Kriechbaumer V, et al. Putting the Squeeze on PD: A role for reticulons in primary PD formation. Plant Physiol. 2015;168(4):1563-1572.

Kotta-Loizou I, Tsaousis GN, Hamodrakas SJ. Analysis of Molecular Recognition Features (MoRFs) in membrane proteins. Biochim Biophys Acta. 2013;1834(4):798-807.

Kriechbaumer V, Botchway SW, Slade SE, Knox K, Frigerio L, Oparka K, Hawes C. Reticulomics: Protein-protein interaction studies with two PD-localized reticulon family proteins identify binding partners enriched at pd, endoplasmic reticulum, and the plasma membrane. Plant Physiol. 2015;169(3):1933-45

Kriechbaumer V, Botchway SW, Hawes C. Localization and interactions between Arabidopsis auxin biosynthetic enzymes in the TAA/YUC-dependent pathway. J Exp Bot. 2016;67(14):4195-207

Kriechbaumer V, Breeze E, Pain C, Tolmie F, Frigerio L, Hawes C. Arabidopsis Lunapark proteins are involved in ER cisternae formation. New Phytol. 2018;219(3):990-1004. A

Kriechbaumer V, Maneta-Peyret L, Fouillen L, et al. The odd one out: Arabidopsis reticulon 20 does not bend ER membranes but has a role in lipid regulation. Sci Rep. 2018;8(1):2310. B

Lai YS, Stefano G, Brandizzi F. ER stress signaling requires RHD3, a functionally conserved ER-shaping GTPase. J Cell Sci. 2014;127(Pt 15):3227-32.

Laloi M, Perret AM, Chatre L, Melser S, Cantrel C, Vaultier MN, Zachowski A, Bathany K, Schmitter JM, Vallet M, Lessire R, Hartmann MA, Moreau P. Insights into the role of specific lipids in the formation and delivery of lipid microdomains to the plasma membrane of plant cells. Plant Physiol. 2007;143(1):461-472.

Lee C, Chen LB. Dynamic behavior of endoplasmic reticulum in living cells. Cell. 1988;54(1):37-46

Lee H, Sparkes I, Gattolin S, Dzimitrowicz N, Roberts LM, Hawes C, Frigerio L. An Arabidopsis reticulon and the atlastin homologue RHD3-like2 act together in shaping the tubular endoplasmic reticulum. New Phytol. 2013;197(2):481-489

Lentze N, Auerbach D. Membrane-based yeast two-hybrid system to detect protein interactions. Curr Protoc Protein Sci. 2008 May;Chapter 19:Unit 19.17

Letunic I, Khedkar S, Bork P. SMART: recent updates, new developments and status in 2020. Nucleic Acids Res. 2021;49(D1):D458-D460

Levy A, Zheng J, Lazarowitz S. Synpatotagmin SYTA forms ER-plasma membrance junctions that are recruited to PD for plant virus movement. Curr Biol 2015;25(15):2018-2025.

Li M, Song J. The N- and C-termini of the human Nogo molecules are intrinsically unstructured: bioinformatics, CD, NMR characterization, and functional implications. Proteins. 2007;68(1):100-108.

Li S, Kim JE, Budel S, Hampton TG, Strittmatter SM. Transgenic inhibition of Nogo-66 receptor function allows axonal sprouting and improved locomotion after spinal injury. Mol Cell Neurosci. 2005;29(1):26-39.

Lin JH, Li H, Yasumura D, Cohen HR, Zhang C, Panning B, Shokat KM, Lavail MM, Walter P. IRE1 signaling affects cell fate during the unfolded protein response. Science. 2007;318(5852):944-9.

Lin JS., Lai EM. (2017) Protein–Protein Interactions: Co-Immunoprecipitation. In: Journet L., Cascales E. (eds) Bacterial Protein Secretion Systems. Methods in Molecular Biology, vol 1615. Humana Press, New York, NY.

Lin S, Sun S, Hu J. Molecular basis for sculpting the endoplasmic reticulum membrane. Int J Biochem Cell Biol. 2012;44(9):1436-1443.

Liu JX, Srivastava R, Che P, Howell SH. An endoplasmic reticulum stress response in Arabidopsis is mediated by proteolytic processing and nuclear relocation of a membrane-associated transcription factor, bZIP28. Plant Cell. 2007;19(12):4111-4119.

Liu TY, Bian X, Sun S, et al. Lipid interaction of the C terminus and association of the transmembrane segments facilitate atlastin-mediated homotypic endoplasmic reticulum fusion. Proc Natl Acad Sci U S A. 2012;109(32):E2146-E2154.

Lu L, Ladinsky MS, Kirchhausen T. Cisternal organization of the endoplasmic reticulum during mitosis. Mol Biol Cell. 2009;20(15):3471-3480.

Madeira F, Park YM, Lee J, Buso N, Gur T, Madhusoodanan N, Basutkar P, Tivey ARN, Potter SC, Finn RD, Lopez R. The EMBL-EBI search and sequence analysis tools APIs in 2019. Nucleic Acids Res. 2019;47(W1):W636-W641

Malhis N, Jacobson M, Gsponer J. MoRFchibi SYSTEM: software tools for the identification of MoRFs in protein sequences. Nucleic Acids Res. 2016;44(W1):W488-W493

Maneta-Peyret L, Lai YS, Stefano G, Fouillen L, Brandizzi F, Moreau P. Phospholipid biosynthesis increases in RHD3-defective mutants. Plant Signal Behav. 2014;9(9):e29657.

Manu MS, Ghosh D, Chaudhari BP, Ramasamy S. Analysis of tail-anchored protein translocation pathway in plants. Biochem Biophys Rep. 2018;14:161-167.

Marchi S, Patergnani S, Missiroli S, et al. Mitochondrial and endoplasmic reticulum calcium homeostasis and cell death. Cell Calcium. 2018;69:62-72.

Martin WF, Garg S, Zimorski V. Endosymbiotic theories for eukaryote origin. Philos Trans R Soc Lond B Biol Sci. 2015;370(1678):2014033

Maule AJ. PD: structure, function and biogenesis. Curr Opin Plant Biol. 2008;11(6):680-686.

McFarlane HE, Kyoung-Lee E, Van-Bezouwen L, Ross B, Rosado A, Samuels A. Multiscale structural analysis of the plant ER-PM contact sites. Plant and Cell Physiology. 2017;58(3):478-484.

Merrill AH Jr. De novo sphingolipid biosynthesis: a necessary, but dangerous, pathway. J Biol Chem. 2002;277(29):25843-25846.

Mészáros B, Erdős G, Dosztányi Z. IUPred2A: context-dependent prediction of protein disorder as a function of redox state and protein binding. Nucleic Acids Research. 2002;46(W1):329-337

Mészáros B, Tompa P, Simon I, Dosztányi Z. Molecular principles of the interactions of disordered proteins. J Mol Biol. 2007 Sep 14;372(2):549-61.

Mészáros B, Simon I, Dosztányi Z. Prediction of protein binding regions in disordered proteins. PLOS Computational Biology. 2009;5(5):e1000376.

Mészáros B, Erdos G, Dosztányi Z. IUPred2A: context-dependent prediction of protein disorder as a function of redox state and protein binding. Nucleic Acids Res. 2018;46(W1):W329-W337.

Mohan A, Oldfield CJ, Radivojac P, et al. Analysis of molecular recognition features (MoRFs). J Mol Biol. 2006;362(5):1043-1059.

Möller S, Croning MD, Apweiler R. Evaluation of methods for the prediction of membrane spanning regions. Bioinformatics. 2001 Jul;17(7):646-53.

Moriya K, Nagatoshi K, Noriyasu Y, et al. Protein N-myristoylation plays a critical role in the endoplasmic reticulum morphological change induced by overexpression of protein Lunapark, an integral membrane protein of the endoplasmic reticulum. PLoS One. 2013;8(11):e78235

Moss TJ, Andreazza C, Verma A, Daga A, McNew JA. Membrane fusion by the GTPase atlastin requires a conserved C-terminal cytoplasmic tail and dimerization through the middle domain. Proc Natl Acad Sci U S A. 2011;108(27):11133-11138.

Nilsson T, Jackson M, Peterson PA. Short cytoplasmic sequences serve as retention signals for transmembrane proteins in the endoplasmic reticulum. Cell. 1989;58(4):707-18

Nixon-Abell J, Obara CJ, Weigel AV, Li D, Legant WR, Xu CS, Pasolli HA, Harvey K, Hess HF, Betzig E, Blackstone C, Lippincott-Schwartz J. Increased spatiotemporal resolution reveals highly dynamic dense tubular matrices in the peripheral ER. Science. 2016;354(6311):aaf3928

Nziengui H, Bouhidel K, Pillon D, Der C, Marty F, Schoefs B. Reticulon-like proteins in Arabidopsis thaliana: structural organization and ER localization. FEBS Lett 2007;581(18):3356-62.

Oates ME, Romero P, Ishida T, Ghalwash M, Mizianty MJ, Xue B, Dosztányi Z, Uversky VN, Obradovic Z, Kurgan L, Dunker AK, Gough J. D^2P^2: database of disordered protein predictions. Nucleic Acids Res. 2013:D508-16.

Orso G, Pendin D, Liu S, et al. Homotypic fusion of ER membranes requires the dynamin-like GTPase atlastin. Nature. 2009;460(7258):978-983.

Overall RL, Blackman LM (1996) A model of the macro-molecular structure of PD. Trends Plant Sci 1: 307–311.

Pain C, Kriechbaumer V, Kittelmann M, Hawes C, Fricker M. Quantitative analysis of plant ER architecture and dynamics. Nat Commun. 2019;10(1):984.

Pain C, Kriechbaumer V. Defining the dance: quantification and classification of endoplasmic reticulum dynamics. J Exp Bot. 2020;71(6):1757-1762.

Park CJ, Park JM. Endoplasmic Reticulum Plays a Critical Role in Integrating Signals Generated by Both Biotic and Abiotic Stress in Plants. Front Plant Sci. 2019;10:399.

Park SH, Zhu PP, Parker RL, Blackstone C. Hereditary spastic paraplegia proteins REEP1, spastin, and atlastin-1 coordinate microtubule interactions with the tubular ER network. J Clin Invest. 2010;120(4):1097-1110.

Pastor-Cantizano N, Ko DK, Angelos E, Pu Y, Brandizzi F. Functional Diversification of ER Stress Responses in Arabidopsis. Trends Biochem Sci. 2020;45(2):123-136.

Pawson T, Nash P. Protein-protein interactions define specificity in signal transduction. Genes Dev. 2000 May 1;14(9):1027-47.

Pérez-Sancho J, Vanneste S, Lee E, McFarlane HE, Esteban del Valle A, Valpuesta V, Friml J, Botella MA, Rosado A. The Arabidopsis synaptotagmin1 is enriched in endoplasmic reticulum-plasma membrane contact sites and confers cellular resistance to mechanical stresses. Plant Physiology. 2015;168(1):132-143.

Pietrosemoli N, García-Martín JA, Solano R, Pazos F. Genome-wide analysis of protein disorder in Arabidopsis thaliana: implications for plant environmental adaptation. PLoS One. 2013;8(2):e55524.

Pomorski T, Menon AK. Lipid flippases and their biological functions. Cell Mol Life Sci. 2006;63(24):2908-2921.

Powers RE, Wang S, Liu TY, Rapoport TA. Reconstitution of the tubular endoplasmic reticulum network with purified components. Nature. 2017;543(7644):257-260.

Putney JW. Capacitative calcium entry: sensing the calcium stores. J Cell Biol. 2005;169(3):381-382

Radivojac P, Iakoucheva LM, Oldfield CJ, Obradovic Z, Uversky VN, Dunker AK. Intrinsic disorder and functional proteomics. Biophys J. 2007;92(5):1439-1456.

Rahier A, Darnet S, Bouvier F, Camara B, Bard M. Molecular and enzymatic characterizations of novel bifunctional 3beta-hydroxysteroid dehydrogenases/C-4 decarboxylases from Arabidopsis thaliana. J Biol Chem. 2006;281(37):27264-77.

Rämö O, Kumar D, Gucciardo E, Joensuu M, Saarekas M, Vihinen H, Belevich I, Smolander OP, Qian K, Auvinen P, Jokitalo E. NOGO-A/RTN4A and NOGO-B/RTN4B are simultaneously expressed in epithelial, fibroblast and neuronal cells and maintain ER morphology. Sci Rep. 2016;6:35969.

Rapoport TA. Protein translocation across the eukaryotic endoplasmic reticulum and bacterial plasma membranes. Nature. 2007;450(7170):663-669.

Ridge RW, Uozumi Y, Plazinski J, Hurley UA, Williamson RE. Developmental transitions and dynamics of the cortical ER of Arabidopsis cells seen with green fluorescent protein. Plant Cell Physiol. 1999;40(12):1253-1261.

Riedl J, Crevenna AH, Kessenbrock K, et al. Lifeact: a versatile marker to visualize F-actin. Nat Methods. 2008;5(7):605-607.

Rodríguez-Feo JA, Gallego-Delgado J, Puerto M, Wandosell F, Osende J. Reticulon-4B/Nogo-B acts as a molecular linker between microtubules and actin cytoskeleton in vascular smooth muscle cells. Biochim Biophys Acta. 2016;1863(8):1985-1995.

Rogers JV, McMahon C, Baryshnikova A, Hughson FM, Rose MD. ER-associated retrograde SNAREs and the Dsl1 complex mediate an alternative, Sey1p-independent homotypic ER fusion pathway. Mol Biol Cell. 2014;25(21):3401-3412.

Ruggiano A, Foresti O, Carvalho P. Quality control: ER-associated degradation: protein quality control and beyond. J Cell Biol. 2014;204(6):869-879.

Sapay N, Guermeur Y, Deléage G. Prediction of amphipathic in-plane membrane anchors in monotopic proteins using a SVM classifier. BMC Bioinformatics. 2006;7:255.

Schallus T, Jaeckh C, Fehér K, et al. Malectin: a novel carbohydrate-binding protein of the endoplasmic reticulum and a candidate player in the early steps of protein N-glycosylation. Mol Biol Cell. 2008;19(8):3404-3414.

Schlacht A, Herman EK, Klute MJ, Field MC, Dacks JB. Missing pieces of an ancient puzzle: evolution of the eukaryotic membrane-trafficking system. Cold Spring Harb Perspect Biol. 2014;6(10):a016048.

Schmid M, Davison TS, Henz SR, et al. A gene expression map of Arabidopsis thaliana development. Nat Genet. 2005;37(5):501-506.

Schroeder LK, Barentine AES, Merta H, et al. Dynamic nanoscale morphology of the ER surveyed by STED microscopy. J Cell Biol. 2019;218(1):83-96.

Schuck S, Prinz WA, Thorn KS, Voss C, Walter P. Membrane expansion alleviates endoplasmic reticulum stress independently of the unfolded protein response [published correction appears in J Cell Biol. 2021 Apr 5;220(4):]. J Cell Biol. 2009;187(4):525-536.

Schwab ME, Strittmatter SM. Nogo limits neural plasticity and recovery from injury. Curr Opin Neurobiol. 2014;27:53-60.

Schwarz DS, Blower MD. The endoplasmic reticulum: structure, function and response to cellular signalling. Cell Mol Life Sci. 2016;73(1):79-94. doi:10.1007/s00018-015-2052-6.

Scripture JB, Huber PW. Binding site for Xenopus ribosomal protein L5 and accompanying structural changes in 5S rRNA. Biochemistry. 2011;50(18):3827-39.

Sekar RB, Periasamy A. Fluorescence resonance energy transfer (FRET) microscopy imaging of live cell protein localizations. J Cell Biol. 2003;160(5):629-633.

Sheahan MB, Rose RJ, McCurdy DW. Organelle inheritance in plant cell division: the actin cytoskeleton is required for unbiased inheritance of chloroplasts, mitochondria and endoplasmic reticulum in dividing protoplasts. Plant J. 2004;37(3):379-390.

Shibata Y, Voeltz GK, Rapoport TA. Rough sheets and smooth tubules. Cell. 2006;126(3):435-439.

Shibata Y, Voss C, Rist JM, et al. The reticulon and DP1/Yop1p proteins form immobile oligomers in the tubular endoplasmic reticulum. J Biol Chem. 2008;283(27):18892-18904.

Shibata Y, Shemesh T, Prinz WA, Palazzo AF, Kozlov MM, Rapoport TA. Mechanisms determining the morphology of the peripheral ER. Cell. 2010;143(5):774-788.

Sia W, Wang P, Voigt B, Hussey PJ, Baluska F. Arabidopsis SYT1 maintains stability of cortical endoplasmic reticulum networks and VAP27-1-enriched endoplasmic reticulum-plasma membrane contact sites. J Exp Bot. 2016;67(21):6161-6171.

Singh S, Mittal A. Transmembrane Domain Lengths Serve as Signatures of Organismal Complexity and Viral Transport Mechanisms. Sci Rep. 2016;6:22352.

Sparkes I, Teanby NA, Hawes C. Truncated myosin XI tail fusions inhibit peroxisome, Golgi, and mitochondrial movement in tobacco leaf epidermal cells: a genetic tool for the next generation. J Exp Bot. 2008;59(9):2499-2512.

Sparkes IA, Frigerio L, Tolley N, Hawes C. The plant endoplasmic reticulum: a cell-wide web. Biochem J. 2009;423(2):145-55. A

Sparkes I, Runions J, Hawes C, Griffing L. Movement and remodeling of the endoplasmic reticulum in nondividing cells of tobacco leaves. Plant Cell. 2009;21(12):3937-3949. B

Sparkes I, Tolley N, Aller I, Svozil J, Osterrieder A, Botchway S, Mueller C, Frigerio L, Hawes C. Five Arabidopsis reticulon isoforms share endoplasmic reticulum location, topology, and membrane-shaping properties. Plant Cell. 2010;22(4):1333-1343.

Spitz F, Gonzalez F, Duboule D. A global control region defines a chromosomal regulatory landscape containing the HoxD cluster. Cell. 2003 May 2;113(3):405-17.

Stanley P. Golgi glycosylation. Cold Spring Harb Perspect Biol. 2011;3(4):a005199.

Stefano G, Renna L, Moss T, McNew JA, Brandizzi F. In Arabidopsis, the spatial and dynamic organization of the endoplasmic reticulum and Golgi apparatus is influenced by the integrity of the C-terminal domain of RHD3, a non-essential GTPase. Plant J. 2012;69(6):957-66.

Steiner P, Kulangara K, Sarria JC, Glauser L, Regazzi R, Hirling H. Reticulon 1-C/neuroendocrine-specific protein-C interacts with SNARE proteins. J Neurochem. 2004;89(3):569-580.

Stephenson JLM, Hawes C. Stereology and stereometry of endoplasmic reticulum during differentiation in the maize root cap. Protoplasma. 1986;131, 32–46.

Strasser R. Plant protein glycosylation. Glycobiology. 2016;26(9):926-939.

Strehler EE, Treiman M. Calcium pumps of plasma membrane and cell interior. Curr Mol Med. 2004;4(3):323-335.

Sun J, Movahed N, Zheng H. LUNAPARK Is an E3 Ligase That Mediates Degradation of ROOT HAIR DEFECTIVE3 to Maintain a Tubular ER Network in Arabidopsis. Plant Cell. 2020;32(9):2964-2978.

Sun J, Zhang M, Qi X, Doyle C, Zheng H. Armadillo-repeat kinesin1 interacts with Arabidopsis atlastin RHD3 to move ER with plus-end of microtubules. Nat Commun. 2020;11(1):5510.

Sun J, Zheng H. Efficient ER Fusion Requires a Dimerization and a C-Terminal Tail Mediated Membrane Anchoring of RHD3. Plant Physiol. 2018;176(1):406-417

Tagami S, Eguchi Y, Kinoshita M, Takeda M, Tsujimoto Y. A novel protein, RTN-XS, interacts with both Bcl-XL and Bcl-2 on endoplasmic reticulum and reduces their anti-apoptotic activity. Oncogene. 2000;19(50):5736-5746.

Terasaki M, Jaffe LA. Organization of the sea urchin egg endoplasmic reticulum and its reorganization at fertilization. J. Cell Biol. 1991;114, 929–940

Tolley N, Sparkes IA, Hunter PR, Craddock CP, Nuttall J, Roberts LM, Hawes C, Pedrazzini E, Frigerio L. Overexpression of a plant reticulon remodels the lumen of the cortical endoplasmic reticulum but does not perturb protein transport. Traffic. 2008;9(1):94-102.

Tolley N, Sparkes I, Craddock CP, Eastmond PJ, Runions J, Hawes C, Frigerio L. Transmembrane domain length is responsible for the ability of a plant reticulon to shape endoplasmic reticulum tubules in vivo. Plant J. 2010;64(3):411-8.

Tsirigos KD, Peters C, Shu N, Käll L, Elofsson A. The TOPCONS web server for consensus prediction of membrane protein topology and signal peptides. Nucleic Acids Res. 2015;43(W1):W401-7.

Ueda H, Yokota E, Kutsuna N, et al. Myosin-dependent endoplasmic reticulum motility and F-actin organization in plant cells. Proc Natl Acad Sci U S A. 2010;107(15):6894-6899.

Ueda H, Yokota E, Kuwata K, et al. Phosphorylation of the C Terminus of RHD3 Has a Critical Role in Homotypic ER Membrane Fusion in Arabidopsis. Plant Physiol. 2016;170(2):867-880.

Ueda H, Ohta N, Kimori Y, Uchida T, Shimada T, Tamura K, Hara-Nishimura I. Endoplasmic reticulum (ER) membrane proteins (LUNAPARKs) are required for proper configuration of the cortical ER network in plant cells. Plant Cell Physiol. 2018;59(10):1931-41.

Ueda K, Matsuyama T, Hashimoto T. Visualization of microtubules in living cells of transgenic Arabidopsis thaliana. Protoplasma. 1999;206:201–206.

Ulloa G, Hamati F, Dick A, et al. Lipid species affect morphology of endoplasmic reticulum: a sea urchin oocyte model of reversible manipulation. J Lipid Res. 2019;60(11):1880-1891.

UniProt Consortium. UniProt: the universal protein knowledgebase in 2021. Nucleic Acids Res. 2021;49(D1):D480-D489.

van der Lee R, Buljan M, Lang B, Weatheritt RJ, Daughdrill GW, Dunker AK, Fuxreiter M, Gough J, Gsponer J, Jones DT, Kim PM, Kriwacki RW, Oldfield CJ, Pappu RV, Tompa P, Uversky VN, Wright PE, Babu, M. M. Classification of intrinsically disordered regions and proteins. Chemical Reviews. 2014;114(13):6589–6631.

Voeltz GK, Rolls MM, Rapoport TA. Structural organization of the endoplasmic reticulum. EMBO Rep. 2002;3(10):944-950.

Voeltz GK, Prinz WA, Shibata Y, Rist JM, Rapoport TA. A class of membrane proteins shaping the tubular endoplasmic reticulum. Cell. 2006;124(3):573-86.

Waese J, Fan J, Pasha A, Yu H, Fucile G, Shi R, Cumming M, Kelley LA, Sternberg MJ, Krishnakumar V, Ferlanti E, Miller J, Town C, Stuerzlinger W, Provart NJ. ePlant: Visualizing and Exploring Multiple Levels of Data for Hypothesis Generation in Plant Biology. Plant Cell. 2017;29(8):1806-1821.

Wang N, Rapoport TA. Reconstituting the reticular ER network - mechanistic implications and open questions. J Cell Sci. 2019;132(4):jcs227611

Wang P, Hawkins TJ, Richardson C, Cummins I, Deeks MJ, Sparkes I, Hawes C, Hussey PJ. The plant cytoskeleton, NET3C, and VAP27 mediate the link between the plasma membrane and endoplasmic reticulum. Curr Biol. 2014;24(12):1397-1405

Wang P, Hussey PJ. NETWORKED 3B: a novel protein in the actin cytoskeleton-endoplasmic reticulum interaction. J Exp Bot. 2017;68(7):1441-1450.

Wang P, Richardson C, Hawkins TJ, Sparkes I, Hawes C, Hussey PJ. Plant VAP27 proteins: domain characterization, intracellular localization and role in plant development. New Phytol. 2016;210(4):1311-26.

Wang P, Hawes C, & Hussey PJ. Plant endoplasmic reticulum-plasma membrane contact sites. Trends in Plant Sci. 2017;22(4):289-297.

Wang S, Tukachinsky H, Romano FB, Rapoport TA. Cooperation of the ER-shaping proteins atlastin, lunapark, and reticulons to generate a tubular membrane network. Elife. 2016;5:e18605.

Ward JJ, Sodhi JS, McGuffin LJ, Buxton BF, Jones DT. Prediction and functional analysis of native disorder in proteins from the three kingdoms of life. J Mol Biol. 2004;337(3):635-45.

Walter P, Blobel G. Translocation of proteins across the endoplasmic reticulum. II. Signal recognition protein (SRP) mediates the selective binding to microsomal membranes of in-vitro-assembled polysomes synthesizing secretory protein. J Cell Biol. 1981;91(2 Pt 1):551-556.

West M, Zurek N, Hoenger A, Voeltz GK. A 3D analysis of yeast ER structure reveals how ER domains are organized by membrane curvature. J Cell Bio. 2011;193(2):333-46.

Westheimer FH. Why nature chose phosphates. Science. 1987;235(4793):1173-1178.

Westrate LM, Lee JE, Prinz WA, Voeltz GK. Form follows function: the importance of endoplasmic reticulum shape. Annu Rev Biochem. 2015;84:791-811.

Wickstead B, Gull K. The evolution of the cytoskeleton. J Cell Biol. 2011; 194(4): 513–525.

Winter D, Vinegar B, Nahal H, Ammar R, Wilson GV, Provart NJ. An “Electronic Fluorescent Pictograph” Browser for Exploring and Analyzing Large-Scale Biological Data Sets. PLoS ONE. 2007;2(8): e718

Woese CR, Kandler O, Wheelis ML. Towards a natural system of organisms: proposal for the domains Archaea, Bacteria, and Eucarya. Proc Natl Acad Sci U S A. 1990;87(12):4576-4579.

Wojcik S, Kriechbaumer V. Go your own way: membrane-targeting sequences. Plant Physiol. 2021;185(3):608-618

Wu X, Hammer JA. ZEISS Airyscan: Optimizing Usage for Fast, Gentle, Super-Resolution Imaging. Methods Mol Biol. 2021;2304:111-130.

Wright PE, Dyson HJ. Intrinsically unstructured proteins: re-assessing the protein structure-function paradigm. J Mol Biol. 1999;293(2):321-31

Xie H, Vucetic S, Iakoucheva LM, Oldfield CJ, Dunker AK, Uversky VN, Obradovic Z. Functional anthology of intrinsic disorder. 1. Biological processes and functions of proteins with long disordered regions. J Proteome Res. 2007;6(5):1882-98

Xue B, Romero PR, Noutsou M, Maurice MM, Rüdiger SG, William AM Jr, Mizianty MJ, Kurgan L, Uversky VN, Dunker AK. Stochastic machines as a colocalization mechanism for scaffold protein function. FEBS Lett. 2013;587(11):1587-91.

Yang YS, Strittmatter SM. The reticulons: a family of proteins with diverse functions. Genome Biol. 2007;8(12):234

Zang J, Kriechbaumer V, Wang P. Plant cytoskeletons and the endoplasmic reticulum network organization. J Plant Physiol. 2021;264:153473.

Zeeshan HM, Lee GH, Kim HR, Chae HJ. Endoplasmic Reticulum Stress and Associated ROS. Int J Mol Sci. 2016;17(3):327.

Zhang M, Wu F, Shi J, et al. ROOT HAIR DEFECTIVE3 family of dynamin-like GTPases mediates homotypic endoplasmic reticulum fusion and is essential for Arabidopsis development. Plant Physiol. 2013;163(2):713-720.

Zhang SL, Yu Y, Roos J, et al. STIM1 is a Ca2+ sensor that activates CRAC channels and migrates from the Ca2+ store to the plasma membrane. Nature. 2005;437(7060):902-905.

Zhao G, Zhu PP, Renvoisé B, Maldonado-Báez L, Park SH, Blackstone C. Mammalian knock out cells reveal prominent roles for atlastin GTPases in ER network morphology. Exp Cell Res. 2016;349(1):32-44

Zhao Y, Zhang T, Huo H, Ye Y, Liu Y. Lunapark Is a Component of a Ubiquitin Ligase Complex Localized to the Endoplasmic Reticulum Three-way Junctions. J Biol Chem. 2016;291(35):18252-18262.

Zhou X, He Y, Huang X, Guo Y, Li D, Hu J. Reciprocal regulation between lunapark and atlastin facilitates ER three-way junction formation. Protein Cell. 2019;10(7):510-525.

Zimmerberg J, Kozlov MM. How proteins produce cellular membrane curvature." Nat Rev Mol Cell Biol. 2006;7(1):9-19.